5-2014

Corrosion assessment and enhanced biocompatibility analysis of biodegradable magnesium-based alloys

Luis Enrique Pompa
University of Texas-Pan American

CORROSION ASSESSMENT AND ENHANCED BIOCOMPATIBILITY ANALYSIS OF BIODEGRADABLE MAGNESIUM-BASED ALLOYS

A Thesis

by

LUIS ENRIQUE POMPA

Submitted to the Graduate School of
The University of Texas-Pan American
In partial fulfillment of the requirements of the degree of

MASTER OF SCIENCE

May 2014

Major Subject: Mechanical Engineering

CORROSION ASSESSMENT AND ENHANCED BIOCOMPATIBILITY ANALYSIS OF BIODEGRADABLE MAGNESIUM-BASED ALLOYS

A Thesis
by
LUIS ENRIQUE POMPA

COMMITTEE MEMBERS

Dr. Waseem Haider
Chair of Committee

Dr. Karen Lozano
Committee Member

Dr. Dorina Mihut
Committee Member

Dr. Shivani Maffi
Committee Member

May 2014

ABSTRACT

Pompa, Luis E., Corrosion Assessment and Enhanced Biocompatibility Analysis of Biodegradable Magnesium-Based Alloys. Master of Science (MS), May, 2014, 111 pp., 18 tables, 65 figures, 153 references, 46 titles.

Magnesium alloys have raised immense interest to many researchers because of its evolution as a new third generation material. Due to their biocompatibility, density, and mechanical properties, magnesium alloys are frequently reported as prospective biodegradable implant materials. Moreover, magnesium based alloys experience a natural phenomena to biodegrade in aqueous solutions due to its corrosive activity, which is excellent for orthopedic and cardiovascular applications. However, major concerns with such alloys are fast and non-uniform corrosion degradation. Controlling the degradation rate in the physiological environment determines the success of an implant. In this investigation, three grades of magnesium alloys: AZ31B, AZ91E and ZK60A were studied for their corrosion resistance and biocompatibility. Scanning electron microscopy, energy dispersive spectroscopy, atomic force microscopy and contact angle meter are used to study surface morphology, chemistry, roughness and wettability, respectively. Additionally, the cytotoxicity of the leached metal ions was evaluated by a tetrazolium based bio-assay, MTS.

DEDICATION

The completion of my master's degree would not have been possible without the guidance of my heavenly father, and the love and support of my family and friends. Although the journey was difficult, God's unfailing love inspired me to push through and for that I am very grateful. Thank you for your motivation and love.

ACKNOWLEDGMENTS

I would have never been able to complete my thesis work without the guidance of my committee members (Dr. Maffi, Dr. Lozano, and Dr. Mihut), help from faculty and staff (Alfonso Salinas, Annie Ocanas, Adriana Hinojosa, Julissa Flores and Marcus Montalvo), and support from research assistants (Edgar Munoz, Zia Rahman, Juan Carbone, Juan de Leon, Benito Gonzalez, Jose Patino, Marcos Villarreal, Jerry Contreras). I would like to express my especial and deepest appreciation to all of them.

I am thankful and grateful to Dr. Waseem Haider, chair of my thesis committee, for his excellent guidance, caring, patience, effort, and providing me with an outstanding motivation for doing research. You have been an amazing mentor for me. Your advice on both research as well as on my professional career is very precious to me.

Last, but by no means least, I thank all my friends for their support and encouragement throughout my master's career.

TABLE OF CONTENTS

Page

LIST OF TABLES

Page

LIST OF FIGURES

Page

CHAPTER I

INTRODUCTION

1.1 Background and History

Historically speaking, the concept of implanting foreign objects into the human body has arisen remarkably. Biomaterial science incorporates the study of the properties and composition of materials and the physiological and biological interaction in which they are placed. The biomaterials science is an interdisciplinary research area that is very active. The state of the art biomaterials science ranges from physics, chemistry, and engineering through molecular and cell biology to the field of medicine (1). In the early years of research and development, metal implants confronted corrosion and lack of sufficient mechanical properties difficulties. In the past decades a significant number of biomedical implants have been studied and utilized in the human body. Innovative advanced materials have arisen due to the complexity of designs needed as implant devices. Furthermore, thanks to years of investigation from scientists and engineers many advanced materials, incorporated with surface engineering methods, are now been implemented with great outcomes, but only to some extent. Even though continuous research has been done, the rate of implants failure is quite high leaving research space for developments and improvements for optimum stability of medical devices. Meanwhile, implant materials require important characteristics for temporal and long-term usage in the body, and this information will be learned in the next section.

1.2 Biological Implant Requirements

Overall, before the use of the biomaterials in clinical practices, they must go through scientific testing and analysis. First, the microstructure, physical and mechanical properties of materials have to be studied. Sometimes, the materials have to go through a certain surface treatment or surface modification for properties enhancement. This treatment includes surface morphological modification and/or chemical modification to materials. Table 1 displays important material requirements that must be met for a successful implantation (2).

Table1. Requirements for implants

Compatibility	Tissue reactions, change in properties (mechanical, physical, chemical), degradation leads to: local deleterious changes, harmful systemic effects
Mechanical properties	Elasticity, yield stress ductility, toughness, time dependent deformation, creep, ultimate strength, fatigue strength, hardness, wear resistance
Manufacturing	Fabrication methods, consistency to all requirements, quality of raw materials, superior techniques to obtain excellent surface finish, capability of material to get safe and efficient sterilization, cost of product

The ideal material combination should incorporate the following properties:

1.3 Biocompatibility

In order to successfully employ implants inside the body, a good interaction between metals and living organisms is necessary, in other words a high degree of biocompatibility is required (1,2). The term biocompatibility indicates the ability of a material to perform with an appropriate host response (1). No adverse effects are acceptable or affect local and systemic host environment such as: soft tissues, bone, ionic composition of plasma, and even intra and extracellular fluids (3). In other words, materials intended for medical use should be non-carcinogenic, non-pyrogenic, non-toxic, non-allergic, non-inflammatory, and hemocompatible (3).

The classification of materials based on its interaction with biological environment and response by the human body is given in table 2 (3,4).

Table 2. Classes of materials

Bioinert	Refers to a material that retains its structure in the body after implantation and does not induce any immunologic host reactions
Bioactive	Refers to materials that form direct chemical bonds with bone or even with soft tissue of a living organism
Bioresorbable	Refers to materials that degrade in the body while they are being replaced by regenerating natural tissue; the chemical by-products of the degrading materials are absorbed and released via metabolic process of the body

1.4 Functionality and Properties of Biological Implants

Biomaterials have to match with biological requirements. For instance, shape, inner structure, and design of an implant require to be adapted to the physical and mechanical features of the tissue being implanted (5). For example, bone replacements require load transmissions and stress distributions features. Similarly, articulation movements are necessary for artificial knee joint (6). To discuss properties of materials, most of the implants are exposed to elastic repetitive loads, meaning that the material must have a good combination of strength and ductility (7). These requirements depend on the specific implant application as stated before. To enumerate, stents and grafts are expanded to push up against blood vessels or arteries; therefore, they require plasticity for expansion and rigidity to maintain the dilatation deformation (8). For orthopedic applications, implants must have excellent toughness, rigidity, elasticity, strength and resistance to fracture. For joint replacement, implants must be wear resistant; as a result debris formation due to friction can be evaded. Similarly, dental applications require rigid and strong materials and even shape memory properties for better outcomes (4,9,10). The most common classes of materials used as biological materials are metals, ceramics, and polymers.

1.5 Metallic Materials

Materials used for implants are titanium and its alloys, stainless steel, and cobalt-chrome alloys (1,11). These types of materials are widely used due to their good mechanical properties, high corrosion resistance, strength and unique characteristics. Titanium alloys possesses qualities such as: light weight, corrosion resistance and biocompatibility when compared to other alloys. Ti6Al4V alloy is known for its excellent tensile strength and pitting corrosion resistant (4,12). Moreover, titanium alloyed with nickel (Nitinol), creates devices displaying shape memory effects that can be applied to dental restoration wiring and cardiovascular applications (13). Furthermore, stainless steel are also well known for biomedical applications. For example, AISI 316L, a single phase austenitic stainless steel, is one of the most popular used for implant applications (14,15). This alloy contains about 17-19%Cr, 12-14%Ni, and 2-3%Mo. Research demonstrates that Mo has improved 316L corrosion resistance, and carbon content has been reduced from 0.08 to 0.03 wt% improving its corrosion resistance to chloride solution. The "L" in the designation refers to low carbon. The 316L elastic modulus is about 200 GPa, therefore load-bearing bone applications are considered (16,17). The different metallic alloys vary in their corrosion resistance and in the mechanical properties. Table 3 depicts metallic materials with their respective applications.

Table 3. Metallic materials and applications (3)

Metallic Materials	Common Applications
Stainless Steel alloys	Joint replacements, (hip, knee), bone plate for fracture fixation, dental implant for tooth fixation, heart valve, spinal instruments, surgical instruments, screws, dental root implants, pacer, fracture plates, hip nails, shoulder prosthesis
Cobalt-chromium alloys	Bone plate for fracture fixation, screws, dental root implant, pacer, and suture, dentistry, orthopedic prosthesis, mini plates, surgical tools, bone and joint replacements, dental implants
Titanium alloys	Cochlear replacement, bone and joint replacements, dental implants for tooth fixation, screws, sutures, parts for orthodontic surgery, bone fixation devices like nails, screws and plates, artificial heart valves and surgical instruments, heart pacemakers, artificial heart valves

1.6 Ceramic Materials

The main characteristics of ceramic materials are stiffness, strength, hardness, wear and corrosion resistance, and low density. Ceramics primary purpose is on withstanding compression forces; it is well known that on tension forces, their performance is poor. Some of the applications for ceramics include: dentistry, orthopedic and medical sensors (3,18). There are three main types of ceramics: bioinert, bioactive and bioabsorbable. Alumina (Al_2O_3) and Zirconia (ZrO_2) are examples of bioinert. Bio glass and glass ceramic are bioactive. Calcium phosphate ceramics are bioabsorbable (19). Table 4 represents ceramic materials and their application. Ceramic materials have been less utilized when compared to metals or polymers due to their poor plastic deformation.

Table 4. Ceramic materials and applications (3)

Ceramic Materials	Common Applications
Alumina	Artificial total joint replacement, acetabular and femoral components, vertebrae spacers and extensors, orthodontic anchors, dental implant for tooth fixation
Zirconia	Replacement for hips, knees, teeth, tendons and ligaments, repair for periodontal disease, bone filters after tumor surgery
Pyrolyctic Carbon	Prosthetic heat valves, endosseous tooth replacement implants, permanently implanted artificial limbs
Bioglass-Ceramics	Dental implants, middle ear implants, heart valves, artificial total joint replacement, bone plates, screws, wires, intramedullary nails, spinal fusion, tooth replacement implants
Calcium Phosphates	Skin treatments, dental implants, jawbone reconstruction, orthopedics, facial surgery, ear, nose and throat repair, dental implant

1.7 Degradable and Absorbable Biological Materials

During the last decade, important progress has occurred to develop the third generation of biodegradable materials for medical applications. It is essential to improve and characterize devices for us in the human body to measure, restore, and improve the physical performance. Biodegradable materials are characterized as materials utilized for implants, which permits the devices to degrade in the human body. There are occasions where implants have to be temporal for specific clinical problems. However, they have to provide healing support and perform safely in living organisms. When implanted, materials should sustain their properties until they are not needed and then degrade and absorbed by the body without causing any adverse effects, and without leaving traces.

1.8 Recent Biodegradable Materials

Polymers are the most common biodegradable materials used today. Biodegradable polymer materials include PolyLactid Acid (PLA), PolyDiaxanone, Polyglactin, PolyGlycolic Acid (PGA) (20,21). These materials are being used in several applications, such as: tissue engineering scaffolds, cardio vascular stents, sutures, etc. Table 5 shows some of the synthetic polymeric materials employed and their biomedical applications. The major disadvantage with polymer materials is their low mechanical properties; therefore, they cannot be utilized in applications where high strength is required. It has also been reported that the biodegradation of polymers when implanted takes several years, which is another disadvantage (22,23).

Table 5. Polymeric materials and applications (11)

Polymeric Materials	Common Applications
Polyethylene	Joint replacement
Polypropylene	Sutures
PET	Sutures, vascular prostheses
Polyamides	Soft-tissue augmentation, vascular prostheses
Polyesters	Vascular prostheses, drug delivery systems
Polyurethanes	Blood-contacting devices
PVC	Tubing
PMMA	Dental restorations, intraocular lenses, joint replacement (Bone cements)

CHAPTER II

LITERATURE RIVIEW

2.1 Magnesium Alloys as Biodegradable Implant Materials

Magnesium alloys are considered an alternative material useful for the fabrication of cardiovascular, orthopedic and trauma stomach devices (24,25). Magnesium alloys provides similar density and Young's Modulus to bones (26). Mg^{2+} is a common ion encountered in the human body. It is the fourth most abundant cation in the human body, with an estimation of 1 mol of magnesium in a normal 70 kg adult. In addition, magnesium alloys are considered biodegradable alloys due to their rate of degradation in the human body (27). To illustrate, titanium, cobalt, and stainless steel biomedical devices requires a second surgery to extract out these devices from the body. Magnesium alloys will be preferred and will be an economic impact for patients and doctors due to their rate of degradation (25). However, it is important to take in consideration that the large quantities of magnesium ions released in the human body could be toxic. In order to prevent this, surface techniques are applied to modify the surface and properties of the alloy. Since magnesium alloys are considered biodegradable alloys, they are only able to receive specific types of surface modifications. The type of surface treatment is chosen according to the environment the implant is going to be interacting with (28). For example, coatings are a great technique for ensuring the biocompatibility of the implant with the bones. Since the main purpose of using magnesium is to biodegrade in the human body, the purpose of the coatings will be to decrease the rate of degradation of the material in the human

body. For cardiovascular applications the alloys would not be able to have a coating, but they would need to have a surface modification in order to increase the corrosion resistance. An important part of the degradation of magnesium alloys is that the material is very corrosive in aqueous solutions. It is an excellent material to degrade in the biological systems because of its corrosion activity. A significant objective for using biodegradable alloys is that they require a tremendous amount of surface modification to increase their corrosion resistance. The idea of surface modification is to change the surface of the alloy, so the chemical elements composing the alloy obtain enhanced properties such as corrosion resistance, biocompatibility, and hardness (29,30).

2.2 Corrosion on Magnesium Alloys

Corrosion of magnesium and its alloys has been studied by researchers due to its strong thermodynamic tendency to act as an active material; with high oxidation. Among metals magnesium demonstrates a very low standard potential as seen in table 6 (31). The dissimilitude of standard potential vs. corrosion potential is related to the formation of an oxide film $Mg(OH)_2$ on the surface of the metal (32,33).

The buffering solutions take effect on the generated OH^- turning the conversion from Mg to Mg^{2+}. Previous works have reported that inorganic/organic components such as amino acids, or proteins, chloride ions etc. can influence the corrosion rate and degradation of alloys. Due to the corrosion activity of magnesium alloys, the mechanical integrity can be affected before certain tissue has the appropriate time to heal without any negative effects. Hard-tissue implantation repairs may require at least 12 weeks (34).

Table 6. Standard electromotive force potentials (31)

Reduction Half Reaction	**Standard Potential, e^0 (volts vs. SHE)**
$Au^{3+} + 3e^- = Au$	1.498
$Fe^{3+} + 3e^- = Fe$	0.771
*	*
*	*
*	*
$2H^+ + 2e^- = H_2$	0
$Ni^{2+} + 2e^- = Ni$	-0.25
*	*
*	*
*	*
$Cr^{3+} + 3e^- = Cr$	-0.744
$Al^{3+} + 3e^- = Al$	-1.662
$Mg^{2+} + 2e^- = Mg$	-2.372

Magnesium and its alloys corrode in aqueous solutions and the different oxidation-reduction reactions are affected by the different alloying elements. Typically, the corrosion occurrence of magnesium will produce hydrogen gas evolution and magnesium hydroxide. The hydroxide ions produced through the cathodic reaction generates an increase in the pH of the solution (35). The common anodic and cathodic reactions are expressed as following:

$$\text{Anodic} \qquad Mg \rightarrow Mg^{2+} + 2e^- \qquad (1)$$

$$\text{Cathodic} \qquad 2H_2O + 2e^- \rightarrow H_2 + 2(OH^-) \qquad (2)$$

$$\text{Net reaction} \qquad Mg + 2H_2O \rightarrow Mg(OH)_2 + H_2 \qquad (3)$$

Figure 1 depicts the Pourbaix diagram for magnesium; the diagram helps visualize the effects of potentials and pH and how they affect the thermodynamic regions of corrosion, immunity and passivity. Furthermore, at low pH values the corrosion potential resembles the

region where the stability of hydrogen occurs. This leads to the production of hydrogen, which leads to the dissolution of magnesium. Similarly, it can be seen that there is a strong hydrogen evolution against dissolved oxygen, however not significant (33).

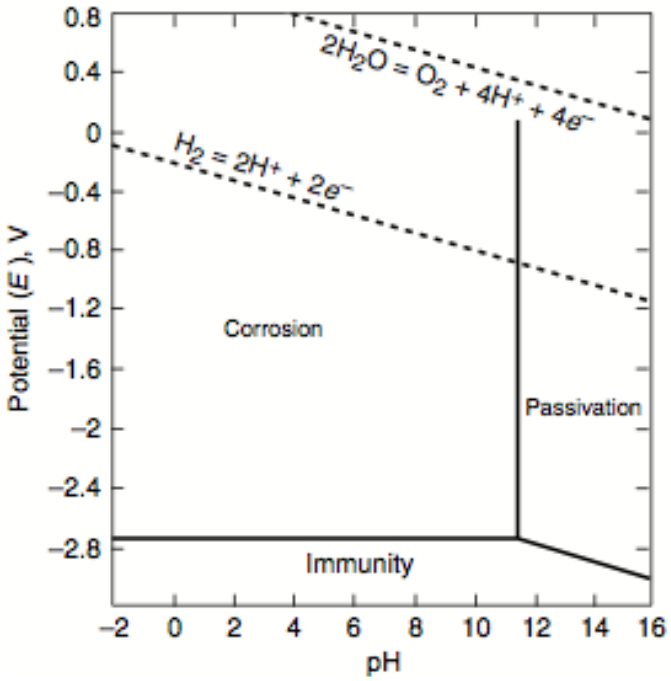

Figure 1. Potential-pH (Pourbaix) diagram for the system of magnesium and water at 25 C (77 F), showing the theoretical domains of corrosion, immunity, and passivation (33).

A major drawback of magnesium is the production of hydrogen gas when placed in contact with physiological environments. The hydrogen evolution may lead to gas pocket formations causing necrosis within tissues and delayed healing at the surgery region area (36). On the other hand, if hydrogen gas is evolved at a slow rate it can be tolerated and released by the body system. According to Song et al (36) a hydrogen evolution rate of 0.01 ml/cm^2/day can be tolerated by the human body. The degradation of magnesium and the generation of hydrogen gas can be controlled by applying appropriate methods such as alloying and surface modification techniques.

2.3 Forms of Corrosion of Magnesium and its Alloys

The common corrosion types of magnesium in physiological environments such as simulated body fluids consist of: galvanic corrosion, pitting corrosion, stress corrosion cracking and corrosion fatigue.

2.4 Galvanic Corrosion

Magnesium has a very low standard electrode potential as shown in table 5. Magnesium possess a value of -2.37 V (vs. SHE) with respect to the hydrogen electrode potential taken as zero and at 25°C it is more active than most metals (31,33). These mentioned characteristics lead to a high susceptibility of magnesium and its alloys to galvanic corrosion. An electrochemical process that occurs when two metals having different electrochemical potentials come in contact with electrolyte is known as galvanic corrosion (37). The metal with more negative potential would act as the anode (the one which is corroding), while the cathode is the one protected against corrosion. The driving force for the galvanic corrosion is governed by the difference of the potential of materials (37). Galvanic corrosion is of a major concern for magnesium alloys in aggressive environments such as SBFs due to the place it possess in the galvanic series which is the most active material with the lowest corrosion potential (31). The galvanic corrosion rate is increased by the following factors: high conductivity of the medium, large potential difference between the anode and cathode, low polarisability of anode and cathode, large area ratio of cathode to anode, and small distance from anode to cathode (38). Furthermore, corrosion of magnesium not only happens when in contact with different metals; galvanic attack is also present between phases and intermetallic particles (39). Magnesium and alloys commonly do not possess a uniform composition and microstructure crystal orientation, which promotes the existence of galvanic couples (37).

2.5 Pitting Corrosion

A severe localized attack at the material surface is known as pitting corrosion. The formation of very small holes called pits is formed throughout the area being damaged. This type of corrosion can be difficult to detect due to the size of pits that could be very small (macro-scale/nano-scale); pits growing downwards and perforating the metal matrix. Pitting corrosion will develop at free corrosion potential of magnesium, when exposed to chloride ions in a non-oxidizing environment (38,40). Magnesium alloys are vulnerable to the formation of pits when the magnesium passive layer consisting of $Mg(OH)_2$ or MgO breaks down at local areas (41,42). Following this event, the corrosion phenomenon can initiate at these broken down local sites where pits act as small anodic surface areas. Furthermore, the pits formed though corrosion could lead to crack initiation sites of stress corrosion cracking and corrosion fatigue (39).

2.6 Stress Corrosion Cracking/Corrosion Fatigue

When an electrochemical potential is developed between stressed or unstressed region areas of a metallic implant under loading conditions, there is an increased chemical activity in the metal. By this corrosion mechanism, the corrosion rate is increased, by two to three times above the normal uniform rate (43). The accelerated rate of corrosion usually results in the formation of small cracks with high concentrated stress within the loaded implant, this mechanism is known as stress corrosion cracking (SCC) (43). SCC in magnesium alloys has been attributed to one of two groups of mechanisms: continuous crack propagation by anodic dissolution at the crack tip or discontinuous crack propagation by a series of mechanical fractures at the crack tip (40). Stress corrosion cracking can happen to magnesium under loading conditions in aggressive physiological environment containing chlorides. If cracks are initiated through SCC, these cracks can grow rapidly and extend between the grains and the metal matrix

leading to fracture and ultimately failure of the implant. Similarly, magnesium is also susceptible to corrosion fatigue in the presence of chloride ion in the body fluids. Corrosion fatigue is the outcome of a material exposed to combined effects such as: cycling loading and corrosive environment (43). Corrosion fatigue is a critical factor in determining the life of metallic implants undergoing cyclic loading conditions (39).

2.7 Corrosion Protection via Alloying Elements

The process of alloying magnesium with other elements leads to an improvement in the corrosion resistance of magnesium (44,45). Before discussing corrosion in detail, it should be noted that different elements could also contribute to the modification of the mechanical properties of magnesium (46). Magnesium alloys may contain a variation of elemental additions as shown in table 7 (47).

Table 7. ASTM codes for magnesium alloying elements

Abbreviation Letter	Alloying Element	Abbreviation Letter	Alloying Element
A	Aluminum	N	Nickel
B	Bismuth	P	Lead
C	Copper	Q	Silver
D	Cadium	R	Chromium
E	Rare earths	S	Silicon
F	Iron	T	Tin
H	Thorium	W	Yttrium
K	Zirconium	Y	Antimony
L	Lithium	Z	Zinc
M	Manganese		

The American Society for Testing and Materials (ASTM) created a system for selecting and naming different elements alloyed with magnesium. The system uses two letters followed by two numbers. The first letter tells the element with the highest portion in the alloying

addition. For example, the composition of AZ91 magnesium is approximately 9 wt. % aluminum, and 1 wt. % Zinc. Another example, WE43 has 4 wt. % yttrium and 3 wt. % rare earths.

Again, table 7 exhibits different magnesium compositions that are being targeted for their mechanical properties capabilities. Some of the alloys compositions have attracted more attention compared to others and tailored them for a specific application. Magnesium in its elemental state has been used, as well as other elements incorporating: aluminum, zinc, calcium, manganese, lithium, zirconium, yttrium, and some of the rare earth metals (25,48–52). Below it is a general explanation of some of the most common alloying elements and their benefits.

Aluminum – Metals alloyed with aluminum have a good combination of mechanical properties and good die-castability (53). Aluminum possess a low density and acts as a passivating alloying element, which offers better corrosion properties (54).

Zinc – Magnesium is frequently alloyed with zinc which increase its yield strength (55). Magnesium alloys as well as other implant materials should have a Young's modulus of 20 GPa which is similar to bone's Young modulus (56). Similar to aluminum, zinc can improve the corrosion resistance and some mechanical properties of magnesium alloys for example, strengthen of magnesium through a solid solution hardening mechanism (57). Further on, zinc is one of the most abundant essential elements in the human body. It is found in all body tissues with 85% of the whole body zinc in muscle and bone, 11% in the skin and the liver and the remaining in all other tissues (58).

Calcium – Several studies demonstrated that calcium additions increase the corrosion resistance, increase mechanical properties, influences grain growth and serves as a grain refinement agent (9,25,59–61) . In the case of the biological functions, calcium is an essential component of

bones, and cartilage. It is essential for the normal clotting of blood, by stimulating the release of thromboplastin from the blood platelets (62).

Manganese – It is the most common alloying addition, which is used to neutralize the effect of iron and to help modifying the morphology and type of intermetallic phases (63). Modifications in the morphology improve tensile strength, elongation, and ductility. Manganese alloying addition also gives an increase of high temperature strength and creep resistance (63). Biologically, Mn is associated with bone development, amino acid, lipid and carbohydrate metabolism (64).

Iron – It is also a very important element for the corrosion resistance of magnesium alloys at controlled additions and has the ability to grain refine in magnesium alloys (65). Fe is found in different proteins especially proteins for storage and transport (64).

Table 8. Summary of most common alloying elements (53–64,66)

Element	Positive Effects	Negative Effects
Zinc	Corrosion resistance, tensile strength	-
Aluminum	Corrosion resistance, mechanical properties, hardness, castability	Stress corrosion cracking, porosity
Yttrium	Corrosion resistance, tensile strength, castability	Liability of cracks
Zirconium	Grain refinement, tensile strength	Ultimate strain
Calcium	Grain refinement, castabiliy	Liability of cracks
Rare earths	Reduce porosity	-
Silicon	Hardness, compressive strength	Castability, ultimate strength
Manganese	Corrosion resistance, tensile strength, castability, ductility	-

As stated before, alloying elements possess the potential to improve magnesium's mechanical properties and corrosion resistance. However, there are several factors that need to be considered like electrochemical characteristics such as; passivation, exchange current density, electronegativity, and density. A variety of different grades of alloys have been designed and developed to deliver a span of characteristics and properties that are needed for specific applications. Below are listed some of the most frequent magnesium alloys currently used in the industry, table 9.

Table 9. Magnesium Alloy Grades (67)

ASTM Designation	Ag	Al	Fe max	Mn	Ni max	Rare Earth	Zn	Zr	Forms
AM50A		4.9	0.004	0.32	0.002		0.22		DC
AM60B		6	0.005	0.42	0.002		.22 max		DC
AS41B		4.2	0.0035	0.52	0.002		0.12		DC
AZ91D		9	0.005	0.33	0.002		0.7		DC
AZ31B		3	0.005	0.6	0.005		1		S, P, F, E
AZ61A		6.5	0.005	0.33	0.005		0.9		F, E
AZ80A		8.5	0.005	0.31	0.005		0.5		F, E
AZ81A		7.6		0.24			0.7		SC, PM, IC
AZ91E		9	0.005	0.26	0.0001		0.7		SC, PM
EZ33A						3.2	2.5	0.7	SC, PM,
WE43A				0.15	0.005	A	0.2	0.7	SC, PM, IC
WE54A				0.15	0.005	B		0.7	SC, PM, IC
ZE41A				0.15		1.2	4.2	0.7	SC, PM, IC
ZE63A						2.6	5.8	0.7	SC, PM, IC
ZK40A							4	0.7	E
ZK60A							5.5	0.7	F, E

A = 4 Yttrium; 3 RE
B = 5.1 Yttrium; 4 RE
C = 2.0 Strontium
D = 2.5 Strontium
E = 2.0 Calcium

DC = die casting; E = extrusion; F = forgin; IC = investment casting; P = plate; PM = permanent mold; S = sheet; SC sand casting

2.8 Magnesium Alloys and Grades

Mg-Al series of magnesium alloys had been studied and reports demonstrate that with some percentage of aluminum addition to the matrix ductility, yield strength and ultimate tensile strength of a material decreased while the hardness increased(68). However, Mg-Zn series gives high strength and high tenacity with very low aluminum content or nothing at all. Zinc elements can influence magnesium alloys to achieve better properties enhancing yield strength and tensile strength with a Zn content less than 6%. The opposite takes effect when increasing the Zn

content over 6%, which lead to a decrease in elongation and tensile strength. Creep strength is also improved in Mg-Zn alloys (68,69). Mg-rare earth (RE) and Mg-Y series alloys have been reported to produce excellent solid solution strengthening and aging reinforcement combined with grain refinement, strength and ductility (68). RE elements ensure an improved corrosion resistance to Mg alloys (70). Mg-RE-Zr series improve mechanical properties in magnesium alloys (71). Figure 2 exhibits typical optical images of the microstructure morphology of magnesium alloy AZ31.

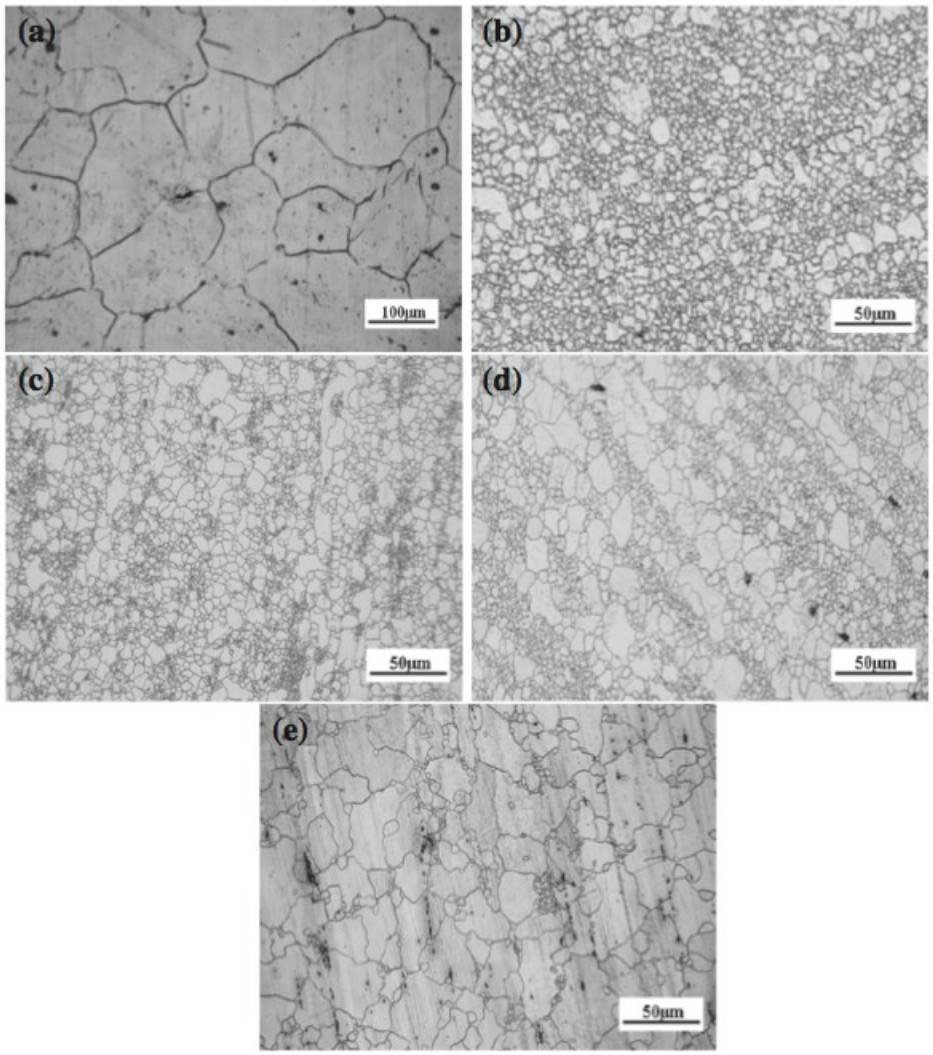

Figure 2. Optical microstructures of Mg alloy AZ31 at different processing states: (a) homogenized at 673 K for 14 h, (b) (c) (d) extruded at 623 K, 673 K, 723 K parallel to the ED–TD plane, (d) annealed at 623 K for 2 h (72).

2.9 Electrochemical Testing and Applications

There are two important electrochemical techniques for testing magnesium alloys: Cyclic Potentiodynamic Polarization and Electrical Impedance Spectroscopy. Cyclic polarization theory targets the concept that the steady state corrosion rate of a material can be altered by changing the applied voltage and accordingly obtaining a change in the current density. The corrosion behavior of a material is characterized by performing an analysis on a cyclic polarization curve of potential versus a logarithmic current density. Cyclic potentiodynamic curves can deliver information that is related to biological implants such as pitting potential (E_P), breaking potential (E_B), hysteresis and terminating current density (i_T) (54,73). Electrical Impedance Spectroscopy is another significant technique for studying the corrosion phenomenon. However, this particular technique needs a more complex understanding and interpretation on the results. The information given from EIS is related to the corrosion rate, which is governed, by kinetics and thermodynamics (63). Figure 3 shows typical potentiodynamic curves performed in phosphate buffer saline and albumin protein (74). Similarly, figure 4 shows some Nyquist plots tested at different potentials (74).

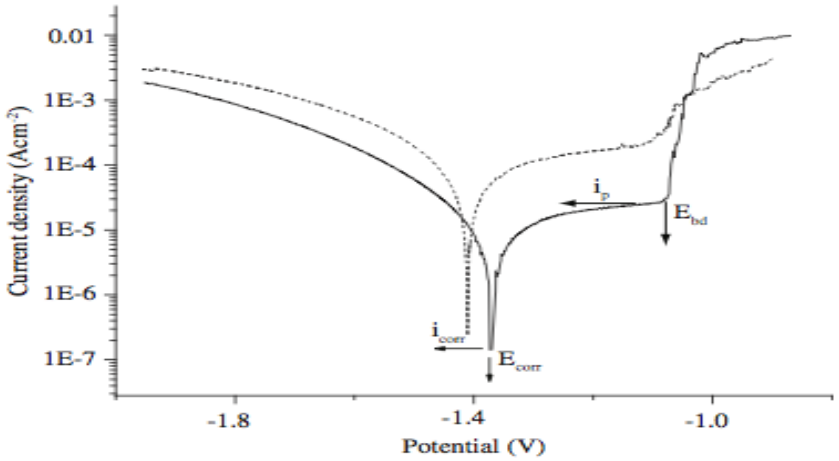

Figure 3. Log i vs. potential polarization curve made in PBS + 0.1 g/L albumin. Passive and corrosion currents (i_p i_{corr}), the breakdown and corrosion potentials (E_{bd}, E_{corr}) are indicated. Dashed line corresponds to the control polarization curve made in PBS.

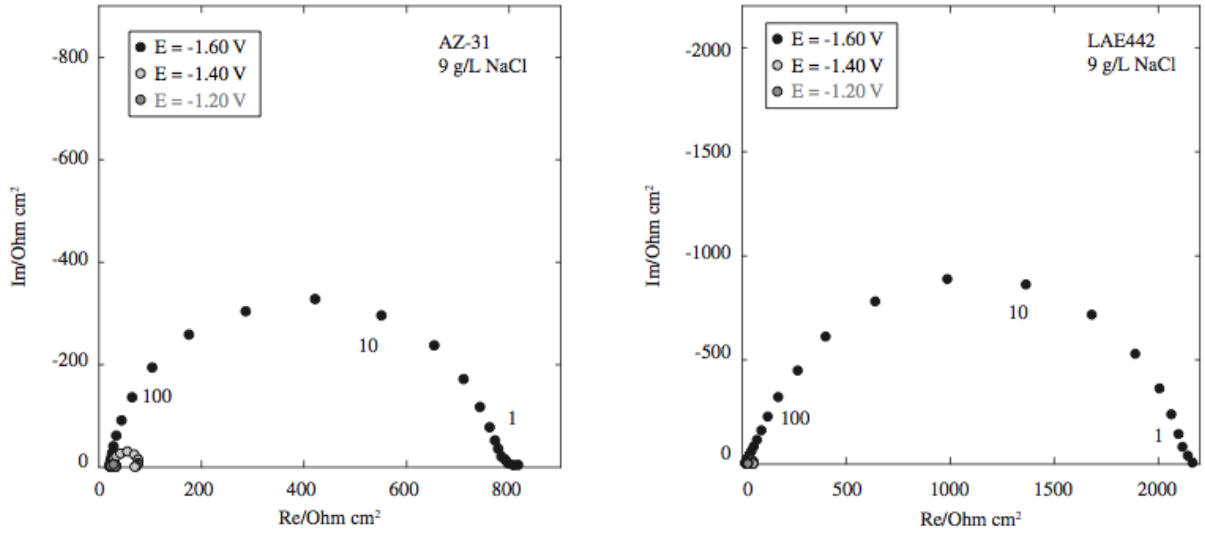

Figure 4. Impedance diagrams (Nyquist plots) of magnesium alloys in 9 g/L NaCl solution at different operational potentials (-1.6 V, -1.4 V, -1.2 V). a) AZ31 alloy; b) LAE442 alloy.

2.10 Surface Modification of Magnesium Alloys

The interactions between biomaterials and biological environment such as tissues, cells, blood, proteins take place on the biomaterials surface. Biological responses depend mainly on the surface properties such as; surface charge, surface chemistry, roughness, wettability and surface energy. Surface characteristics play an important role in the biocompatibility of biological materials. Surface engineering modification is effective for improving corrosion resistance and biocompatibility of metallic biological implants (75). Furthermore, surface engineering assist on the modification of the material without distressing the bulk properties. With such modification techniques, it is potentially possible to select certain material focusing on the bulk properties and afterwards apply engineering approaches to design its surface with the required set of properties (76). A large body of methods exist for surface treatment on magnesium alloys including: oils and waxes, physical and chemical conversions treatments, alkali heat treatments etc. (76,77). However, some of these methods are intended for industrial

applications and might include chemicals and materials that are toxic. For medical implants applications, there are several different techniques that have also been reported for optimization of corrosion resistance as well as the biocompatibility (77).

2.11 Ion Implantation

Ion implantation comprises bombarding ionized particles on the surface of a substrate. The ionized particles penetrate the surface and become embedded in the sub-surface of the substrate. The ionized particles soon neutralize in the interstitial positions within the grain structure forming a solid solution. During this process physiochemical changes take place in the sub-surface of the substrate, while the bulk properties of the substrate remain unchanged (43,75). Ruizhen Xu et. al, conducted corrosion experiments on different test samples, pure magnesium blocks (99.95% pure; 10 mm × 10 mm × 5 mm), AZ31 blocks (Mg with 3 wt% Al and 1 wt% Zn; 10 mm × 10 mm × 5 mm), and AZ91 blocks (Mg with 9 wt% Al and 1 wt% Zn; 10 mm × 10 mm × 5 mm) and pure magnesium implanted with zinc and aluminum. Samples were immersed in simulated body fluid (SBF).

Pure magnesium exhibited the lowest negative corrosion potential (−1.976 V). The implanted sample (−1.8125 V) had a similar corrosion potential as AZ91 (−1.8368 V). AZ31 showed the highest corrosion potential (−1.7038 V) as seen in figure 5. The results indicated that the implanted sample had higher corrosion potential compared to pure magnesium (over 160 mV) indicating better corrosion resistance.

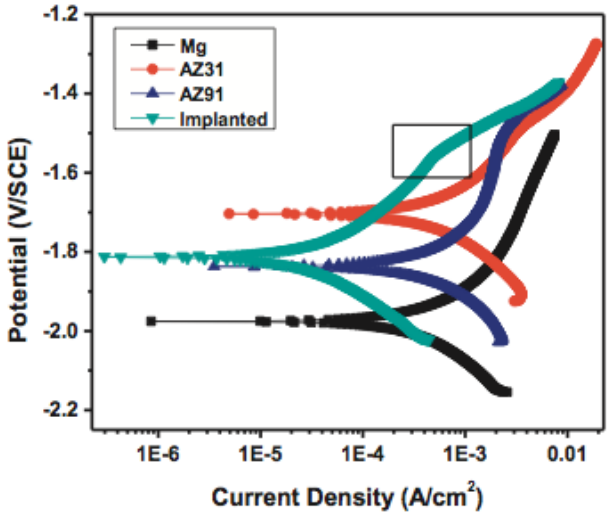

Figure 5. Potentiodynamic polarization curves and its magnesium alloys. (78)

The electrochemical behavior of the samples was analyzed by (EIS). The diameters of the capacitive loops depict a representation of the corrosion resistance indicating higher corrosion rates with enlarged capacitive loop. As Mg, AZ31, and AZ91 have similar diameters in the capacitive loops, they have similar corrosion resistance. The results showed good agreement with those of potentiodynamic polarization.

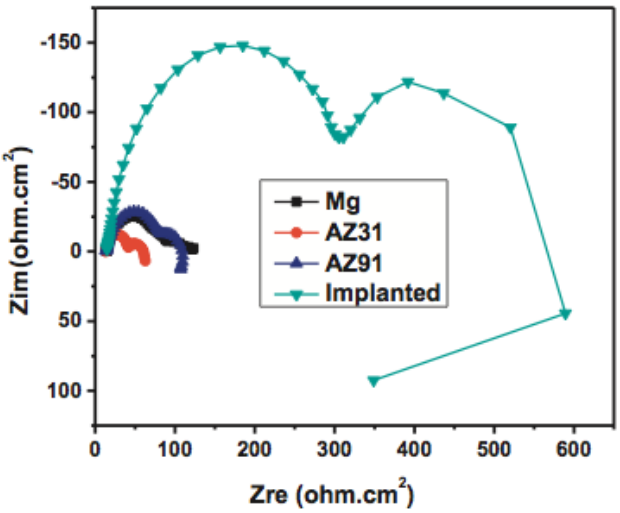

Figure 6. Electrochemical impedance spectra of different samples (78)

Ion implantation of Zn and Al showed enhanced results over pure magnesium, AZ31 and

AZ91. Better corrosion resistance was observed in the immersion tests having a better oxide surface film protecting from pitting corrosion attack.

2.12 Calcium Phosphate Surface Coatings

Biologically calcium phosphate (CaP) belongs to the orthophosphate group and naturally occurs in biological structures like bone and teeth (79). Due to a high degree of biocompatibility, non-toxic, bioactivity and bone inductivity, CaP has been widely used as a coating for orthopedic implant materials (80). Calcium phosphates include hydroxyapatite (HA), which is commonly thermally sprayed. HA coatings are primarily employed to enhance the osseointegration of bone implants. HA consists of $[Ca_5(PO_4)_3OH]$, which are chemically similar to mineral components of bones and hard tissues (81,82). Also, HA coatings have the capacity to shorten the healing time of metal-based implants (81). In addition to being biocompatible, it has been proved that different types of CaP coatings have decreased the corrosion rate of magnesium alloys (77). XU Li-ping et. al. studied calcium phosphate coatings on Mg alloys. It was concluded a better corrosion behavior over untreated Mg alloys as shown in figure 7 (83). In another study by Fu-zhai, CaP was successfully formed on AZ31 alloy. The results showed that the degradation rate of the coated samples was significantly decreased. Figure 8 indicates that the CaP coating was very effective in protecting the Mg alloy from a rapid degradation (80).

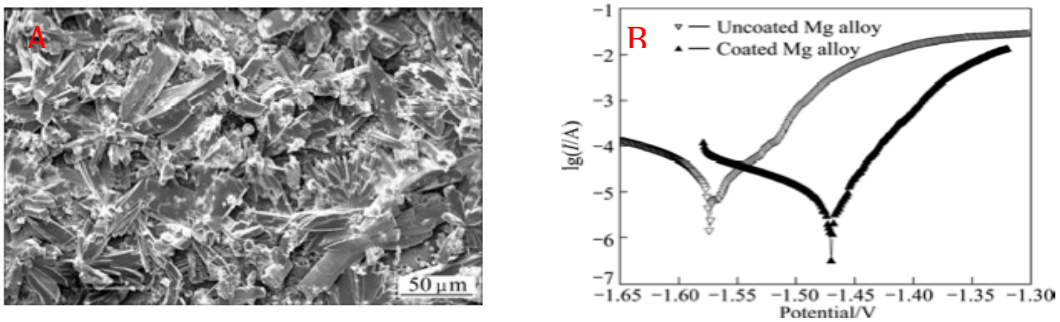

Figure 7. a) SEM surface morphology of calcium phosphate coating, b) Electrochemical polarization curves of Mg alloy samples with and without calcium phosphate coating

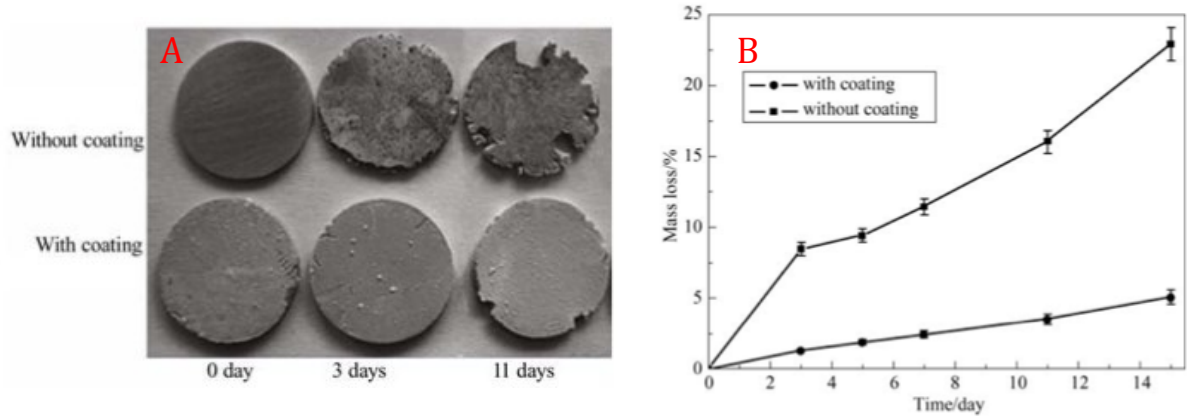

Figure 8. a) Comparison of the degradation behavior of AZ31 samples with and without coating after different immersion time of 0, 3 and 11 days during the degradation process. b) Variation of the mass loss percentage of samples with coating and control samples without coating with immersion time in the NaCl aqueous solution (3 wt.%)

2.13 Anodization Treatment

The anodization treatment, is an electrochemical treatment that changes the surface chemistry of the metal by oxidation, producing a stable anodic oxide layer. A thin layer at the metal-oxide interface, followed by a less dense porous oxide layer, characterizes the structure of the oxide film [69]. The anodizing behavior is strongly influenced by the voltage, current, temperature, and concentration of electrolyte [68, 69]. Anodization can increase the film thickness, corrosion resistance, hardness, resistance to wear, and even can influence addition properties. Koji Murakami et. al. conducted a study on corrosion protection of pure magnesium, AZ31, and AZ91 influenced by anodization treatments. The results showed a better corrosion behavior that could be due to sacrificial effect of the anodized layers. Figures 9 and 10 depict some of the results obtained by the authors (84).

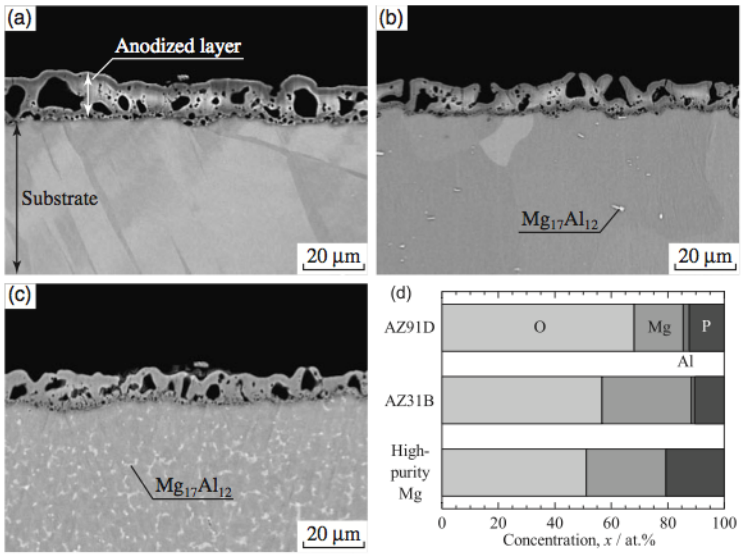

Figure 9. Cross-sectional backscattered electron images and compositions of the anodized layers (a) High-purity magnesium, (b) AZ31B, (c) AZ91D, (d), Compositions of anodized layers

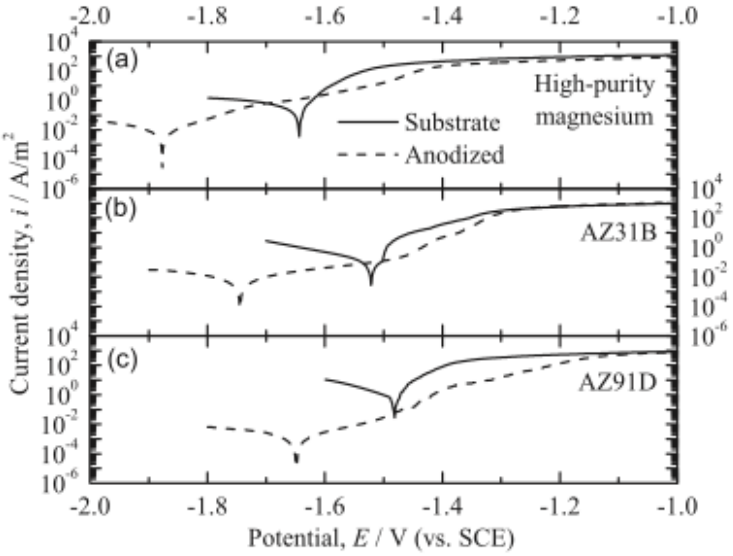

Figure 10. Anodic polarization curves of the raw and anodized surfaces obtained in 5 mass% sodium chloride solution (a) High-purity magnesium, (b) AZ31B, (c) AZ91D, Sweep rate 1 mV/s.

Apart from the above mentioned ion implantation, CaP and anodization treatments, many techniques have evolved to control and improve magnesium alloys aiming them for potential cardiovascular and orthopedic implant materials. Some of the techniques include: alkali heat treatments, physical and chemical treatment, biodegradable polymers, composites, fluoride conversion coating and even carbonate treatments (76,77).

2.14 In Vitro and In Vivo Experiments of Biodegradable Magnesium Alloys

In vitro tests are often performed for evaluation of potential effects of a material on the host organism before implantation. These experiments are simulated in a physiological environment in the lab and within the glass. In order to commence evaluating and testing a material, cytotoxicity tests should be performed. There are various *in vitro* approaches that are employed to examine biomaterials and cell behavior. The material is tested by applying direct contact and indirect contact experiments. The most common methods for biomaterial screening are cytotoxicity assays and cell proliferation. To illustrate, table 10 summarizes cell viability of different cell lines cultured in magnesium alloys extracts. Furthermore, tests *in vivo* play an important role to give understandings on the sample behavior on in-service conditions.

Table 10. Cell viability in magnesium and its alloys extracts (85) (86) (87) (88) (57) (89) (90)

Material	Cell line	Cell viability (%)
Pure Mg	L929	65.7
	NIH3T3	90.6
	MC3T3-E1	87.5
	ECV304	76.8
	VSMC	93.6
Mg - 1Ca	L929	81.8
Mg - 3Ca	L929	55
Mg - 1Zn	L929	111.8
	NIH3T3	114.1
	MC3T3-E1	112.7
	ECV304	98.9
	VSMC	110.6
Mg - 6Zn	L929	100
Mg-1Zn-Mn	L929	100
Mg-1Zn-1Ca	L929	75
Mg-2Zn-1Ca	L929	70
Mg-3Zn-1Ca	L929	72
Mg-1Si	L929	88.3
	NIH3T3	102.4
	MC3T3-E1	119
	ECV304	80.5
	VSMC	95.1
Mg-1Sr	MG63	84
Mg-2Sr	MG63	80
Mg-3Sr	MG63	68
Mg-4Sr	MG63	50

As mentioned previously, magnesium alloys are being considered as orthopedic implant biomaterials. Traditional medical procedures favor the selection of metals such as stainless steel, titanium alloys, and cobalt alloys. It has also been said that some of the orthopedic implantations are not permanent and require a second surgery once the healing process has been fulfilled. Comparing to the commonly biomaterials stated before, Mg alloys posses many outstanding features including being included to human metabolism, biocompatibility, and biodegradability (80). Biodegradable magnesium alloys are being evaluated and reported for use in bone screws, plates, and scaffolds for bone and cartilage repair (91–93). *In vitro* and *in vivo* studies have been performed and reported. Z. Li et. al. developed Mg-Ca alloys for use as biodegradable metals with bone. Cytocompatability evaluation on L-929 cells was observed as shown in figure 11. Also, Mg-Ca alloy pin was implanted *in vivo* and was gradually degraded within 90 days and new formation of bone was observed as shown on figure 12.

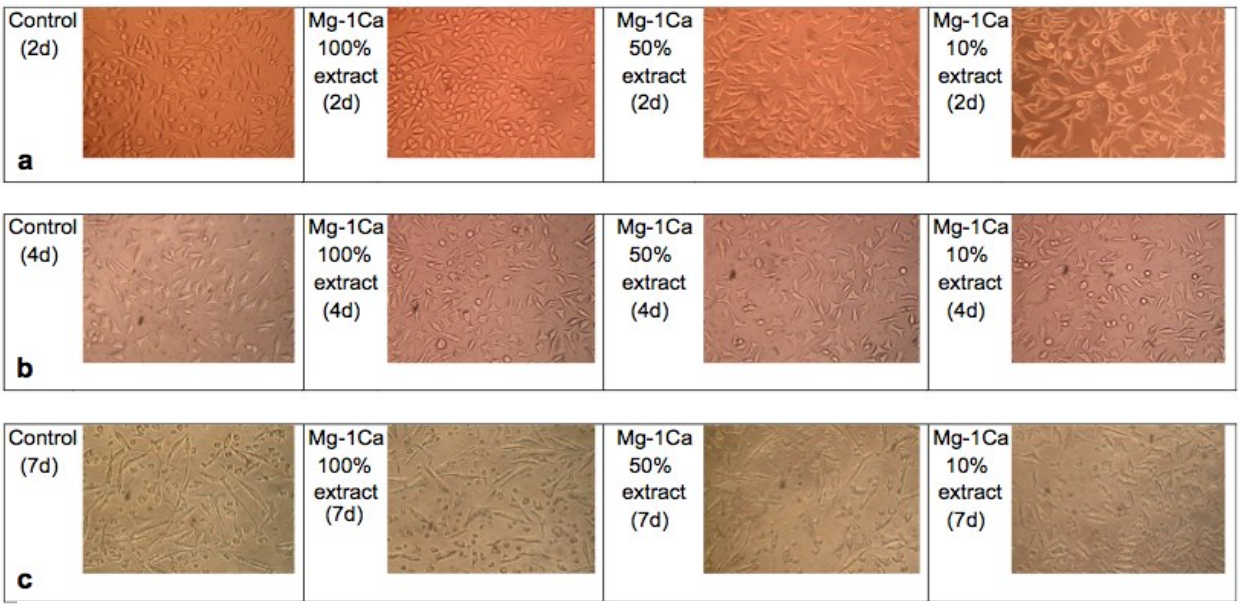

Figure 11. Optical morphologies of L-929 cells that were cultured in the control and 100%, 50%, and 10% concentration Mge1Ca alloy extraction medium for (a) 2 days, (b) 4 days and (c) 7 days [79].

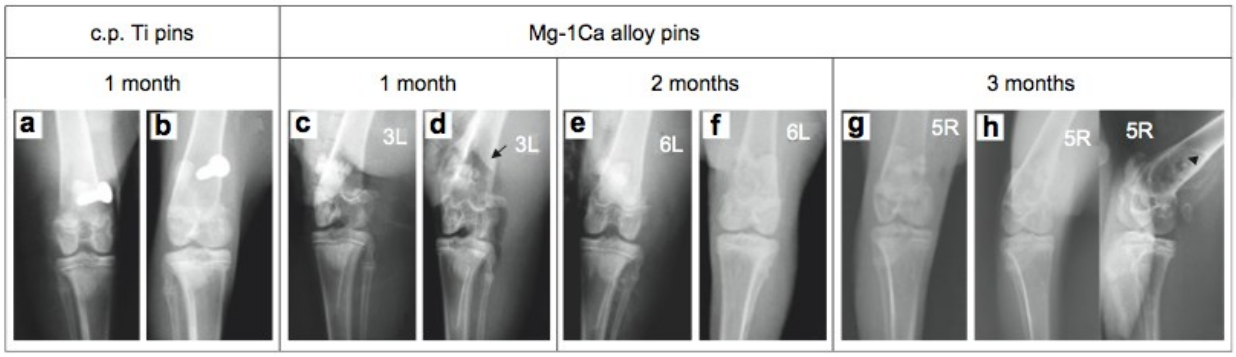

Figure 12. Femora radiographs of rabbit with implants for different periods after surgery. (a and b) c.p. Ti pin at 1 month postoperation; (c and d) Mge1Ca alloy pins at 1 month postoperation (the arrow marks the gas shadows); (e and f) Mge1Ca alloy pins at 2 months postoperation; (g and h) Mge1Ca alloy pins at 3 months postoperation (the black triangle marks the circumferential osteogenesis) [79].

F. witte et al. conducted a case study where the aim of the assessment was to investigate the degradation mechanism at the bone-implant interface of different degrading magnesium alloys in bone and to determine their effect on the surrounding bone. The corrosion layer of the magnesium alloys was in direct contact with the surrounding bone during the degradation process. The magnesium alloys used for the study were: AZ31, AZ91, WE43, and LAE442. The results demonstrated that the metallic magnesium implants degraded in the *in-vivo* experiment performed. An osteoblast response to the degrading alloys in the guinea pig femur was studied (45) . In another investigation by Erdmann et al. magnesium alloy (MgCa0.8) and stainless steel (S316L) screws were investigated and compared for their biomechanical properties. Moreover, in vivo degradation behavior of MgCa0.8 was also investigated. It was demonstrated that the MgCa0.8 magnesium alloys had good tolerability and biomechanical properties comparable with S316L in the first 2-3 weeks after implantation. Furthermore, MgCa0.8 gradually degraded during the in vivo implantation. Further studies were suggested in order to investigate whether the reduce power holding strength is sufficient for secure internal fracture fixation (94). The next in vivo study by Kraus et al. investigated the bone and tissue response to degrading magnesium pin implants in rats. The magnesium alloys selected for this

investigation were ZX50 and WZ21. The difference of the alloys was in their degradation rates. The ZX50 alloys had higher corrosion rate compared to WZ21alloys. Implants made of WZ21 maintained their integrity for 4 weeks and corroded subsequently ~0.5% volume loss per day compared to ZX50 which had a degradation rate of ~1.2% daily volume loss. It was observed that WZ21 alloys generated enhanced bone neoformation around the implant. Bone recovered after complete degradation of the magnesium implant (95) . Chen et al. investigated composite coatings with hydroxyapatite (HA), octa-calcium phosphate (OCP) in electrochemical deposition (ED) layers and MgO, $Mg_3(PO_4)_2$ in microarc oxidation (MAO) were prepared o MgZnCa alloy to improve corrosion resistance and bone response. Materials and coated samples were implanted in the femur shaft of rabbits to observe in vivo degradation behavior during 50 weeks. The results concluded that the coated samples degradation rate was slower than the substrates. The composite coatings prevented the fast degradation of the magnesium alloys and demonstrated good bioactivity in the pathological examination. New formed bone tissue was found around the coated alloys (96). Several more Mg-based alloys have been investigated, including Mg-RE (Di Mario et al. 2003; Peeters et al. 2005; Witte et al. 2005; Waksman et al. 2006; Hanzi et al. 2009), Mg-Al (Heublein et al. 2003; Levesque et al. 2003; Xin et al. 2007) and Mg-Ca (Zhang and Yang 2008; Li et al. 2008)

CHAPTER III

EXPERIMENTAL

3.1 Sample Preparation

The specimens were made out of AZ31B (3.0 wt. % Al, 1.0 wt. % Zn, Mg balance), AZ91E (9.0 wt. % Al, 1.0 wt. % Zn, Mg balance) and ZK60A (6.0 wt. % Zn, 0.45 wt. % Zr, Mg balance) magnesium alloys. The alloys were received in the form of rods and were cut using a high speed saw into small disks with following dimensions: 19 mm diameter and 4 mm thickness. Each sample was mechanically ground up to 1200-grit SiC paper, ultrasonically cleaned and degreased using ethanol and then air-dried. Magnesium samples were sent out to different companies for treatments and coatings. Alloys were anodized by Electrobright® (Macungie, PA, USA). Hydroxyapatite coating was plasma-sprayed by APS® Materials. Butvar® B-98, a polymeric material was used to dip-coat magnesium alloys as a protective coating.

3.2 Material Characterization

The surface morphology of the specimens was analyzed by scanning electron microscopy (Sigma VP Carl Zeiss, Germany). The element distribution on the surface of the alloys was investigated by energy dispersive spectroscopy (EDS) (Carl Zeiss, Germany). The surface roughness was analyzed (20 X 20 μm area) by atomic force microscopy (Nanoscope IV MultiMode in air, Digital Instruments, Santa Barbara, CA, USA). The contact angle, surface free energy and work of adhesion were investigated by applying the sessile drop method using the

Kyowa angle meter (DM-CE1 Japan).

3.3 Corrosion Experiments

Corrosion studies were evaluated by electrochemical tests in phosphate buffer saline (pH 7.4) at 37 °C in a humidified atmosphere having 5% CO_2 (Sigma Aldrich) following standards ASTM: G102-89 (97), ASTM: G3-89 (98) and ASTM: G31-72 (99). Electrochemical tests were carried out using a classical three electrode cell with a graphite bar as the counter electrode, saturated calomel electrode SCE (+0.242 V vs SHE) as the reference electrode and magnesium alloys as the working electrodes using a GAMRY potentiostat-reference 600. The potentiodynamic polarization curves were acquired at a constant voltage scan rate of 1.0 mV/s. For the electrochemical impedance spectroscopy (EIS) measurements, the scan frequency ranged from 100 kHz to 10 mHz, with a perturbation amplitude of 10 mV.

For the immersion experiment, three specimens with a total surface area of ~8 cm^2 were immersed in phosphate buffer saline for 168 hours. The solution volume was adjusted according to solution volume/surface area (SV/SA) ratio 66.7. The volume of the evolved hydrogen was measured every 24 hours. The pH values of the solutions were also recorded every day. The sample weight was measured before and after the immersion procedure. After the immersion test, the samples were removed from the electrolyte and cleaned in 20 ml of chromic acid solution to remove corrosion products from the material. The samples were rinsed afterwards with deionized water and then air dried. The weight of the dried specimens was measured and the corrosion rate was calculated.

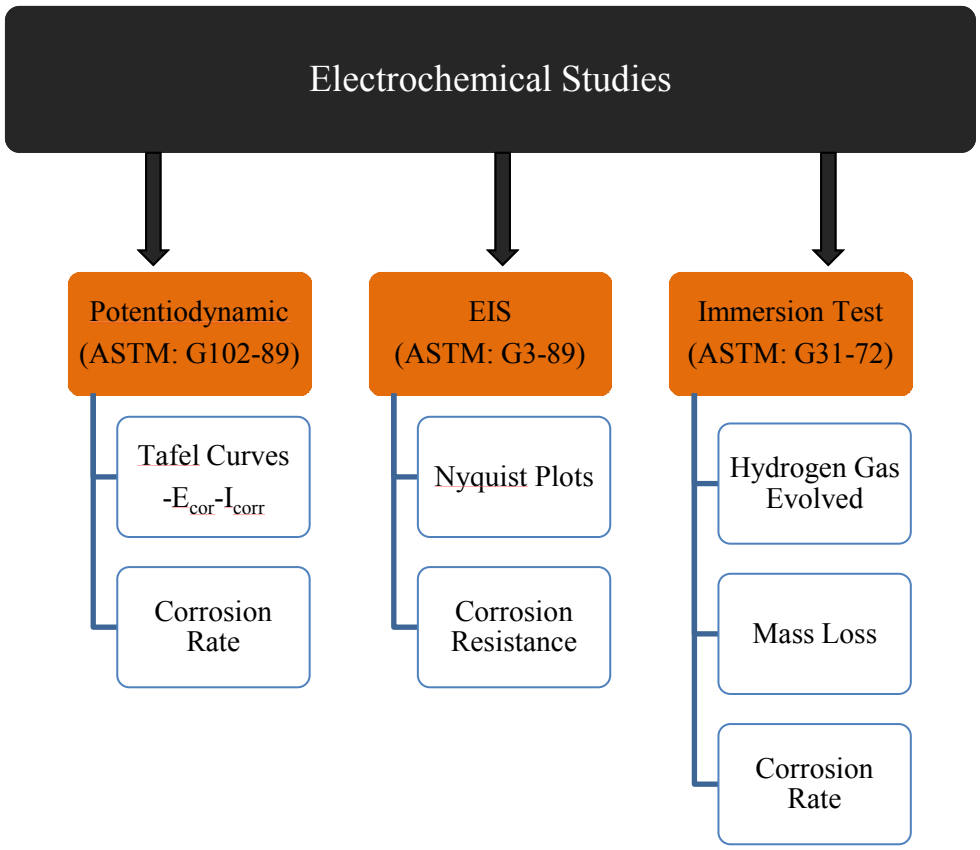

Figure 13. Classification of techniques used for corrosion studies of magnesium alloys

3.4 Indirect Cell Viability

The effect of metal ions released from magnesium alloys was assessed by using MTS assay (G3580, Celltiter 96® AQ_{ueous} One Solution Reagent, Promega Corporation) to determine the percentage of viable MC3T3-E1 (ATCC® CRL-2A593™) cells in extract solutions exposed to different concentrations. The cells were cultured in MEM alpha modification media (Thermo Scientific™ HyClone™ SH3026501), 10% fetal bovine serum, FBS, (Thermo Scientific™ HyClone™ SH3008803HI), and Penicillin-Streptomycin (Sigma-Alridch P4333) at 37 °C in a humidified atmosphere having 5% CO_2. The AZ31B, AZ91E, and ZK60 mg alloys were immersed in MEM alpha modification media for 21 days and the media was changed and collected after every 3 days. Cells were counted (2 x 10^4 cells) using hemocytometer and plated

in 96-well plates with 200 µl of culture media per well. The cells were incubated for 24 hours to allow attachment. After the 24-hour incubation, the culture media was replaced with culture media exposed to magnesium alloys (100% concentrations). Pure culture media with cells was used as control. The cells were incubated for 24 hours. After the 24 hours, 100 µl of media were removed from the 96-well plates, the remaining 100 µl media was treated with 20 µl/well with Celltiter 96® AQ_{ueous} One Solution Reagent. The 96-well plates were placed in the incubator for 4 hours. Immediately after the incubation period, the optical density measurements were recorded using ELx800™ BioTek absorbance microplate reader controlled by Gen5 software with a 490 nm absorbance excitation filter. Statistical analysis was executed to evaluate the difference in cell viability by the analysis of variance. One-way ANOVA was used to determine the significance of pairwise comparisons. Differences were considered statistically significant ($P < 0.05$) and not significant ($P > 0.05$). P values can be found in the appendix section for reference.

3.5 Direct Cell Viability

The MC3T3-E1 (ATCC® CRL-2593™) cell line was cultured in MEM alpha modification media (Thermo Scientific™ HyClone™ SH3026501), 10% fetal bovine serum, FBS, (Thermo Scientific™ HyClone™ SH3008803HI), 100 U ml^{-1} penicillin and 100 µg ml^{-1} streptomycin (Sigma-Alridch P4333) at a temperature of 37 °C in a humidified atmosphere of 5% CO_2. Cells were seeded onto specimen surfaces at a cell density of 7 x 10^4 and each well containing 250 µl of culture media to completely cover the specimen surfaces. After 24 hour incubation, cell staining was performed using the commercially available NucBlue® Live Cell Stain Ready Probes™ (R37605, Invitrogen Inc.) to stain the cell nuclei. Fluorescent images of cells were captured using the EVOS® FL Cell Imaging System (AMF4300, Invitrogen Inc.).

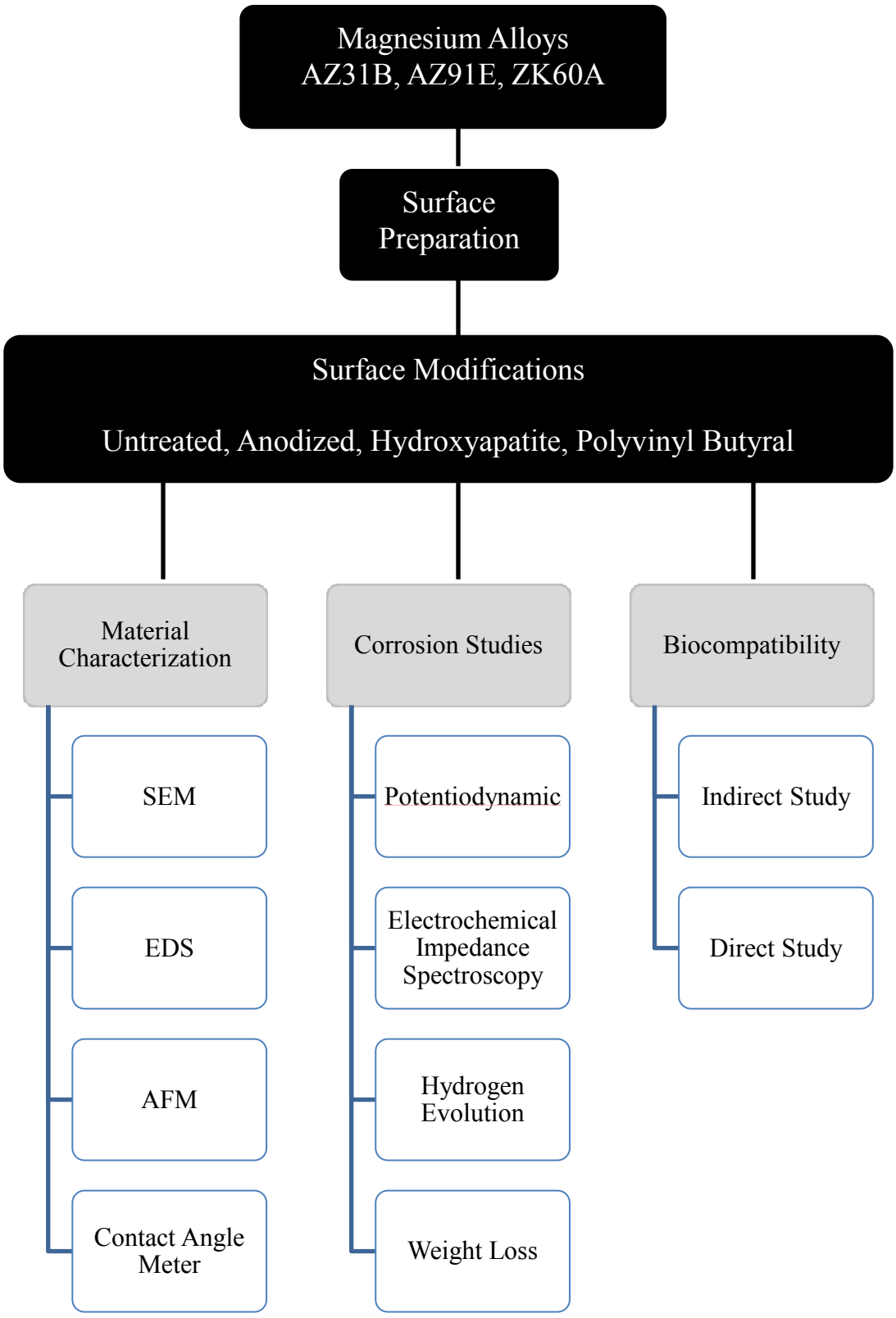

Figure 14. Schematic diagram of research summary

CHAPTER IV

RESULTS AND DISCUSSION

4.1 Surface Morphology and Chemistry

Surface engineering assists in the modification of the material without distressing bulk properties. Surface modifications can deliver properties such as corrosion resistance and biocompatibility of metallic biomedical implants (76). Moreover, surface coatings can be chosen as a strategy to control the corrosion behavior of magnesium as well.

The surface of biomaterials dictates the interactions between biomaterial and biological environment such as tissues, cells, blood and proteins. Biological responses depend on biomaterials' physiochemical properties such as surface topography, chemistry and wettability. Figure 15 shows the surface morphologies and elemental surface distribution information of magnesium alloys with respective treatments and coatings. Different surface morphologies were observed before and after the anodization treatment, plasma sprayed hydroxyapatite coating, and PVB dipped coating. Figures 15a, 16a and 17a exhibit the untreated alloys with typical grinding marks. In the other hand, figure 15b, 16b and 17b show anodized magnesium alloys with micro-textured morphologies. The anodization treatment produced an oxide film, which is intended to improve the corrosion resistance (100). Anodization treatments by Tu et al. formed passive film on samples influenced the corrosion resistance displaying an excellent anti corrosion performance (101). The anodized morphologies demonstrate some micro-texture patterns throughout the treated surface for AZ31 and AZ91; however ZK60 morphology shows the grain

boundaries of the alloy. Furthermore, the EDS demonstrated the surface composition for each of the alloys. The increased oxygen content was observed for anodized alloys when compared to untreated alloys. High oxygen concentration indicates that the anodic film is made up of magnesium oxides and hydroxides (102). Salman et al. demonstrated that passive film was made of Mg(OH) and MgO for anodized materials (102).

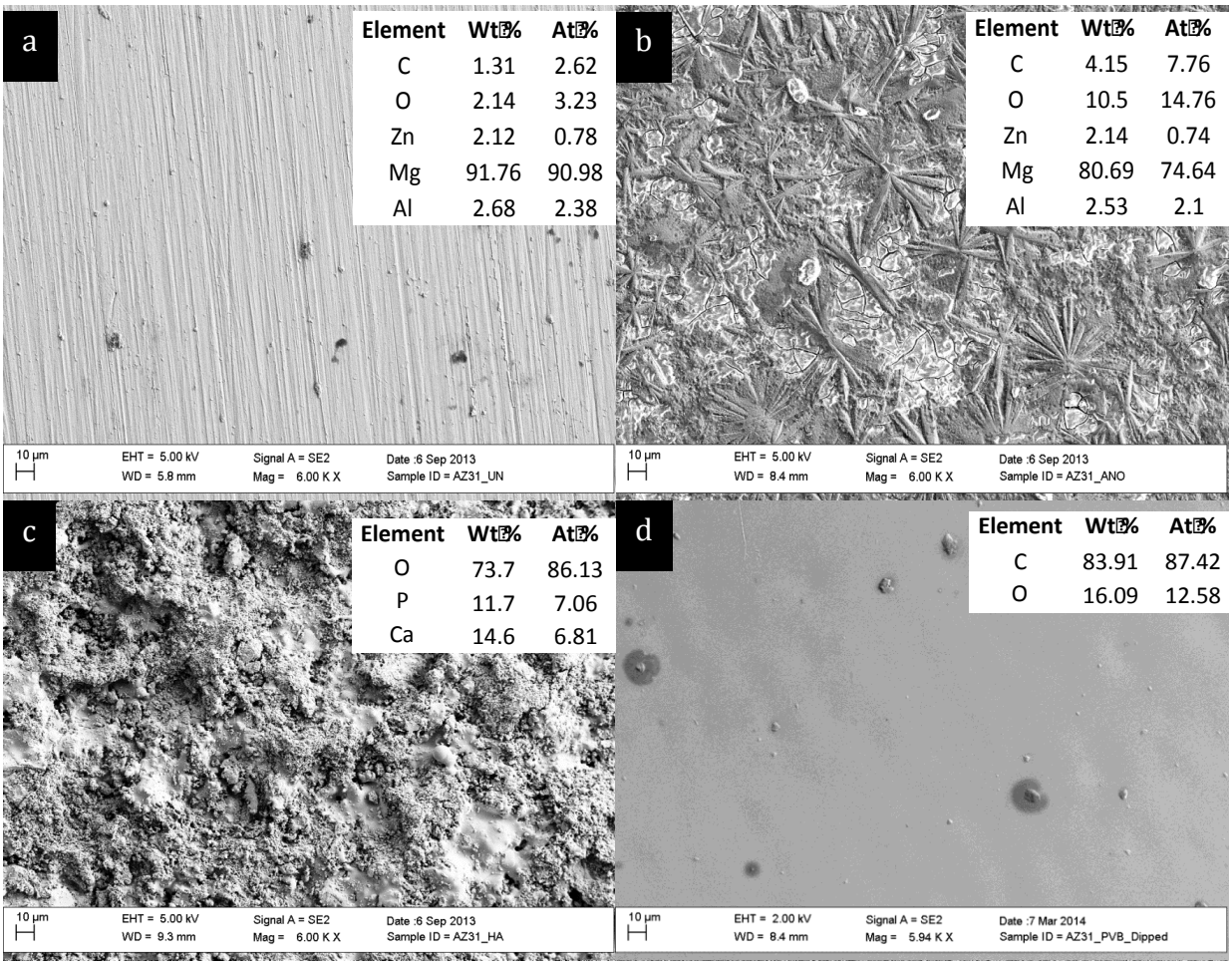

Figure 15. SEM images of AZ31B magnesium: a) Untreated b) Anodized, c) Hydroxyapatite coating, d) PVB coating

The second surface treatment studied was a calcium phosphate ceramic material. Calcium phosphate bio-ceramics have been used in medicine for about 30 years in areas such as: dental applications, augmentation, orthopedics, maxillofacial procedures, and otolaryngology (103). Calcium and phosphorus are the main elements in bone tissues, especially

osteoconductive minerals such as hydroxyapatites (29). The biocompatibility of HA has been demonstrated to be a significant impact in many studies. Results in *in-vivo* implantations have proved no local systemic toxicity, no inflammation symptoms, and no foreign responses (104–106). Furthermore, hydroxyapatite mineral materials have been used to rebuild and construct new bones and promote osteointegration on biomedical implants (29,107). The theoretical composition of pure hydroxyapatite is 39.68% Ca, 18.45wt% P, delivering a Ca/P weight ratio of 2.151 and a molar ratio of 1.6667 (107).

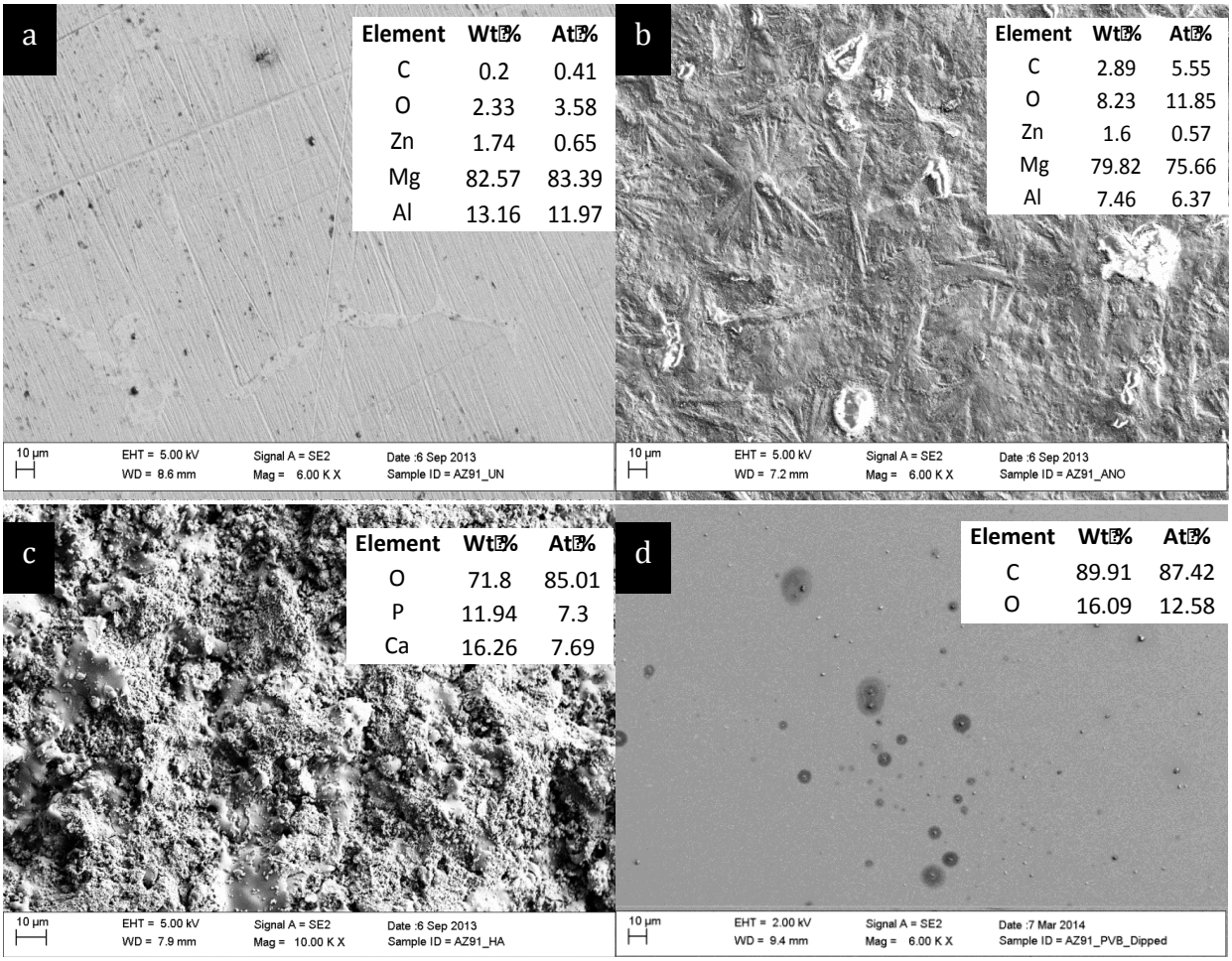

Figure 16. SEM images of AZ91B magnesium: a) Untreated b) Anodized, c) Hydroxyapatite coating, d) PVB coating

Figures 15c, 16c, and 17c, present the SEM morphologies of characteristic microstructure plasma sprayed hydroxyapatite coating on the magnesium alloy substrates. The degree of particle melt in plasma spray process depends upon many factors such as heat content of plasma to which they are exposed, location of particles in plasma, the velocity and size of particles (108). The overall coating is massive with high porosity features. The EDS information for AZ31-HA and AZ91-HA showed that the Ca/P weight and molar ratio were below than the theoretical composition ratios implying that the coatings were Ca-deficient hydroxyapatite. The EDS data for ZK60-HA showed that weight and molar ratios were in good agreement with theoretical ratios.

The third type of surface modification applied to magnesium alloy surfaces was made out of a polymer. Polymers are long-chain molecules of small repeating units. Polymeric materials can be either natural (DNA, proteins, cellulose, and starch), or synthetic (PVC, PE, PP, PMMA, etc.). They have drawn attention in the biomedical field due to the ease of manufacture to be attained in different forms as fibers, textiles, rods, and viscous liquids (109).

Biodegradable polymers for clinical applications comprise a promising alternative in order to improve the corrosion resistance and biocompatibility of magnesium based alloys. Dip-coatings from organic and inorganic polymers have obtained significant attention for the enhancement of surface properties on magnesium-based materials. The dip coating method involves in basically dipping the material in a certain solution for a specific time to allow the wetting of the surface, then withdrawing the material and letting dry in the desired environment. Several studies reported coatings using polymeric materials. Li et al. used polylactic-co-glycolic acid (PLGA) for the production of polymer coatings. Corrosion and biocompatibility studies were carried out to study coated samples. Results revealed an improvement in corrosion

resistance and enhanced cell attachment (110). Chen et al. presented research in the experimental work with polymeric materials. Polycaprolactone (PCL) and polylactic acid (PLA) coatings were successfully prepared on the surface of pure magnesium. Polarization and immersion corrosion test were performed in SBF to characterize corrosion rate and corrosion resistance (111). There are many more studies that are suggesting the use of biodegradable polymers for the production of protective coatings on magnesium alloys (112–115).

In this investigation polyvinyl butyral (PVB) polymer was selected as biodegradable polymer coating. Figures 15d, 16d, and 17d, show SEM images of magnesium samples treated with 14% PVB dissolved in ethanol. The surface morphologies demonstrated a smooth, plain non-porous coating when viewed under scanning electron microscope.

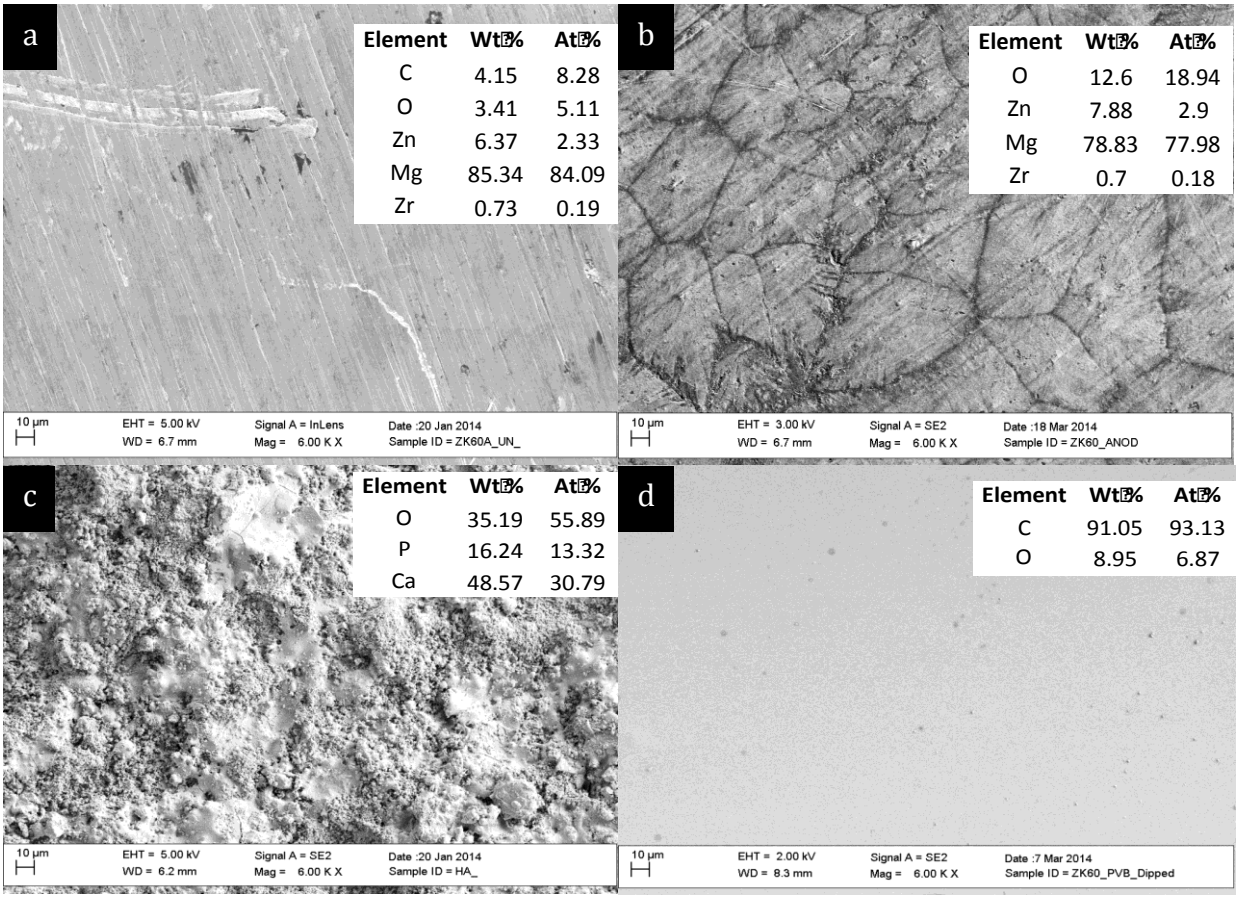

Figure 17. SEM images of ZK60A magnesium: a) Untreated b) Anodized, c) Hydroxyapatite coating, d) PVB coating

4.2 Surface Roughness

Atomic force microscopy (AFM) is a technique to obtain images at extremely high resolution (nanometer range). The basic principle of this technique is that a probe is maintained in closed contact with the sample surface by a feedback mechanism as it scans over the surface, and the movement of the probe to stay at the same probe-sample distance is taken to be the sample topography. Usually, scans are obtained using a silicon or silicon carbide probe with a sharp integrated tip. The vertical bending (deflection) of the cantilever due to the forces acting on the tip is detected by a laser focused on the back of the cantilever (116). The laser is reflected by the cantilever onto a distant photodetector as seen in figure 18.

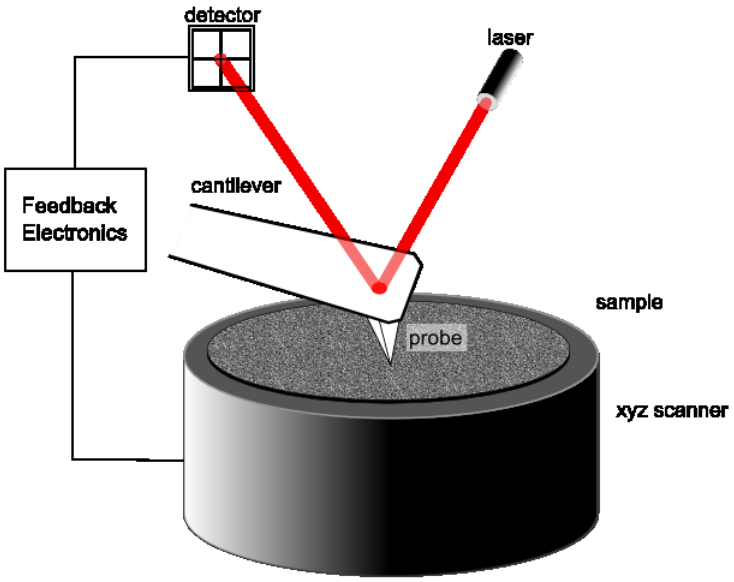

Figure 18. Schematic of AFM operation (116)

Some of the most common modes used are called tapping mode (TM-AFM), and noncontact mode (NC-AFM). Tapping and noncontact are also known as dynamic modes because the cantilever is oscillated when operating. The difference between tapping and noncontact modes is that during the tapping mode, the tip of the probe actually touches the sample, and moves completely away from the sample in oscillation cycle. In noncontact mode,

the cantilever stays close to the sample all the time, and has a much smaller oscillation amplitude; the figure 18 representing the schematic of AFM operation (116).

The surface roughness of magnesium alloys has been studied. AFM scans were recorded on a 20 μm by 20 μm area for each specimen. Each sample was viewed at three different locations on the surface by using the tapping mode. The roughness reading was taken at each of the three locations using the roughness analysis feature on the AFM, thus allowing an average roughness reading to be taken for each specimen. The average roughness is illustrating the comparison in topography between all the specimens.

Figures 19, 20, and 21 show the surface topography of magnesium alloys. The average surface roughness (R_a), root mean squared roughness and standard deviation were calculated and recorded for all untreated, anodized, HA coated, and PVB coated alloys as shown in table 10. The results for the AZ31B, AZ91E and ZK60A untreated alloys did not have any significant change in the surface roughness, since the materials where grounded down with same grit size (1200) using SiC abrasive paper. However, R_a values increased for the anodized alloys. PVB coated alloys showed the lowest surface roughness, while the highest roughness was measured for HA coated specimens.

The surface of an implant or scaffold for bone tissue engineering programs should replicate, as close as possible the natural bone architecture. This includes possessing an ordered and adequate network of interconnected pore distribution in order to allow neobone tissue ingrowth, blood vessel invasion and nutrient delivery, while allowing outward flow of biological waste (117).

In order to facilitate favorable conditions for protein and subsequently cell (tissue) adhesion, certain surface attributes must exist. Therefore, the surface topography of the

magnesium alloys must be designed with osseointergration in mind. Several studies have shown implant success does not only depend on the physiochemical properties such as interfacial free energy, but also on its roughness (118). Interaction between tissues and implants surfaces is typically controlled by the finishing and texture of the implant material. Rough surfaces exhibit more surface area and reveal a better bone integration via the osseointegration process. Micro-textured surface characteristics allow in growth of the tissues (119,120). In *Methods to Characterize the Surface Roughness of Metallic Implants* (121), Ungersbock and Rahn concluded that the roughness of the surface of implants is one of the key factors that plays a dominant role in the soft tissue reaction at the interface between natural tissue and biomaterials. In deep, the degree of roughness mimics or resembles the porous surface of natural bone tissue, thus, allowing the infiltration of important proteins to adhere and commence the process of osseointergration.

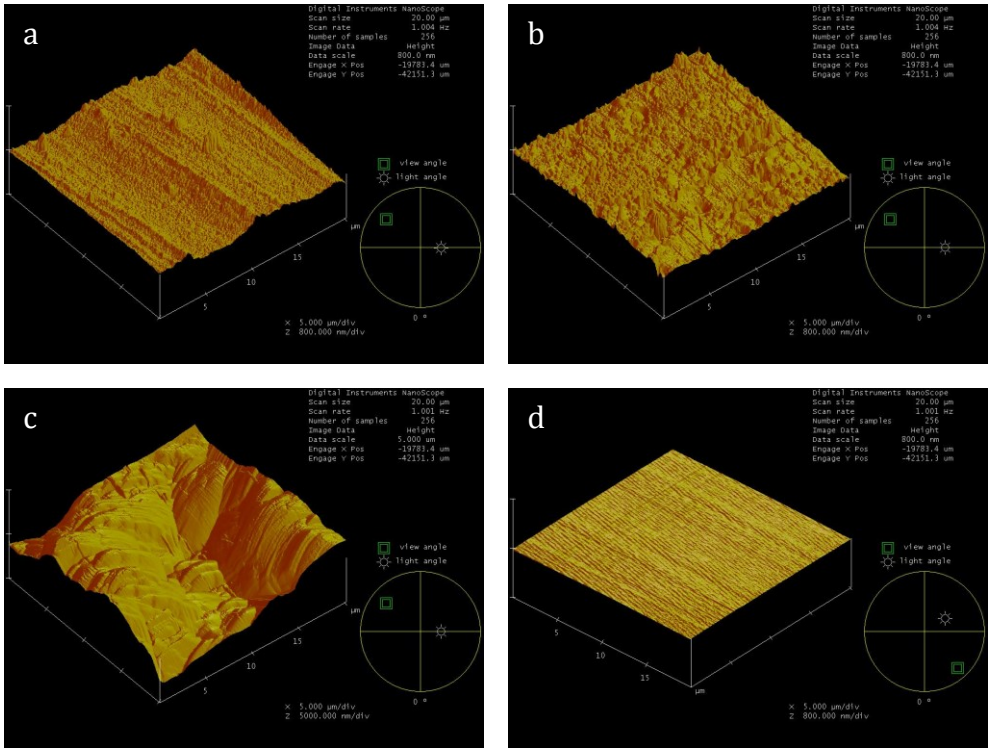

Figure 19. AFM images of AZ31B magnesium: a) Untreated b) Anodized, c) Hydroxyapatite coating, d) PVB coating

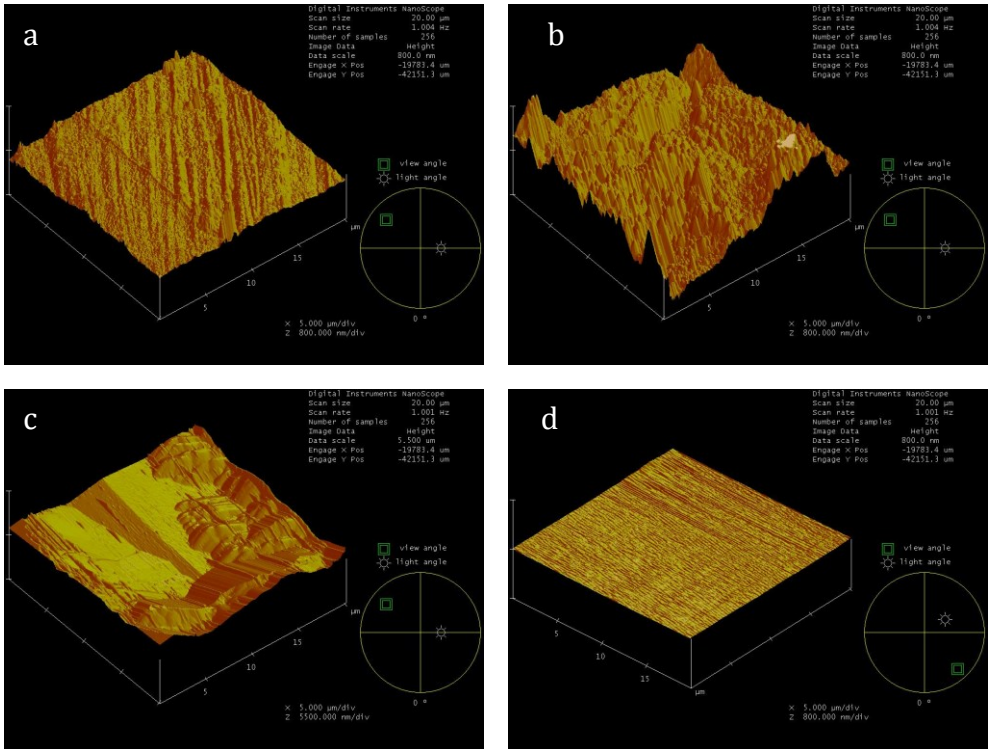

Figure 20. AFM images of AZ91E magnesium: a) Untreated b) Anodized, c) Hydroxyapatite coating, d) PVB coating

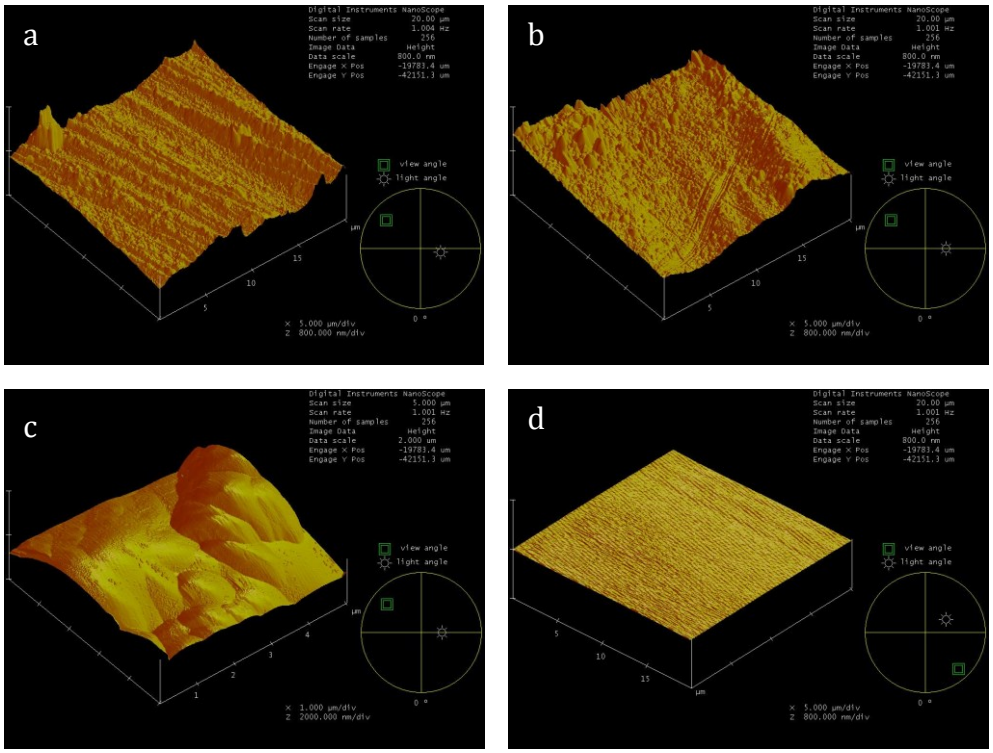

Figure 21. AFM images of ZK60A magnesium: a) Untreated b) Anodized, c) Hydroxyapatite coating, d) PVB coating

Figures 22, 23, and 24 depict the average roughness and root mean squared roughness obtained from AFM scan readings.

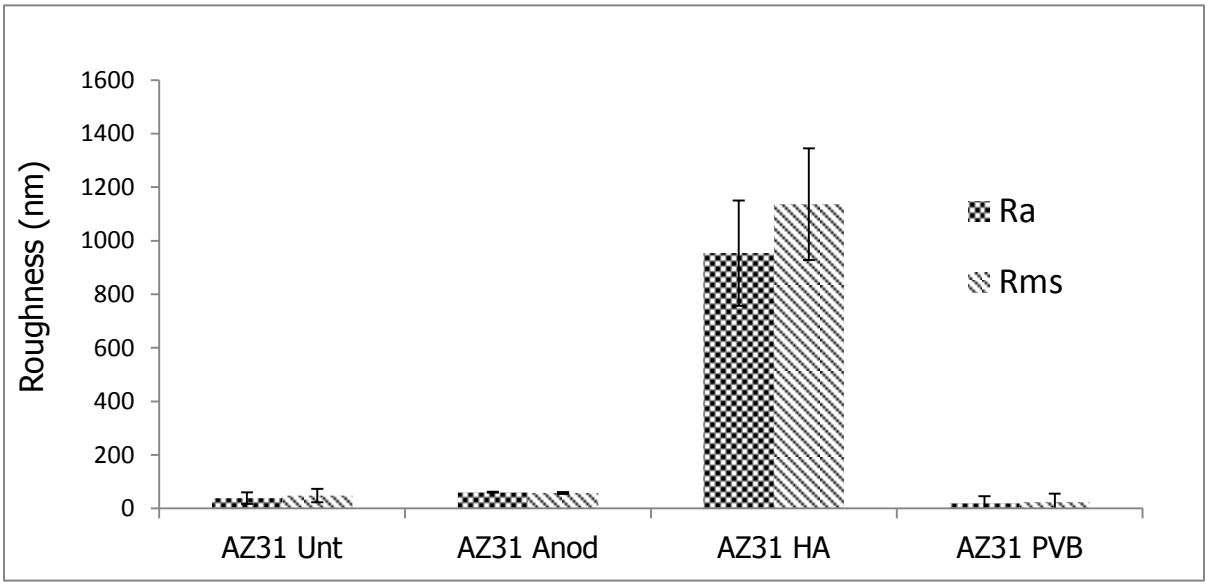

Figure 22. AFM data of AZ31 samples

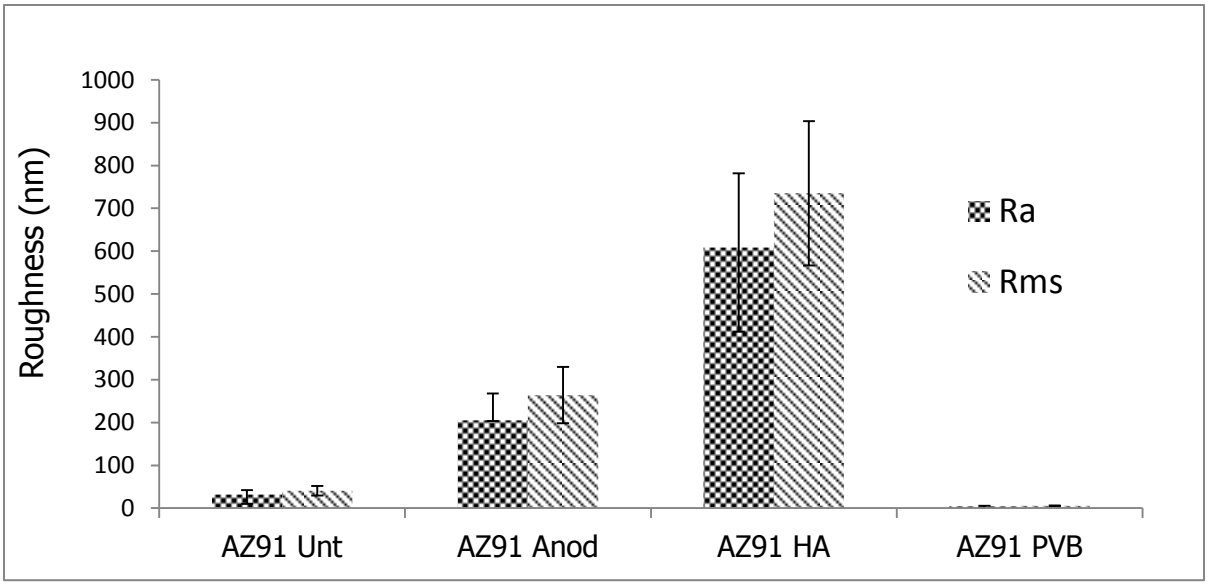

Figure 23. AFM data of AZ91 samples

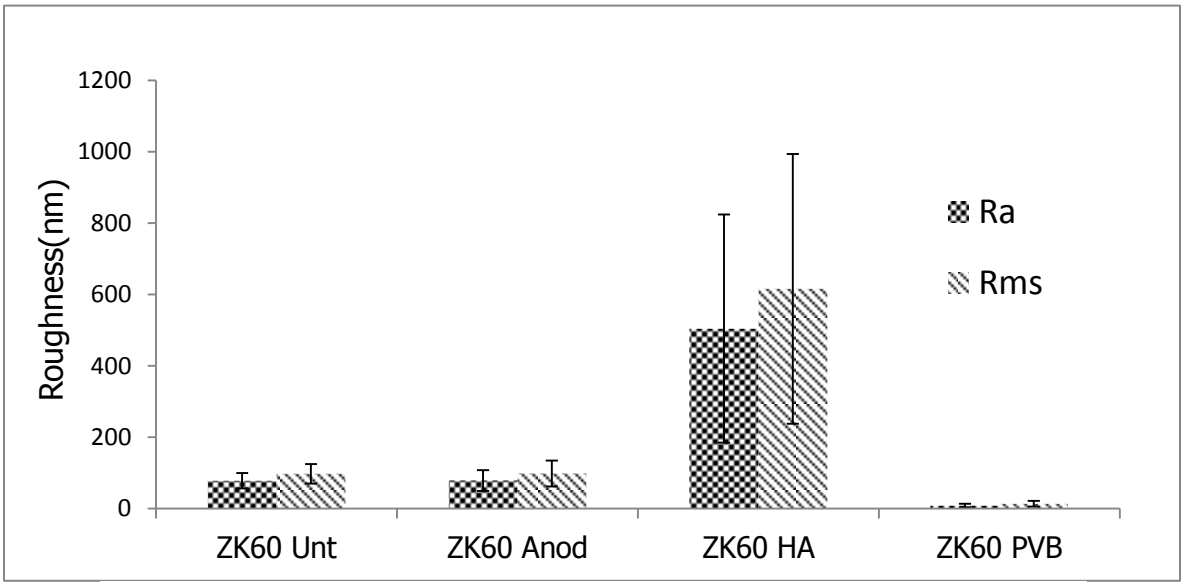

Figure 24. AFM data of ZK60 samples

Table 11. Atomic force microscopy data *(mean ± std)*

Magnesium Alloys	Root mean square Rq (nm)	Average roughness Ra (nm)	Average max Height Rpm (nm)	Average max depth Rvm (nm)
AZ31 Untreated	48.0 ± 25	38.4 ± 21	85.7 ± 28	-78.4 ± 26
AZ31 Anodized	57.9 ± 3	43.2 ± 2	85.2 ± 8	-71.9 ± 1
AZ31 HA	1136.8 ± 208	953.8 ± 196	1709.3 ± 430	-1012.3 ± 1887
AZ31 PVB	24.1 ± 30	20.1 ± 25	24.9 ± 31	-52.5 ± 78
AZ91 Untreated	40.7 ± 11	31.4 ± 10	57.0 ± 14	-45.3 ± 11
AZ91 Anodized	263.7 ± 65	204.8 ± 62	347.4 ± 43	-294.7 ± 68
AZ91 HA	735.1 ± 168	608.1 ± 173	637.4 ± 552	-979.9 ± 251
AZ91 PVB	5.2 ± 1	4.1 ±1	6.7 ±2	-6.3 ± 29
ZK60 Untreated	97.8 ± 27	78.3 ± 21	122.1 ± 38	-108.9 ±
ZK60 Anodized	98.8 ± 36	78.9 ± 29	130.3 ± 52	-111.5 ± 41
ZK60 HA	616.1 ±377	504.6 ± 319	1357.9 ± 1124	622.2 ± 833
ZK60 PVB	13.4 ± 8	8.8 ± 4	22.8 ± 20	-15.1 ± 8

4.3 Wettability Studies

Contact angle is a quantitative measure of the wetting of a solid by a liquid. It is described geometrically as the angle formed by a liquid at the three-phase boundary where a liquid, gas and solid intersect (122). Surface analysis or wettability studies include the measurement of contact angles as the primary data. Angles lower than (<90 degrees) are related to high wettability or hydrophilic behavior, while large angles over (>90 degrees) correspond to low wettability or hydrophobic behavior (123).

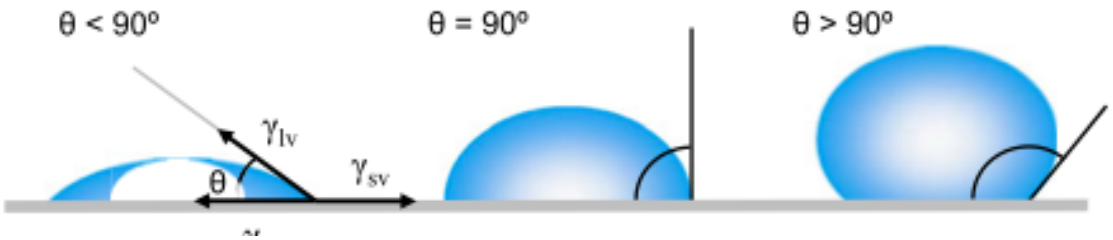

Figure 25. Illustration of contact angles formed by sessile liquid drops on a smooth homogenous solid surface (123)

There exists a fundamental science behind wetting and contact angle phenomena. Also, there are different techniques employed to determine contact angles. Most of the techniques can be categorized in two groups: the direct optical method and the indirect force method. In this investigation, the wettability of samples was determined employing the direct optical method.

The contact angles on samples were analyzed using a Kyowa contact angle meter model DM-CE1 (figure 26). The sessile drop method was adopted by selecting three different solvent probes: mildly polar (Deionized water); neutral (ethylene glycol) and highly polar (diiodomethane). Ten readings were performed per solvent on three of each untreated and treated alloy at locations separated by sufficient spacing to avoid potential influences from previous droplets. Figure 25 shows contact angles formed by a liquid droplet resting on a solid substrate (124).

Figure 26. Kyowa contact angle meter, DM-CE1

Contact angle measurement, first stated in qualitative form by Thomas Young in 1805 (125). This method remains the most accurate technique for determining the interaction between liquid (L) and solid (S). The angle between the solid surface and the liquid droplet, is denoted as equilibrium contact angle. According to the Young-Dupre equation the contact angle (θ) can be represented as (123):

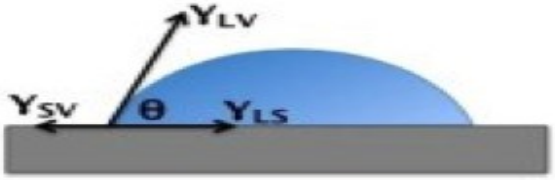

$$\gamma_{lv}cos\theta = \gamma_{sv} - \gamma_{sl} \quad (4)$$

Figure 27. Schematic representation of interfacial forces and contact angle

where, γ_{sv} is solid-vapor, γ_{sl} is the solid-liquid, and γ_{lv} is liquid vapor interfacial tensions. θ is the cotact angle.

FAMAS analysis software was utilized to calculate the surface free energy, interfacial free energy, and work of adhesion of samples employing two theories: Acid-Base interaction (table 13 and 14) and Kitazaki-Hata (table 15 and 16). The SFE can be calculated using:

$$\gamma^{total} = \gamma^{d} + \gamma^{p} + \gamma^{h} \tag{5}$$

Where, γ^{total} is the total surface free energy; γ^{d} is the surface free energy dispersion component; γ^{p} is the surface free energy polar component; and γ^{h} is the surface free energy hydrogen bond component. Moreover, the following parameters make the energy balanced equation (123,126,127) :

$$\gamma_i(1 + \cos\theta_i) = 2\left(\sqrt{\gamma_i^d \gamma_s^d} + \sqrt{\gamma_i^+ \gamma_s^-} + \sqrt{\gamma_i^+ \gamma_s^-}\right) \tag{6}$$

where,

$$\gamma_i = \gamma_i^d + 2\left(\sqrt{\gamma_i^+ \gamma_i^-}\right) \tag{7}$$

and,

$$\gamma_s = \gamma_s^d + 2\left(\sqrt{\gamma_s^+ \gamma_s^-}\right) \tag{8}$$

Table 12. Surface free energy parameter calculations

Testing drop	**Testing surface**
θ_i Contact angle between solid and liquid	γ_s Surface tension of solid sample
γ_i Surface tension of drop	γ_s^d Dispersion portion of surface tension
γ_i^d Dispersion portion of surface tension	γ_s^+ Surface tension contribution by acid
γ_i^+surface tension contribution by acid	γ_s^- surface tension contribution by base
γ_s^- surface tension contribution by base	

The interactions between biomaterials and biological environment such as tissues, cells, blood, proteins take place on the bare surface. Biological responses depend mainly on the surface properties such as surface charge, surface chemistry, roughness, wettability and surface energy (75,128). The wettability (contact angle, surface free energy) plays an important role on the biocompatibility of the implant materials. It has been reported that wettability has a significant influence on cellular interactions with biomaterials (129). Cell adhesion and cell spreading are important parameters for implant devices. For example, for biological active materials, tissue generation is conditioned by the cell adhesion and proliferation on the implant surface (118), whereas inert materials are independent of cell activity at the surface. Contact angle measurements deliver information on the wettability properties of a biomaterial, and wettability can influence protein absorption and cell activity. It has been proven that materials with moderate hydrophilic surfaces tend to enhance cell proliferation and biocompatibility as compared to highly hydrophilic surfaces (130–134).

In this experimental wettability analysis, the water contact angle of untreated, anodized, HA coated and PVB coated ranged between 50° - 100°. Contact angle increased (hydrophobic behavior) with the three liquid probes for the anodized alloys. Contact angles behaved hydrophobic to AZ31 and AZ91 HA coated samples. However, it was observed that droplet on ZK60 HA coated sample was completely absorbed. Contact angle measurements for PVB coated samples did not show a significant change; with values very close to the ones of untreated samples. Surface free energy is lower for the anodized alloys, AZ31-HA, and AZ91-HA when compared with untreated alloys. Images of water droplet on experimental specimens are represented in figure 28. Tables 12-15 and figures 29-31 summarize the results of contact angle, work of adhesion and surface free energy measurements.

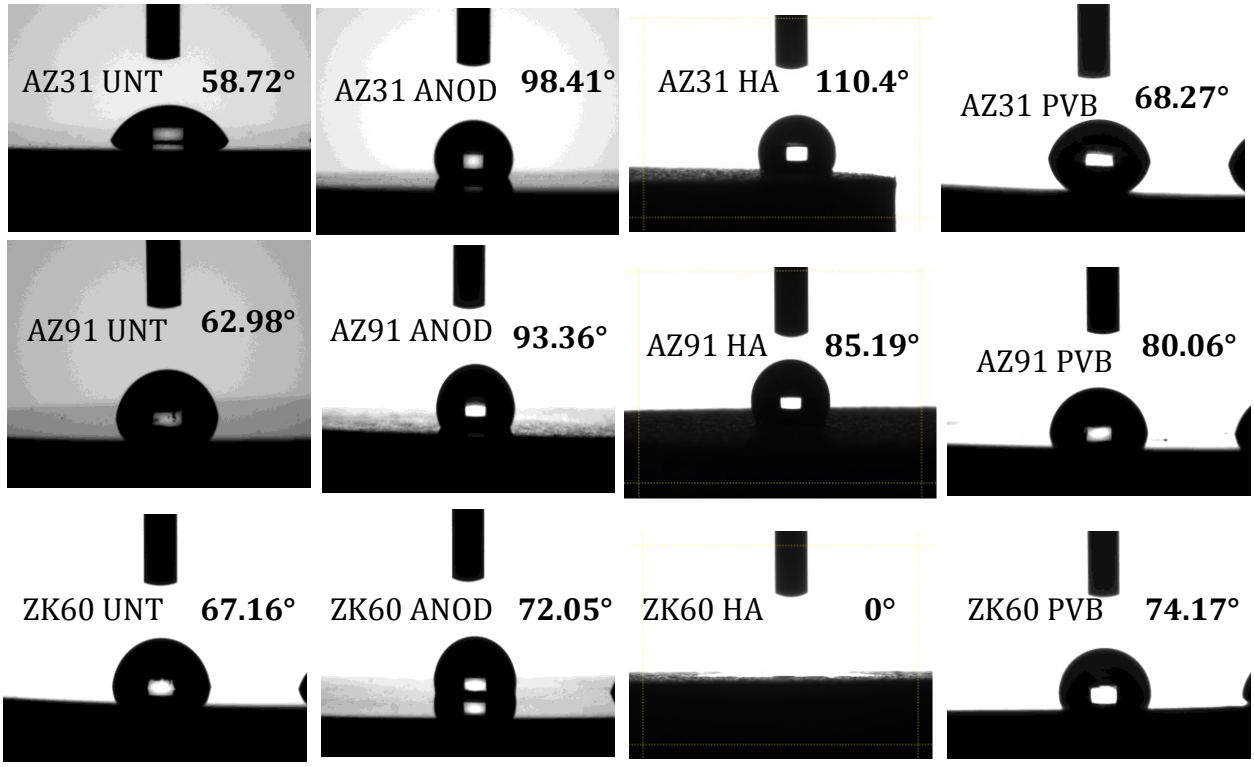

Figure 28. Optical images of contact angle analysis

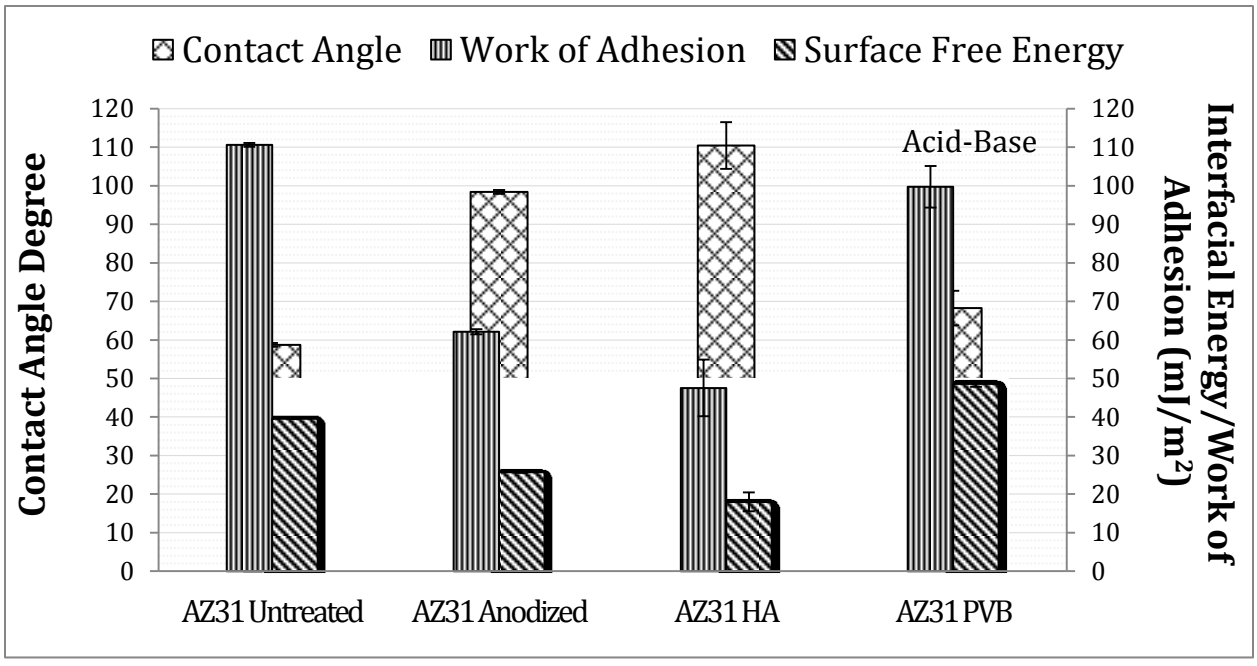

Figure 29. Acid-Base theory contact angle, work of adhesion, and surface free energy for AZ31 samples (n = 10)

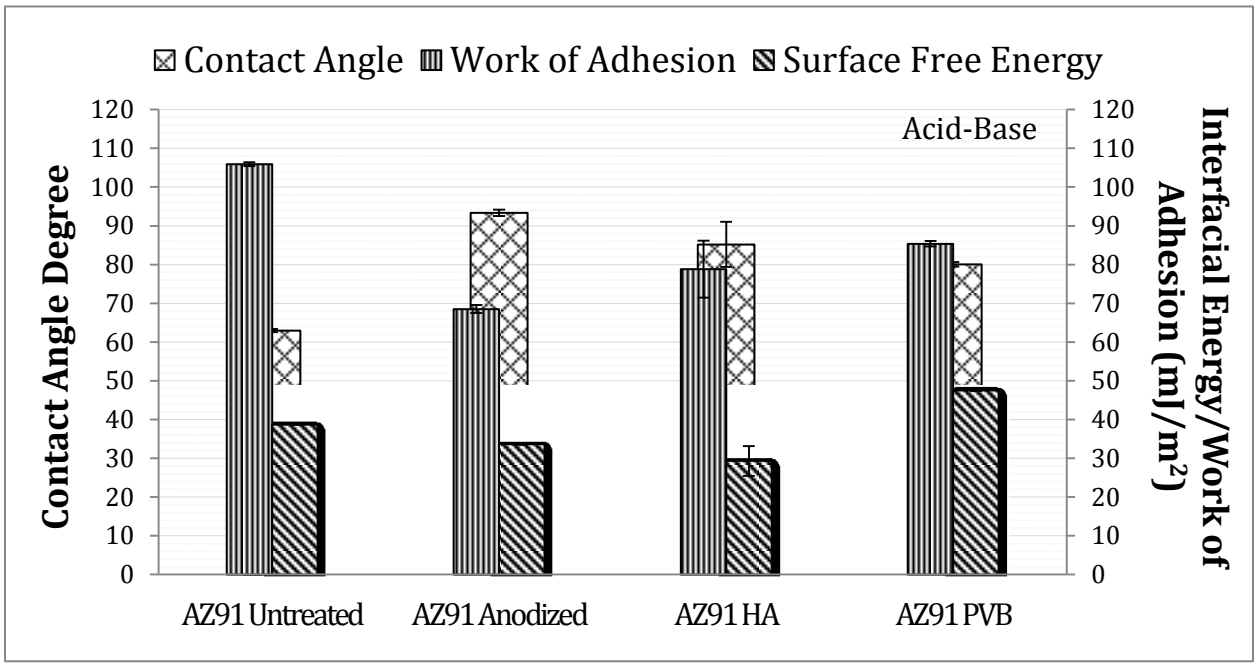

Figure 30. Acid-Base theory contact angle, work of adhesion, and surface free energy for AZ91 samples (n = 10)

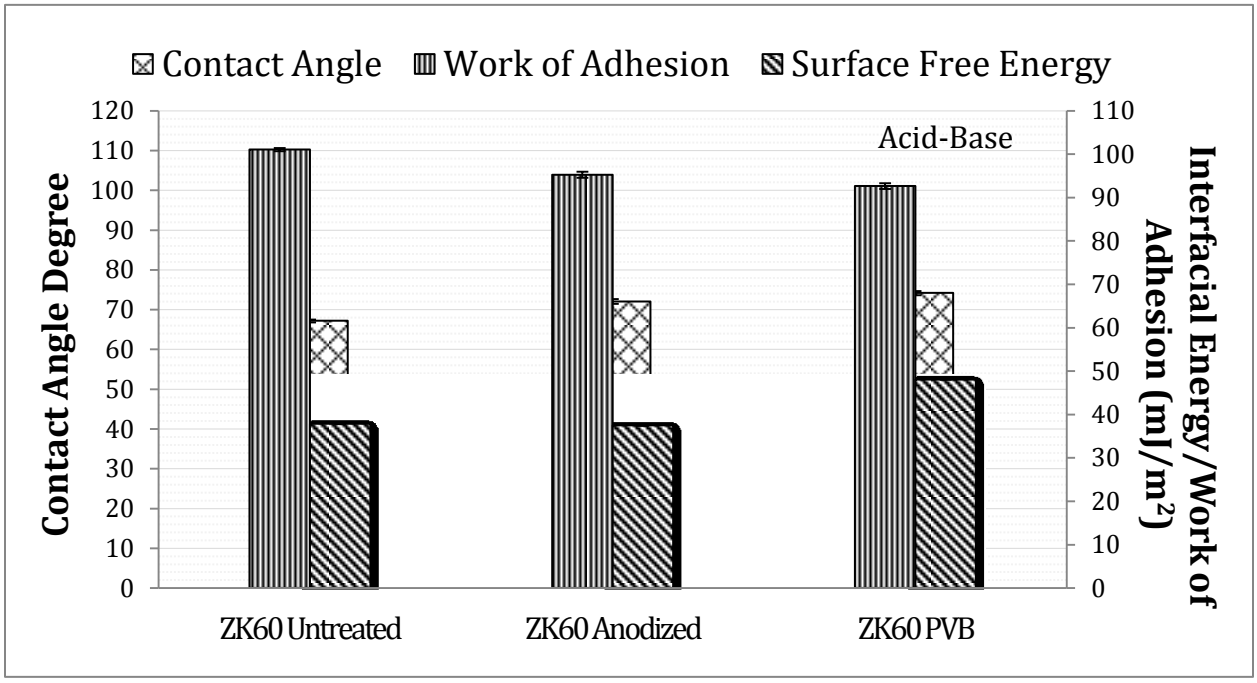

Figure 31. Acid-Base theory contact angle, work of adhesion, and surface free energy for ZK60 samples (n = 10)

Table 13. Acid-Base average values of C.A, interfacial free energy, and work of adhesion (*n = 10)*

Sample	Contact angle deg (*std ≤ 15)*			Interfacial free energy (mJ/m^2) (*std ≤ 5)*			Work of adhesion (mJ/m^2) *(std ≤ 5)*		
	Water	ethylene glycol	diiodo-methane	water	ethylene glycol	diiodo-methane	water	ethylene glycol	diiodo-methane
AZ31 Untreated	58.7	44.8	40.2	1.7	5.5	0.7	110.6	81.9	89.6
AZ31 Anodized	98.4	71.5	66.9	36.3	10.5	5.7	62.1	63.1	70.7
AZ31 HA	110.4	86.5	79.2	43.3	15.4	8.5	47.5	50.5	60.3
AZ31 PVB	68.3	38.91	18.2	21.7	11.3	0.4	99.7	85.2	99.0
AZ91 Untreated	62.9	47.9	41.8	5.6	6.6	0.8	105.9	80.0	88.7
AZ91 Anodized	93.4	67.3	51.2	37.9	15.2	1.7	68.5	66.4	82.7
AZ91 HA	85.2	58.9	61.2	24.3	5.9	5.8	78.8	72.3	75.3
AZ91 PVB	80.1	41.4	25.4	34.9	11.6	1.6	85.4	83.8	96.7
ZK60 Untreated	67.2	50.8	43.4	9.6	7.6	0.9	101.1	78.1	87.7
ZK60 Anodized	72.1	53.6	44.2	15.0	9.0	1.0	95.3	76.3	87.3
ZK60 PVB	74.2	44.2	19.2	28.1	13.6	0.0	92.7	82.3	98.8

Table 14. Acid-Base average values of surface free energy components *(mJ/m^2) (n=10, std ≤ 5)*

Samples	Lifshitz-Van der Waals LW	Acidic (Electron Acceptor) +	Basic (Electron Donor) -	Total
AZ31 Untreated	39.5	0.0	26.2	39.5
AZ31 Anodized	24.6	0.2	1.1	25.6
AZ31 HA	18.0	0.6	0.5	18.0
AZ31 PVB	48.3	0.0	11.7	48.6
AZ91 Untreated	38.7	0.0	22.3	38.7
AZ91 Anodized	33.6	0.0	1.9	33.6
AZ91 HA	27.9	0.7	5.8	29.3
AZ91 PVB	46.0	0.2	2.9	47.5
ZK60 Untreated	37.8	0.0	18.6	37.8
ZK60 Anodized	37.5	0.0	14.2	37.5
ZK60 PVB	48.0	0.0	7.5	48.0

Table 15. Kitazaki-Hata average values of C.A, interfacial free energy, work of adhesion (*n = 10)*

Sample	Contact angle deg (*std ≤ 15)*			Interfacial free energy (mJ/m^2) (*std ≤ 5)*			Work of adhesion (mJ/m^2) (*std ≤ 5)*		
	water	ethylene glycol	diiodo-methane	water	ethylene glycol	diiodo-methane	water	ethylene glycol	diiodo-methane
AZ31 Untreated	57.9	50.3	36.6	54.1	62.4	52.1	111.5	78.2	91.6
AZ31 Anodized	97.6	72.9	66.4	36.9	13.4	6.9	63.2	61.6	71.2
AZ31 HA	107.6	99.0	73.2	59.4	44.9	22.9	50.9	40.3	65.4
AZ31 PVB	67.2	35.4	18.2	26.2	15.5	6.1	100.9	86.5	99.0
AZ91 Untreated	62.0	53.8	37.9	51.9	57.8	45.9	106.9	75.9	90.9
AZ91 Anodized	92.4	73.7	46.9	42.5	26.1	4.7	69.7	61.1	85.5
AZ91 HA	107.6	99.0	73.2	59.4	44.9	22.9	50.9	40.3	65.4
AZ91 PVB	80.4	42.3	25.7	37.9	14.7	4.3	84.9	82.9	96.6
ZK60 Untreated	66.4	55.8	40.2	44.1	46.5	34.5	101.9	74.5	89.6
ZK60 Anodized	70.7	61.9	38.4	53.6	55.2	37.8	96.8	70.1	90.6
ZK60 PVB	72.7	39.8	19.2	28.4	13.4	2.08	94.4	84.3	98.8

Table 16. Kitazaki-Hata surface free energy components *(mJ/m^2) (n=10, std ≤ 5)*

Samples	Dispersion (d)	Polar (p)	Hydrogen Component (h)	Total	Frictional Polarity
AZ31 Untreated	19.5	60.8	12.6	92.9	63.9
AZ31 Anodized	27.0	0.0	0.3	27.3	0.0
AZ31 HA	12.8	24.5	0.2	37.5	26.4
AZ31 PVB	40.9	9.4	4.0	54.3	9.6
AZ91 Untreated	19.9	55.9	10.3	86.0	58.7
AZ91 Anodized	27.6	11.6	0.2	39.5	12.1
AZ91 HA	26.7	4.5	3.0	34.2	4.7
AZ91 PVB	49.6	0.0	0.5	50.1	0.0
ZK60 Untreated	21.3	43.9	8.1	73.3	45.9
ZK60 Anodized	20.6	51.2	5.9	77.6	53.7
ZK60 PVB	43.7	4.4	1.9	50.1	4.5

4.4 Electrochemical Corrosion Experiments

A potentiostat is used to monitor the electrochemical behavior of materials. The potentiostat is an electronic instrument that controls the voltage difference between a working electrode and a reference electrode. Both electrodes are contained within an electrochemical cell. The potentiostat implements the control by injecting current into the cell through an auxiliary or counter electrode (135). In almost all applications, the potentiostat measures the current flow between the working and counter electrodes. The controlled variable in a potentiostat is the cell potential and the measured variable is the cell current (135). A potentiostat requires an electrochemical cell with three electrodes as shown below in figure 32. W/WS denote the working and working sense. R denotes the reference electrode and C denotes the counter electrode (135).

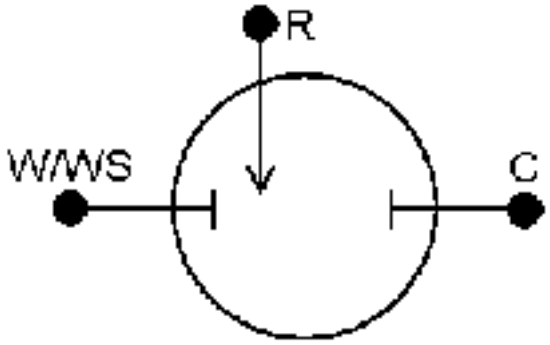

Figure 32. Three point electrode cell schematic (135)

During the corrosion testing, the working electrode is the corroding metal. Generally, the working electrode is not the actual metal structure being studied. Instead, a small sample is used to represent the structure. This is analogous to testing using weight loss coupons. The working electrode can be bare or coated metal/alloy (135). The reference electrode is used in measuring the working electrode potential. A reference electrode should have a constant electrochemical potential as long as no current flows through it. The most common lab reference electrodes are

the saturated calomel electrode (SCE) and the Silver/Silver Chloride (Ag/AgCl) electrodes (135). The counter, or auxiliary, electrode is a conductor that completes the cell circuit. The counter electrode is generally an inert conductor like platinum or graphite (135).

A typical three-electrode corrosion cell and a potentiostat (GAMRY®) is shown in figure 33. It is used to run the electrochemical experiments (potentiodynamic polarization and electrochemical impedance spectroscopy).

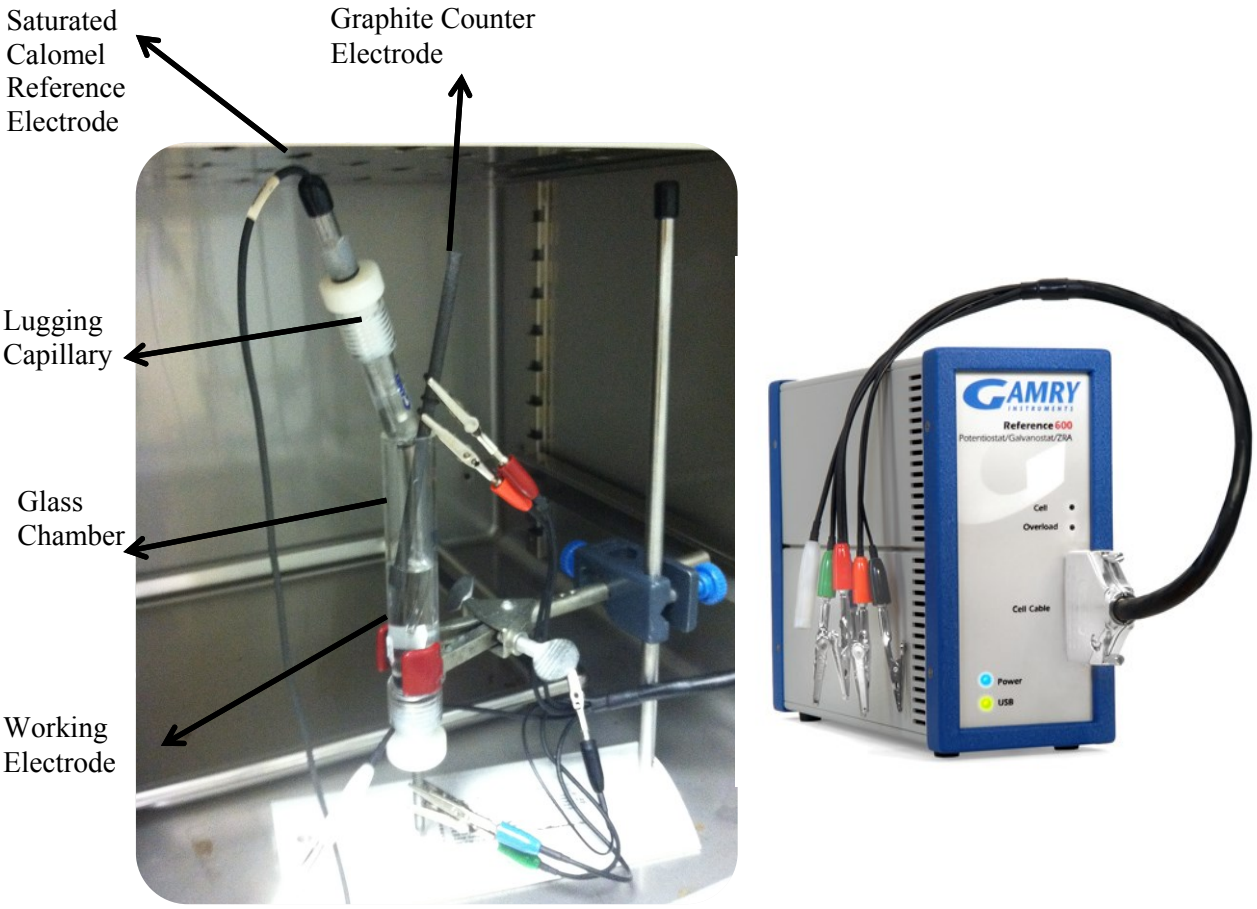

Figure 33. Corrosion cell kit and GAMRY potentiostat 600

4.4.1 Potentiodynamic Polarization

In order to determine the corrosion rates, potentiodynamic polarization test are performed. Potentiodynamic is commonly used to characterize corrosion rates of metallic materials while the corrosion rates can be calculated by the following expressions:

$$\eta = \beta log \frac{i}{i_0} \tag{9}$$

This expression is known as the Tafel equation, where β is the tafel slope, i is the applied current density, and i_0 is the exchange current density. Slopes from the anodic and cathodic reactions may be obtained from the linear regions of the polarization curve, as depicted in figure 34 (136). The corrosion current density (i_{corr}) and the potential (E_{corr}) is at the intersection of anodic and cathodic slopes.

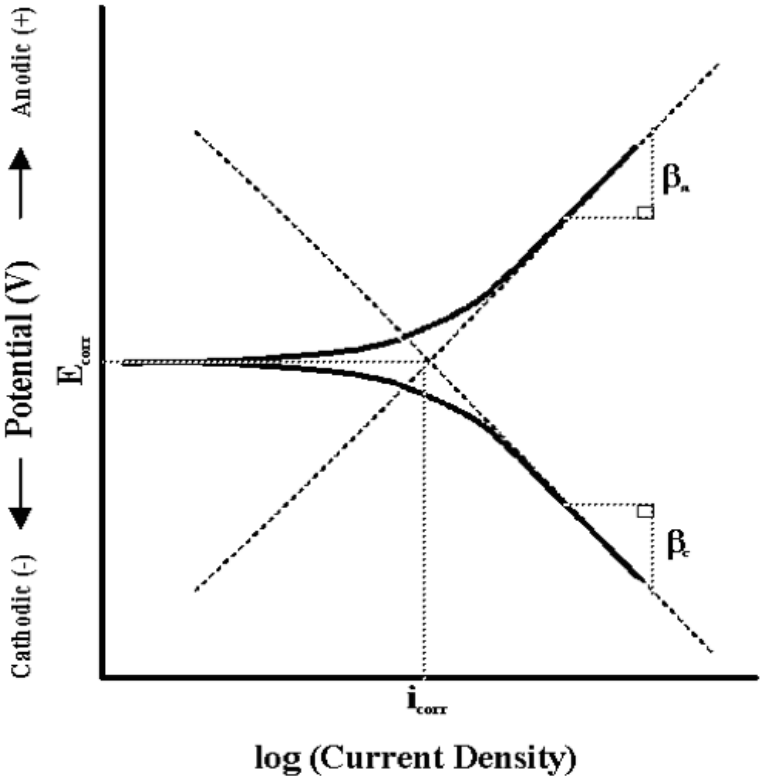

Figure 34. Tafel slope calculation (136)

The corrosion current density may be then combined with Faraday's law:

$$W = \frac{A.W.Q}{zF} \tag{10}$$

Where W is the mass of material removed. A.W. is the atomic weight of the sample, Q is the total charge passed, z is the total number of electrons transferred during the reaction, and F is Faraday's constant. If experiments are performed on alloys, the equivalent weight must be known. For an alloy, the equivalent weight can be expressed as a weighted average of its constituents. The expression to calculate the equivalent weight is represented:

$$Equivalent\ Weight\ (EW) = \left(\Sigma \frac{f_i z_i}{AW_i}\right)^{-1} \tag{11}$$

Where, f_i is the atomic fraction, and z_i is the valence electron of each component. Once the weight is been established, the corrosion rate in terms of depth per unit time, can be calculated through the density (ρ) and exposed surface area (SA) (136):

$$Corrosion\ rate = \frac{W * SA}{\rho} \tag{12}$$

4.4.2 Potentiodynamic Polarization Tests

The electrochemical polarization curves from the different magnesium alloys immersed in PBS are shown in figures 35-37. In theory, the cathodic curve represents the hydrogen evolution through the reduction process, while the anode curve characterizes the oxidation of Mg alloy. According to the results, the cathodic polarization current of hydrogen reduction reaction was much higher for the anodized alloys compared to the untreated alloys (87). Longest

passivation stages were observed for AZ31B and AZ91E anodized compared to ZK60A anodized passivation area. The corrosion potential E_{corr}, the current density I_{corr}, and corrosion rate (C.R.) results extracted from the potentiodynamic polarization curves via tafel fit extrapolation are summarized in Table 17. It was observed that the anodization treatment has enhanced the corrosion resistance. The current densities have decreased for all three alloys; for example the current density for AZ31B shifted from 3.43 E-05 A/cm^2 to 2.72 E-06 A/cm^2, improving the corrosion rate. The same behavior was observed for the other magnesium alloys. The current density of AZ91E shifted from 3.66 E-05 A/cm^2 to 2.50 E-06 A/cm^2, and ZK60A current density shifted from 3.23 E-05 A/cm^2 to 1.86 E-06 A/cm^2. Moreover, compared to untreated magnesium alloys the E_{corr} potentials for the anodized alloys became more positive experiencing a more noble behavior. The corrosion rate for all the alloys decreased with anodization; this can be attributed to the formation of various oxides acting as protective passive films. The anodized coating is harder than other conversion coatings, which leads to higher wear resistance.

Furthermore, the PVB coated samples had a significant decrease in their current densities compared to the untreated alloys. For example AZ31 PVB coated current density shifted to 3.38 E-07, AZ91 PVB coated shifted to 4.74 E-08, and ZK60 PVB coated alloys went to 1.19 E-07. However, for the HA coated alloy, the current density increased for all the magnesium alloys, having a higher corrosion rate. The corrosion parameters obtained from tafel extrapolation are listed in table17.

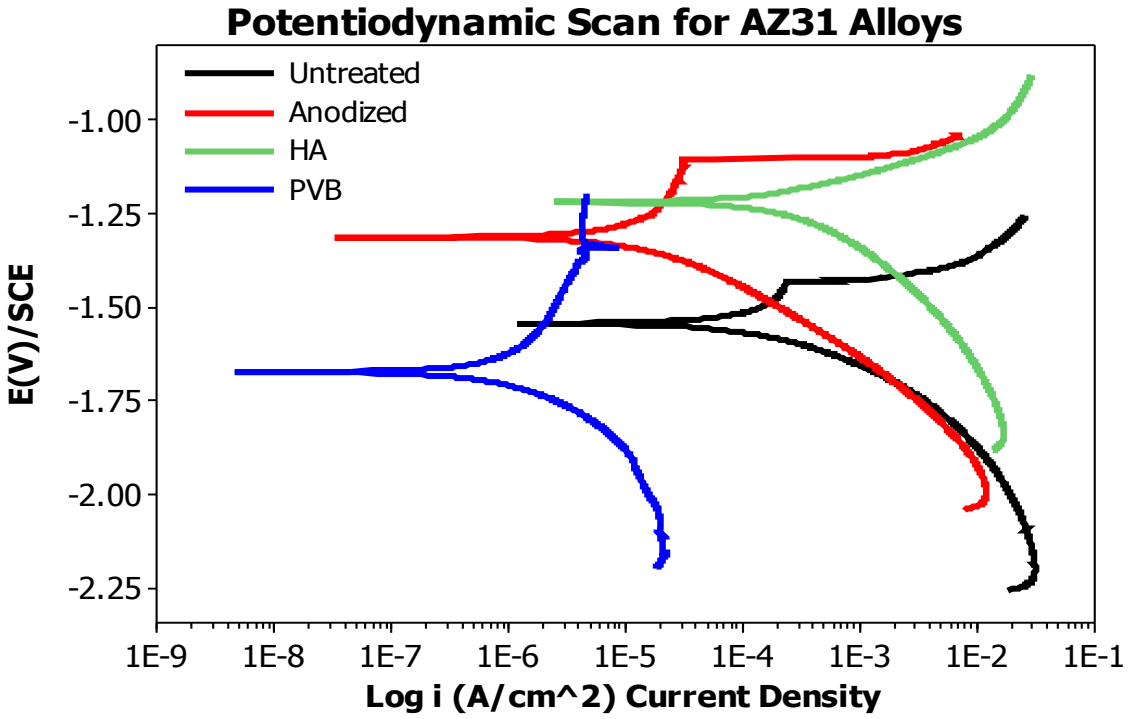

Figure 35. Potentiodynamic curves of AZ31 samples in PBS at 37 °C in a humidified atmosphere with 5% CO_2

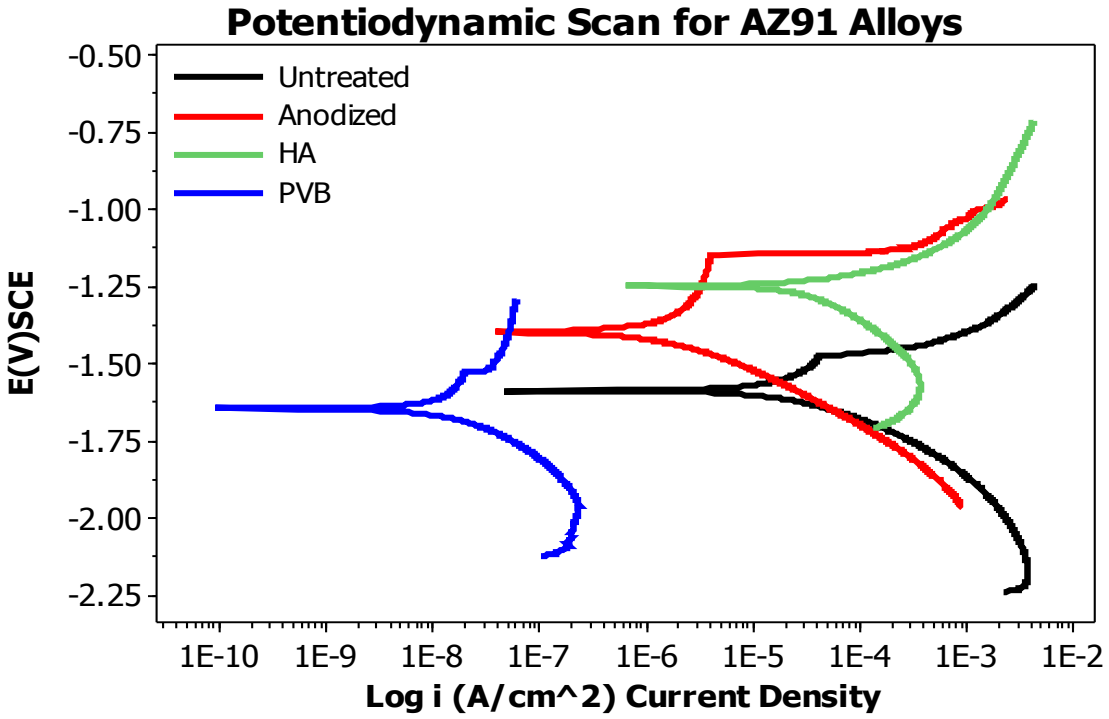

Figure 36. Potentiodynamic curves of AZ91 samples in PBS at 37 °C in a humidified atmosphere with 5% CO_2

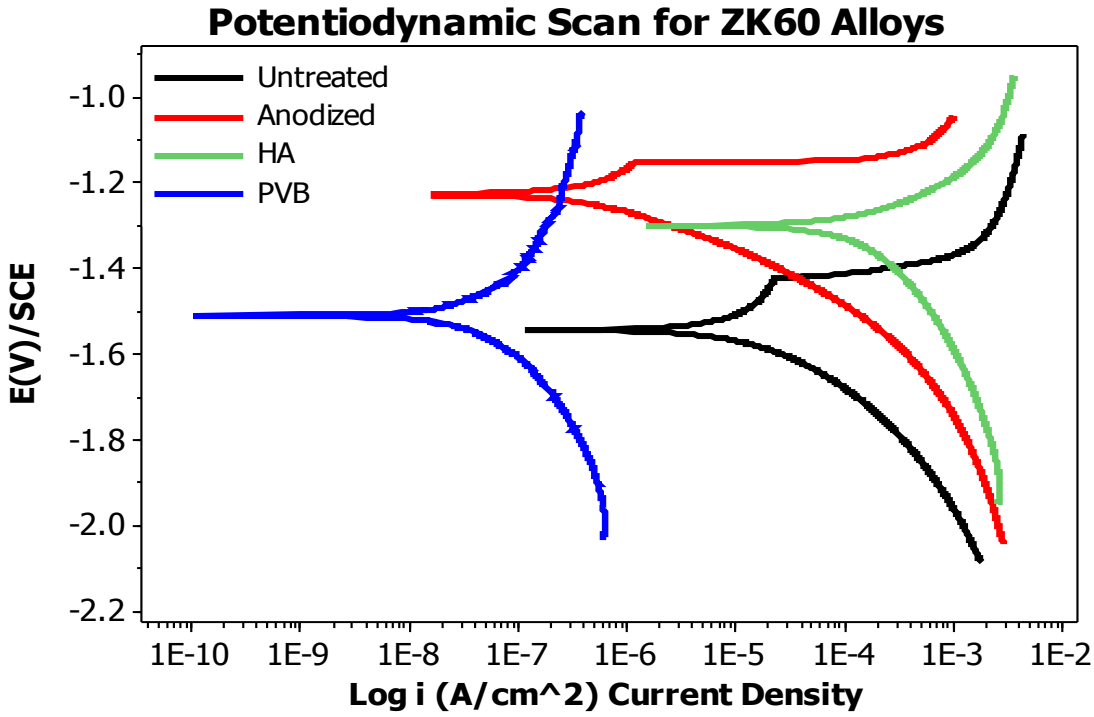

Figure 37. Potentiodynamic curves of ZK60 samples in PBS at 37 °C in a humidified atmosphere with 5% CO_2

Table 17. Average electrochemical results of potentiodynamic polarization of Mg Alloys

Alloy	Icorr (A/cm²)	Ecorr (V)	C.R. (mpy)
AZ31 Untreated	4.4E-05	-1.5	38.5
AZ31 Anodized	2.7E-06	-1.3	2.4
AZ31 HA	2.8E-05	-1.2	43.7
AZ31 PVB	3.3E-07	-1.7	0.3
AZ91 Untreated	3.6E-05	-1.6	30.9
AZ91 Anodized	2.5E-06	-1.4	2.1
AZ91 HA	2.0E-04	-1.3	176.4
AZ91 PVB	4.7E-08	-1.7	0.04
ZK60 Untreated	3.2E-05	-1.6	26.8
ZK60 Anodized	1.8E-06	-1.3	1.5
ZK60 HA	1.6E-04	-1.3	136.2
ZK60 PVB	1.1E-07	-1.5	0.01

4.4.3 Electrochemical Impedance Spectroscopy

Electrochemical impedance spectroscopy (EIS) technique offers an insight into the mechanism of corrosion attack. EIS can characterize corrosion due to pits, pores, or due to diffusion through an oxide film. This electrochemical practice also provides information about the dielectric constant and capacitance of a passive film (137–139). EIS has also been used as an effective tool for characterizing coating systems.

The interface between liquid and solid systems can be discussed in terms of electrical circuits (138,140). The EIS technique permits the characterization of different elements to an over all sample resistance; e.g charge transfer resistance, capacitor resistance, or coating resistance. In order to obtain actual information of the various electrical elements, circuit models are designed for the impedance spectra simulation (140) as shown in figure 38. In addition, to simulating impedance spectra using circuit models, applying variations of capacitance and resistance, it is possible to obtain information regarding the stability of films or coatings.

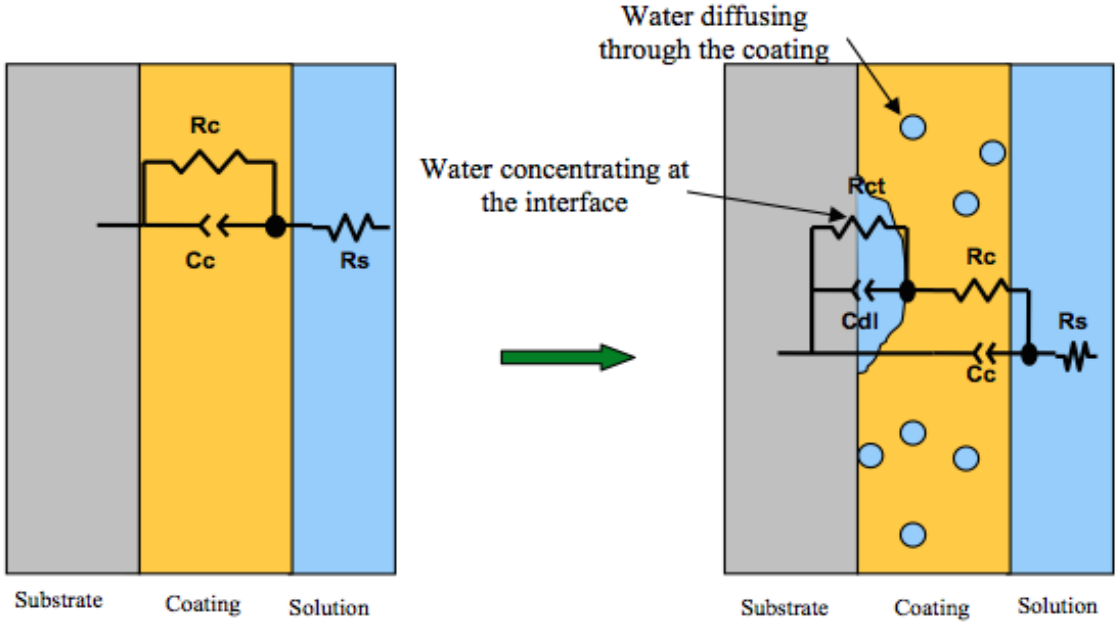

Figure 38. Electronic circuits used to simulate impedance spectra of alloys: (a) exposed to corrosive electrolyte instantly, (b) exposed to corrosive electrolyte for different periods of time (140).

EIS was performed starting with a frequency of 100 kHz and at ending frequency of 10 mHz. Ten data points were recorded per decade. The EIS spectra (nyquist plots) of magnesium alloys are presented in figures 39-42. For the curves obtained for the untreated alloys (AZ31, AZ91, ZK60), two time constants were observed: one was the capacitance arc in the high frequency region and the other was a capacitance arc in the low frequency region. Generally, the capacitance arcs results from charge transfer and film effects (141). The presence of the inductance loops for the untreated sample spectra indicates two surface states (141); the low frequency loop is related to the adsorption of the corrosion products (107). Subsequently, according to the EIS data, obvious change can be found on the anodized specimens. The plot for the anodized alloys contained only one capacitance loop, implying that the passive layer was undamaged (107). Additionally, the capacitance loop diameter was bigger than that of the magnesium substrates. It can be concluded that the anodized layer can reduce the biodegradation rate of magnesium alloy. On the other hand, there is a significant reduced impedance for all the HA coated alloys, suggesting the presence of corrosion activity such as pitting corrosion (142). Results are demonstrating that the stability of the HA coating is very poor and weak. The EIS PVB coated samples data is shown in figure 42. The results were plotted separately due to the data range, which was significant high compared to the untreated, anodized, and HA samples. The results demonstrated that the polymeric coating provides good protection against degradation and hence exhibited one capacitive loop. The results showed good agreement with those of potentiodynamic polarization.

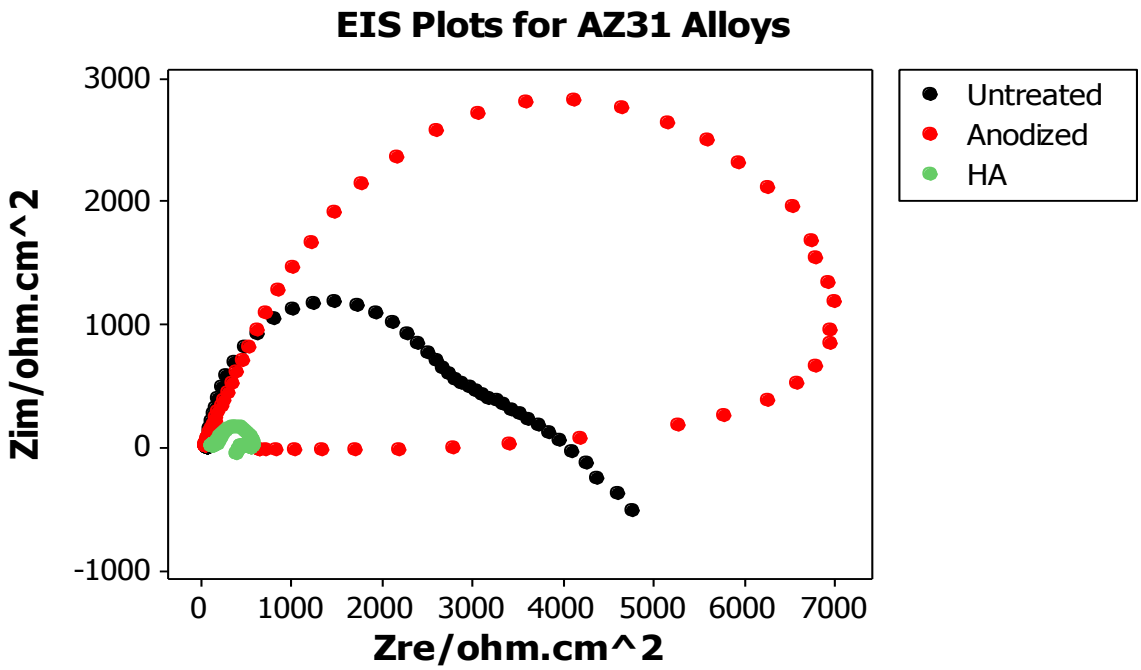

Figure 39. Representative EIS spectra for AZ31 alloys

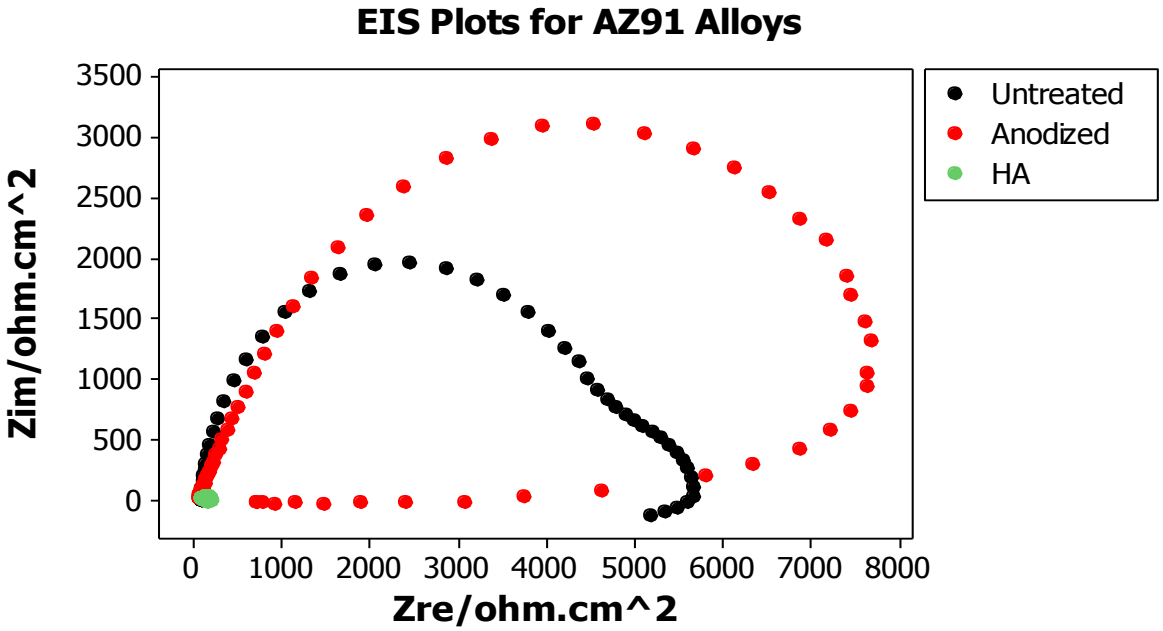

Figure 40. Representative EIS spectra for AZ91 alloys

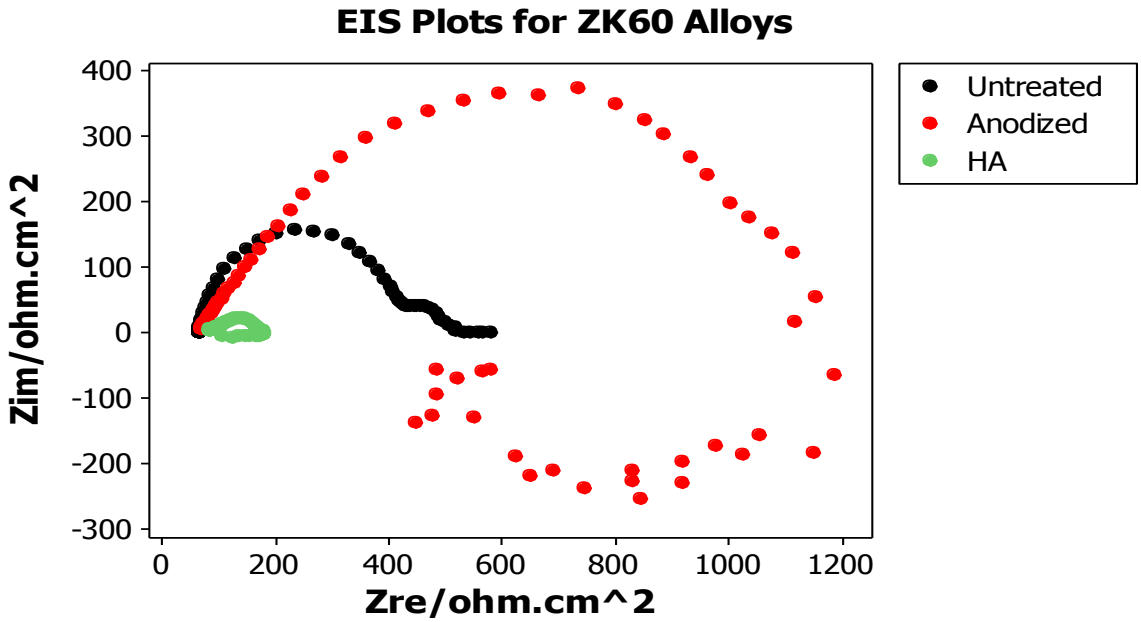

Figure 41. Representative EIS spectra for ZK60 alloys

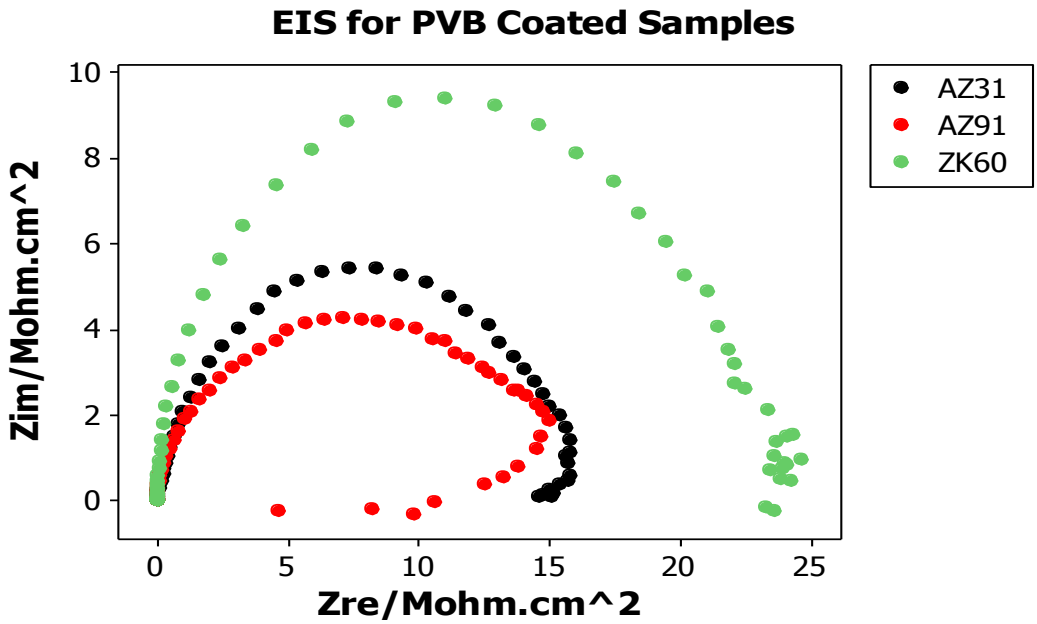

Figure 42. Representative EIS for PVB polymer coated alloys

Taking the physical structure of the electrode system and impedance into account, the equivalent circuit of the tested sample is proposed in figure 43. Furthermore, the EIS fitted results of the experimental samples are presented in table 18. Xu et. al explained R_s, C_c, R_{po}, C_{dl} and R_{ct} circuit components as follows: R_s is the solution resistance between the reference and working electrodes. Its value is determined by the conductivity of the test medium and cell geometry (78). Since the systems are similar, the value of solution resistance is close for all systems. C_c is the constant phase angle CPE component and represents the capacitance of the intact film on the surface. A larger value indicates that the dielectric constant of the surface film increases due to electrolyte penetration and film thickness reduction due to chemical dissolution. R_{po} is the relevant resistance named after pore or ionic conducting defect resistance. Larger R_{po} implies good corrosion resistance of the surface film. C_{dl} is another CPE component, describing the capacitance of the interface electric double layer in the vulnerable regions exposed to electrolyte penetration. The Faraday charge transfer resistance, R_{ct}, is related to the electrochemical reaction in the same region. The higher the R_{ct}, the lower will be the corrosion resistance.

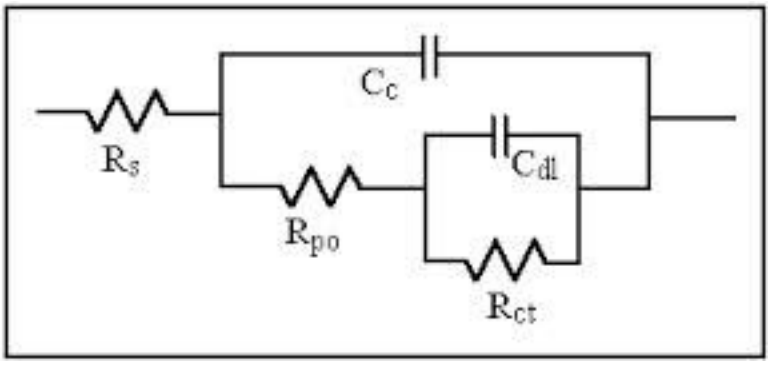

Figure 43. Electrical circuit model for the EIS spectra

Table 18. Fitted results of EIS spectra

Sample	R_s (Ωcm^2)	C_c ($10^{-6}Fcm^{-2}$)	R_{po}(Ωcm^2)	C_{dl} ($10^{-6}Fcm^{-2}$)	R_{ct} (Ωcm^2)
AZ31 Untreated	83.37	5.49E-06	8.00E+02	4.43E-06	2.10E+03
AZ31 Anodized	100.6	1.35E-06	1.80E+03	4.39E-06	2.95E+03
AZ31 HA	144.6	3.86E-07	6.71E+01	8.51E-06	3.63E+02
AZ31 PVB	1285	1.49E-09	4.47E+03	8.08E-08	6.67E+04
AZ91 Untreated	85.92	4.54E-06	1.34E+03	3.96E-06	3.09E+03
AZ91 Anodized	227.2	1.33E-06	2.48E+03	3.22E-06	4.99E+03
AZ91 HA	104	9.19E-07	2.44E+01	1.72E-05	6.15E+01
AZ91 PVB	517.2	5.23E-10	3.63E+06	1.89E-09	9.63E+06
ZK60 Untreated	77.93	1.62E-05	3.66E+02	3.06E-03	9.26E+01
ZK60 Anodized	80.7	8.63E-07	1.45E+02	3.50E-06	5.63E+02
ZK60 HA	95.29	1.42E-06	2.58E+01	2.59E-05	5.71E+01
ZK60 PVB	269	6.18E-10	8.75E+05	3.27E-10	2.73E+07

4.4.4 Immersion Experiments

The degradation of magnesium alloys leads to the evolution of hydrogen gas and alkalization of solution. Hydrogen evolution is a major drawback for the use of magnesium. In the case of implant applications, the hydrogen evolution may lead to gas pocket formations, which may lead to necrosis or even delayed healing symptoms. In animal studies, the formation of gas bubbles was found at different tested body locations (34,44,45).

The corrosion resistance and corrosion rate of magnesium and its alloys is influenced by several factors, such as temperature, pH, proteins, aminoacids, chlorides, dissolved oxygen, etc. These factors lead to different forms of corrosion attack such as galvanic corrosion, pitting corrosion, stress corrosion cracking, corrosion fatigue, etc. It is important to study the degradation phenomenon of magnesium under body-simulated conditions. Several factors considered during *in-vitro* corrosion experimentations, involve the usage of simulated body fluids with a low molarity of dissolved oxygen in a humidified atmosphere with 5% CO_2.

The degradation performance was evaluated by immersing the samples using phosphate buffer saline (PBS) as the simulated body fluid (SBF). The hydrogen evolution rates and corresponding degradation rates were monitored as a function of the immersion time. The average degradation rates after immersion in PBS at about 37 °C and 5% CO_2 for 7 days were calculated by means of weight loss and hydrogen evolution. In the hydrogen evolution test setup depicted in Figure 44, the hydrogen evolution volume was measured, and the degradation rate was deduced from the reaction below:

$$Mg + 2H_2O \rightarrow Mg(OH)_2 + H_2 \quad (3)$$

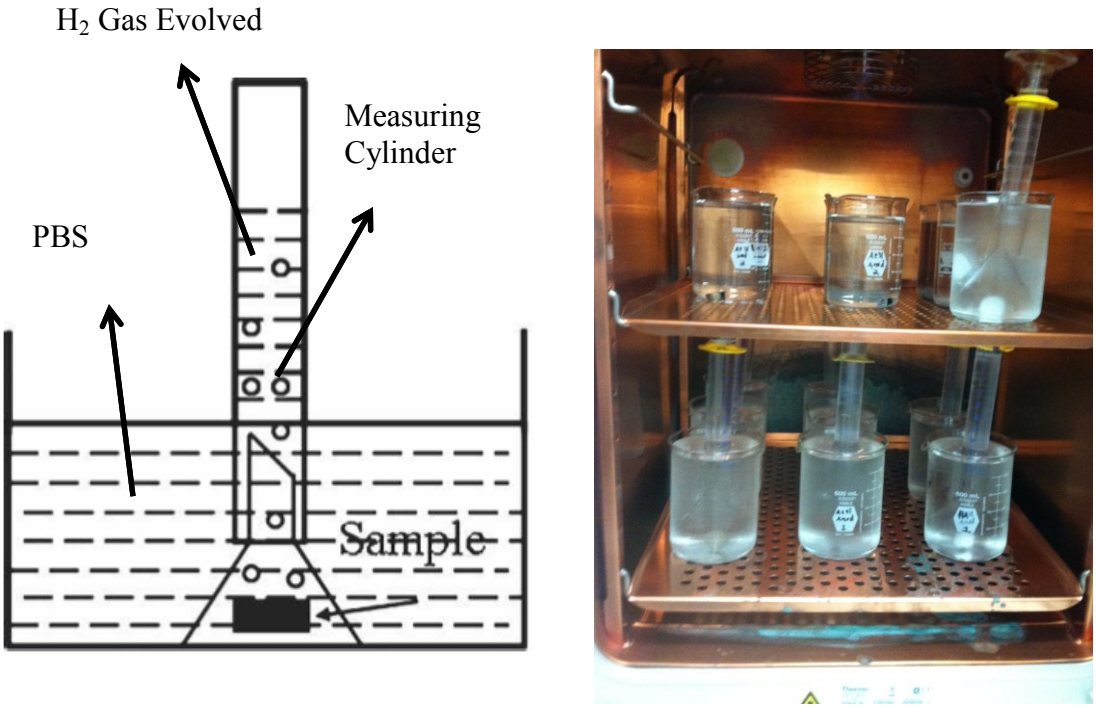

Figure 44. Representation of immersion test set up (142)

Figures 45, 46, and 47 are representing, the hydrogen evolution tendency for AZ31, AZ91, and ZK60 treated specimens during immersion in PBS. It can be seen that HA magnesium coated alloys exhibited the highest hydrogen evolution rate. The PVB coated materials had the lowest hydrogen evolution rates, with a very steady evolution behavior.

The corrosion rates were calculated from the weight change during the immersion test. The corrosion rate (CR) was measured in mils per year (MPY) by the following equation (99):

$$CR = \frac{(K * W)}{(A * t * \rho)} \tag{13}$$

Wher, K is a constant (3.45 x 10^6), W is the mass loss in grams, A is the surface area in cm^2, t is time of immersion exposure in hours, and ρ is the density in g/cm^3. Figure 48-50 summarize the corrosion rate calcualtions for all the magnesium alloys. It can be noted that the hydrogen evolution resluts are linearly related to the corrosion rate calculations.

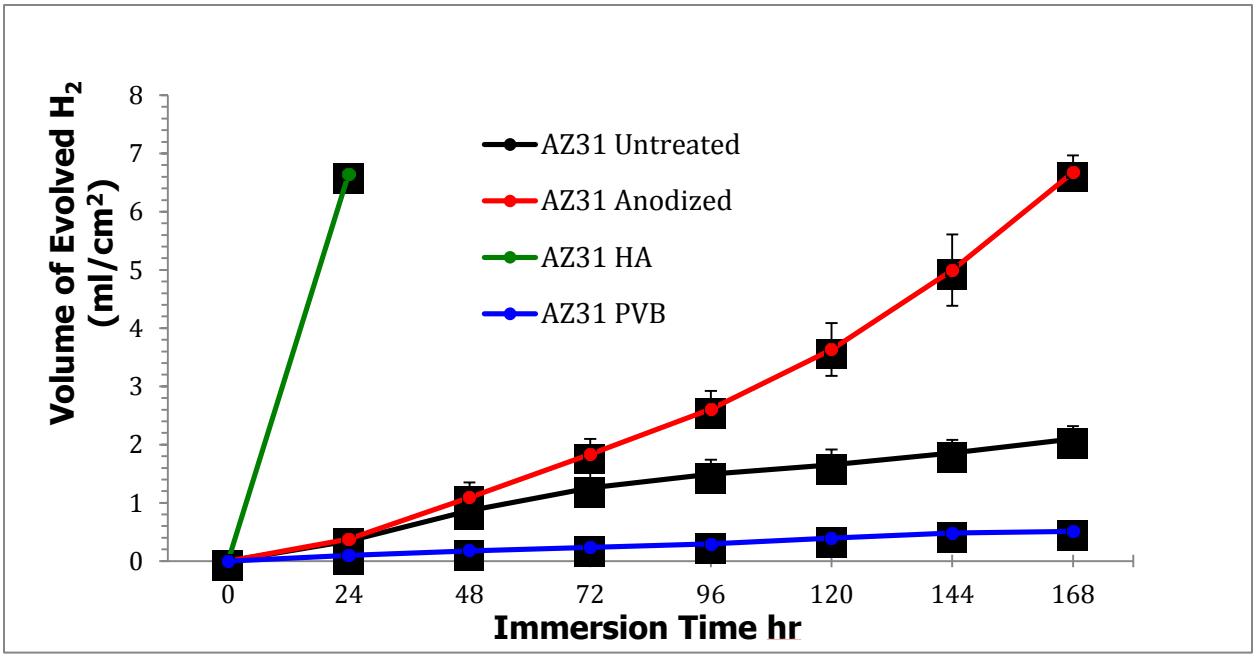

Figure 45. Hydrogen evolution rate for AZ31 alloys

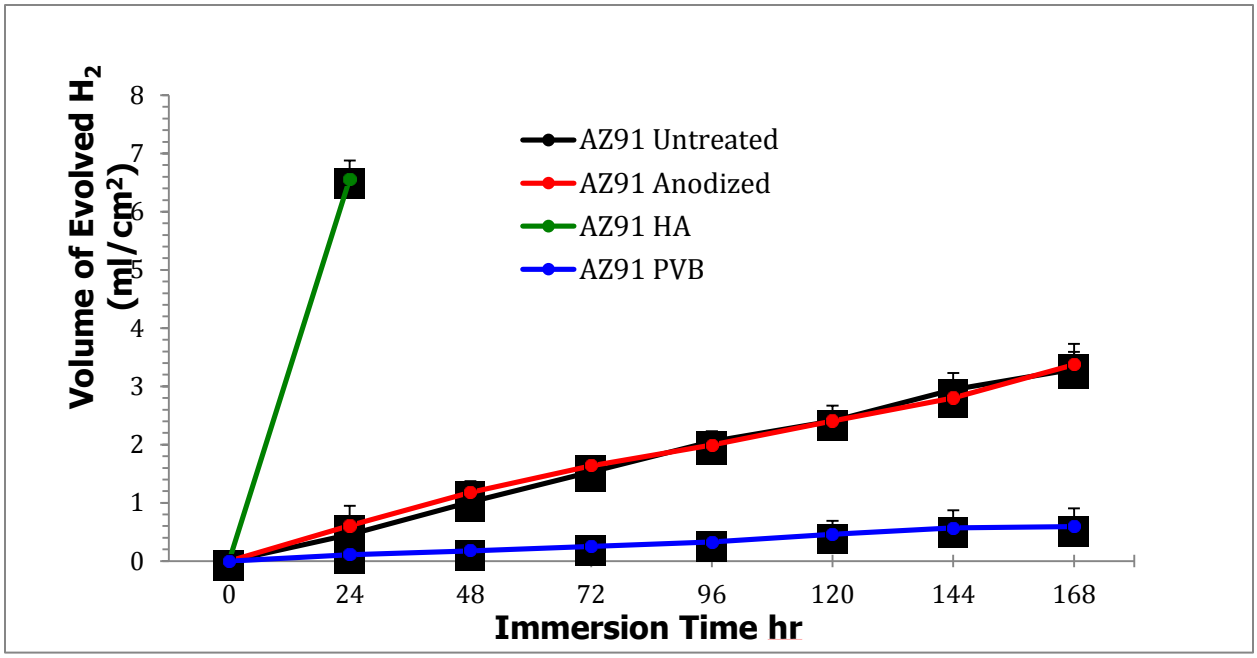

Figure 46. Hydrogen evolution rate for AZ91 alloys

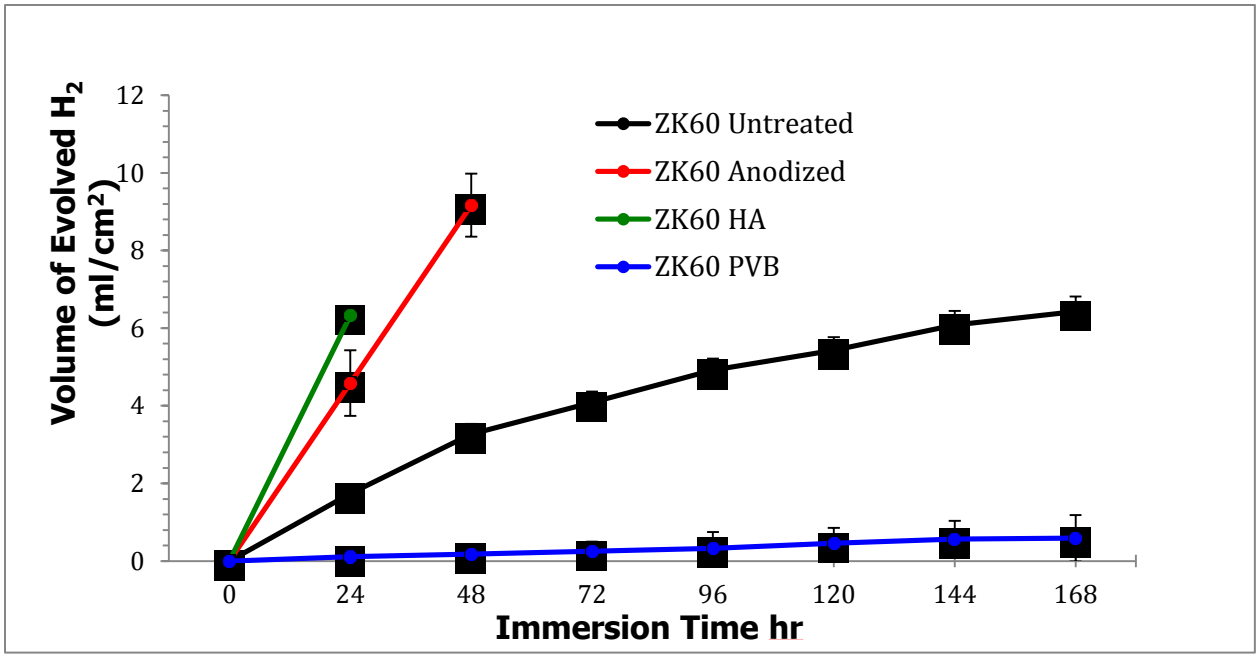

Figure 47. Hydrogen evolution rate for ZK60 alloys

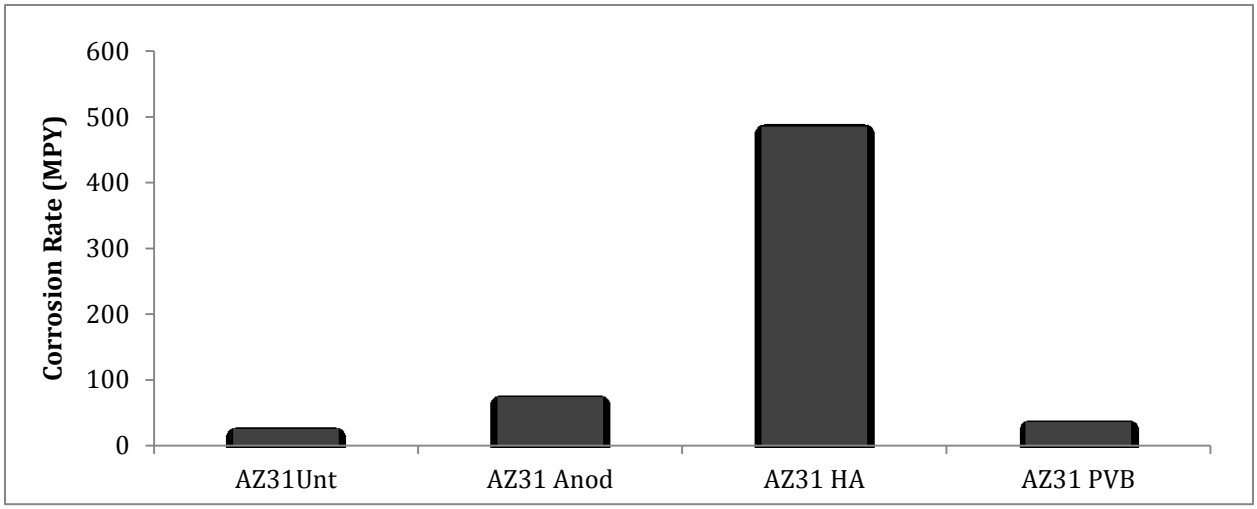

Figure 48. Corrosion rates of AZ31 alloys

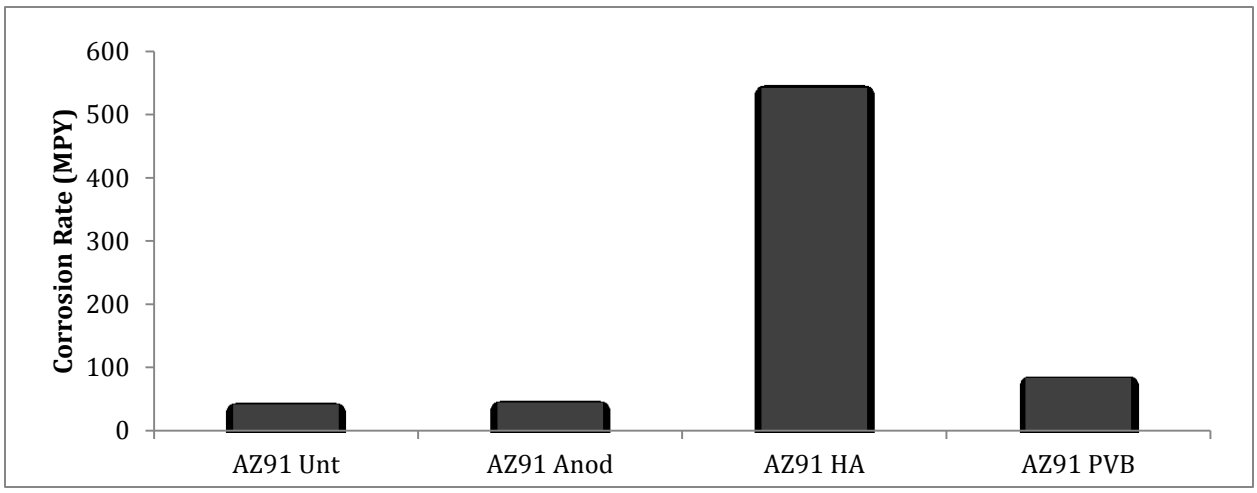

Figure 49. Corrosion rates of AZ91 alloys

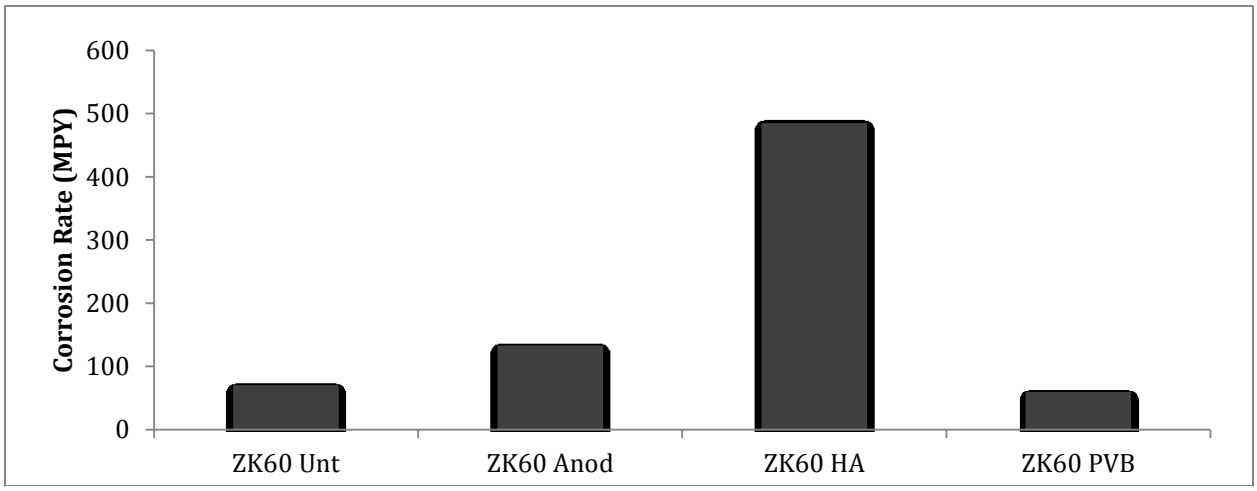

Figure 50. Corrosion rates of ZK60 alloys

4.5 Biological Studies

Stainless steel, titanium and cobalt-chromium alloys are commonly used for orthopedic implants. Most of these orthopedic implants are not permanent and require a second surgery once the healing process has been fulfilled. Magnesium alloys are considered as potential orthopedic implant materials. Compared to the commonly used biomaterials, magnesium alloys posses many outstanding features including being biocompatible, and biodegradable (80). Biodegradable magnesium alloys are being evaluated and reported for use in bone screws, plates, and scaffolds for bones and cartilage repair (91–93).

For a material intended to as an orthopedic fixation implant, an osteoblast cell line is preferable for the evaluation of cytotoxicity. MC3T3-E1, an osteoblast cell line, has been adopted for the biocompatibility studies. There are many techniques available for the assessment of the biocompatibility of materials. *In vitro* tests are often performed for the evaluation of potential effects of the material on the host cells before implantation. Generally, such techniques are based and described by international standards. International standards such as ISO-10993-5 and ISO-10993-12 are commonly used by researchers to evaluate different magnesium grades (86,143–149). There are of direct and in-direct methods suggested as experimental assessments for the biomaterial screening. The in-direct method was adopted and is frequently used. The preparation of the extracted solution samples involves immersing magnesium alloy samples in culture media for a period of time. The extracts are further on prepared making dilutions of various concentrations, and then the treated media is seeded to the cell line selected for the biocompatibility study.

Cell-based assays are often used for screening collections of compounds to determine if the test molecules have effects on cell proliferation or show direct cytotoxic effects that

eventually lead to cell death (150). Regardless of the type of cell-based assay being selected, it is important to know the number of viable cells remaining at the end of the experiment. There are a variety of assay methods that can be used to estimate the number of viable cells. The cell viability can be measured by using different classes of colorimetric tetrazolium reagents. The tetrazolium reduction, resazurin reduction, and protease activity assays measure some aspect of general metabolism or an enzymatic activity as a marker of viable cells (150). All of these assays require incubation of a reagent with a standardized population of cells to convert a substrate to a colored or fluorescent product that can be detected with a plate reader. Under most standard culture conditions, incubation of the substrate with viable cells will result in generating a signal that is proportional to the number of viable cells present. When cells die, they rapidly lose the ability to convert the substrate to product (150). The most commonly used compounds include: MTT-((3-(4, 5-dimethylthiazolyl-2)-2, 5-diphenyltetrazolium bromide), MTS-(3-(4,5-dimethylthiazol-2-yl)-5-(3-carboxymethoxyphenyl)-2-(4-sulfophenyl)-2H-tetrazolium,innersalt), XTT-(2,3-Bis-(2-Methoxy-4-Nitro-5-Sulfophenyl)-2*H*-Tetrazolium-5-Carboxanilide), and WST-1-(2-(4-Iodophenyl)-3-(4-nitrophenyl)-5-(2,4-disulfophenyl)-2H-tetrazolium, monosodium salt).

4.5.1 Percent Cell Viability (MTS assay)

In this investigation, the effect of metal ions released from magnesium alloys was assessed using MTS assay. This improved tetrazolium reagent eliminate a liquid handling step during the assay protocol because a second addition of reagent to the assay plate is not needed to solubilize formazan precipitates, thus making the protocols more convenient (150). This set of tetrazolium reagents is used in combination with intermediate electron acceptor reagents such as phenazine methyl sulfate (PMS) or phenazine ethyl sulfate (PES) which can penetrate viable

cells, become reduced in the cytoplasm or at the cell surface and exit the cells where they can convert the tetrazolium to the soluble formazan product as depicted in figure 51 (150,151).

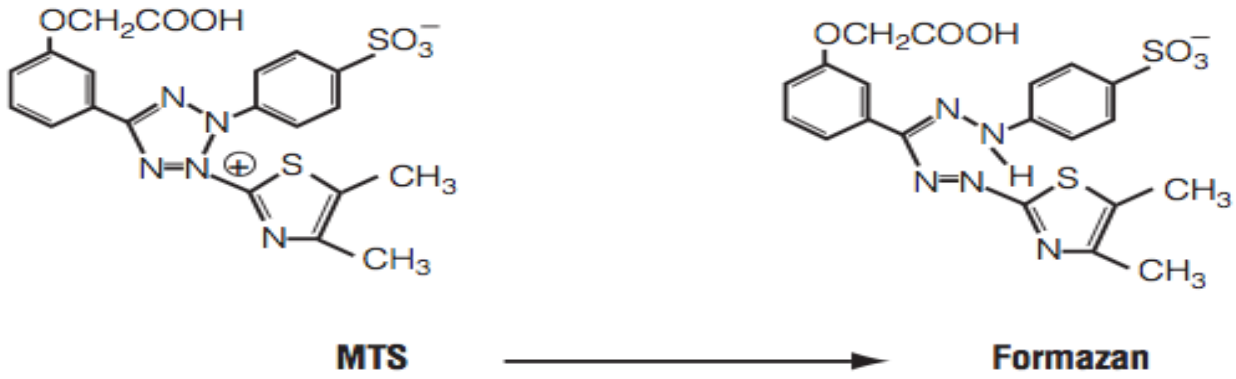

Figure 51. Structures of MTS tetrazolium and its formazan product

Cells and test compounds (MTS) were prepared in 96-well plates containing a final volume of 100 µl/well. An optional set of wells can be prepared with medium for background subtraction. The 20 µl of MTS solution were added to each of the well containing the cell populations. Plates were incubated for 4 hours at 37 °C. Absorbance was recorded at a light wavelength of 490 nm. Figure 52 is a representation of the MTS procedure (152).

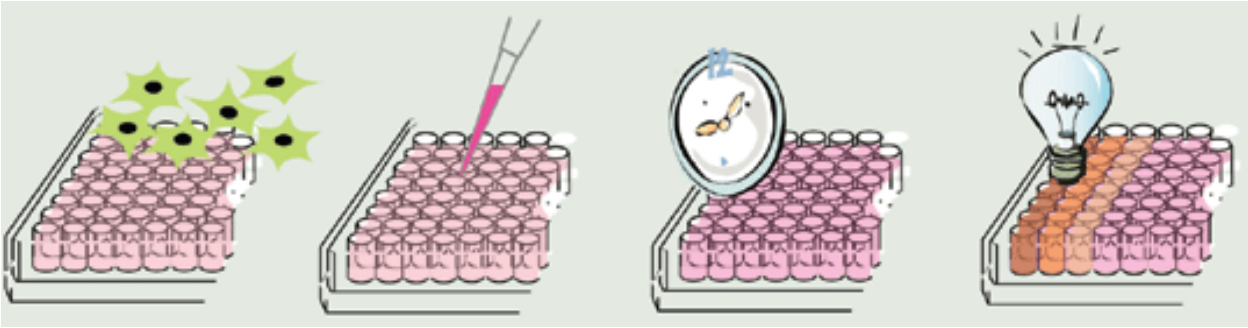

Figure 52. MTS cell viability protocol representation

The cell viability was studied with 50% and 100% concentrated extract culture media. Figures 53-55 depict the MC3T3 cell viability cultured for 24 hours with individual extraction concentrations of AZ31, AZ91, and ZK60 alloys. As explained previously, culture media was

collected every 3 days up to 21 days. The aim for this type of experiment was to monitor the magnesium degradation and the leached metal ions for a period of 21 days. The present results showed that the cytotoxic effect was different for the tested materials. The lowest cell viability of about 25% was observed for the ZK60 anodized alloy. Significant reduced cell viability for AZ31 and AZ91 anodized alloys could be seen during the 3-day period of collected extracts. However, a recovery with steady increase in growth rate was observed for AZ91 anodized alloy for the media collected after the 6-day extracted media. AZ31 and AZ91 untreated alloys showed similar cell viability trend behavior. Overall, AZ31 and AZ91 (untreated and anodized) were less cytotoxic to the MC3T3 cells than ZK60 alloys. The results also showed that the cell viability for most of the alloys was greater than 75% suggesting the cytocompatibility of AZ31, AZ91, and ZK60 (143). Figures 56-61 show optical images of the osteoblast cells cultured for 24 hours in 100% extract media. Net cell growth is related to the MTS plotted data.

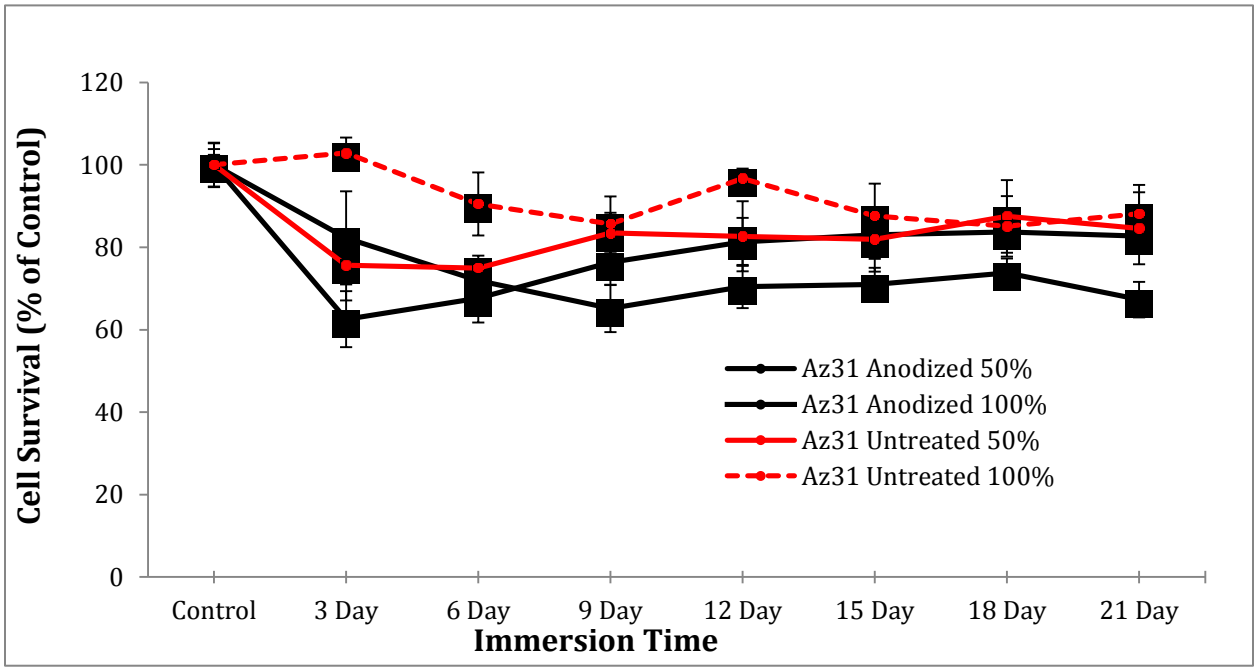

Figure 53. Effect of AZ31alloys on MC3T3 cells after 1 day incubation

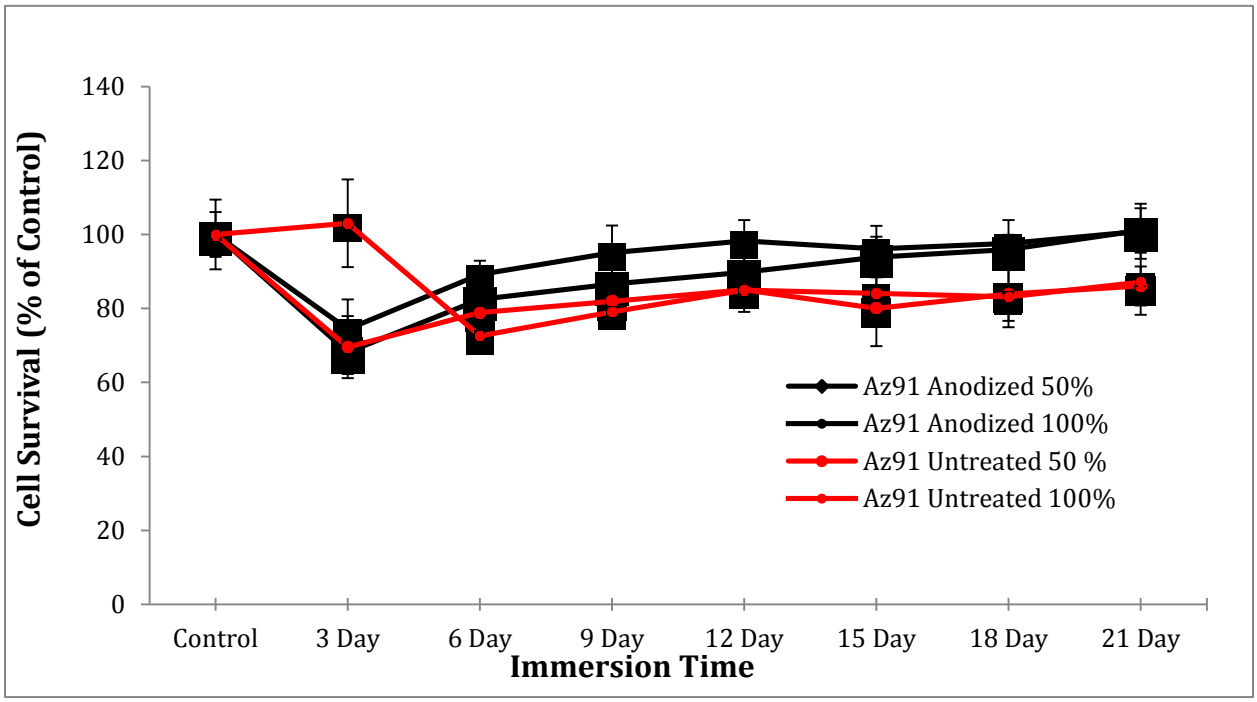

Figure 54. Effect of AZ91 alloys on MC3T3 cells after 1 day incubation

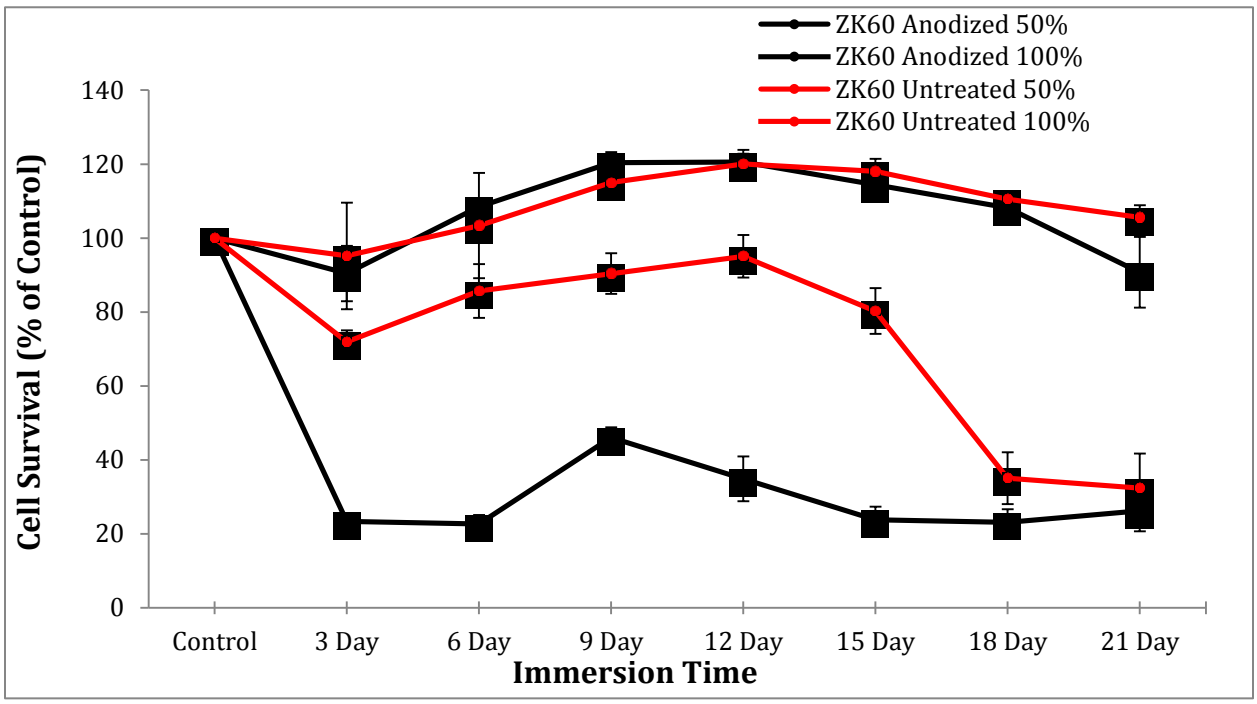

Figure 55. Effect of ZK60 alloys on MC3T3 cells after 1 day incubation

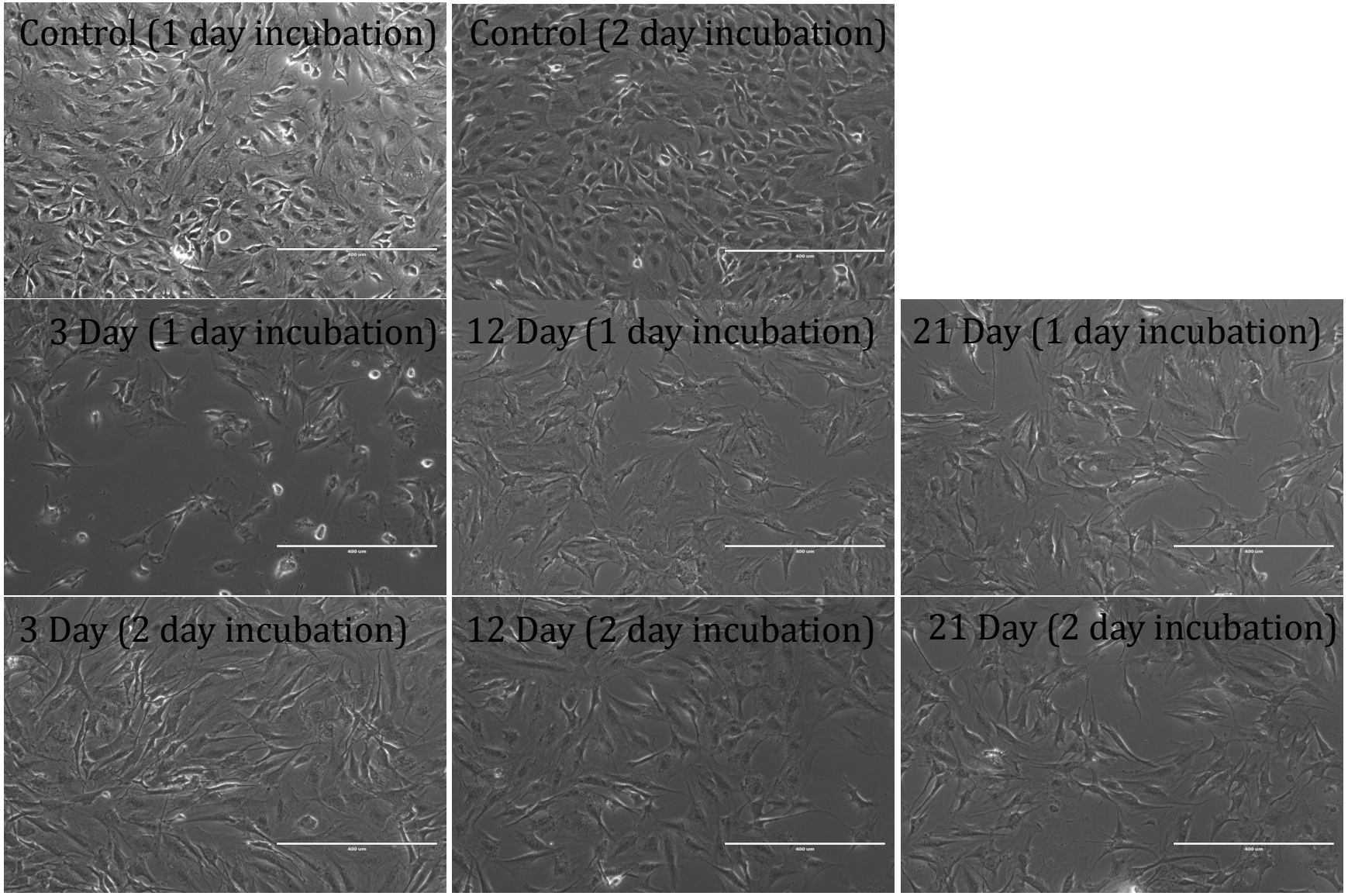

Figure 56 Effect of AZ31 untreated alloys on MC3T3 cells

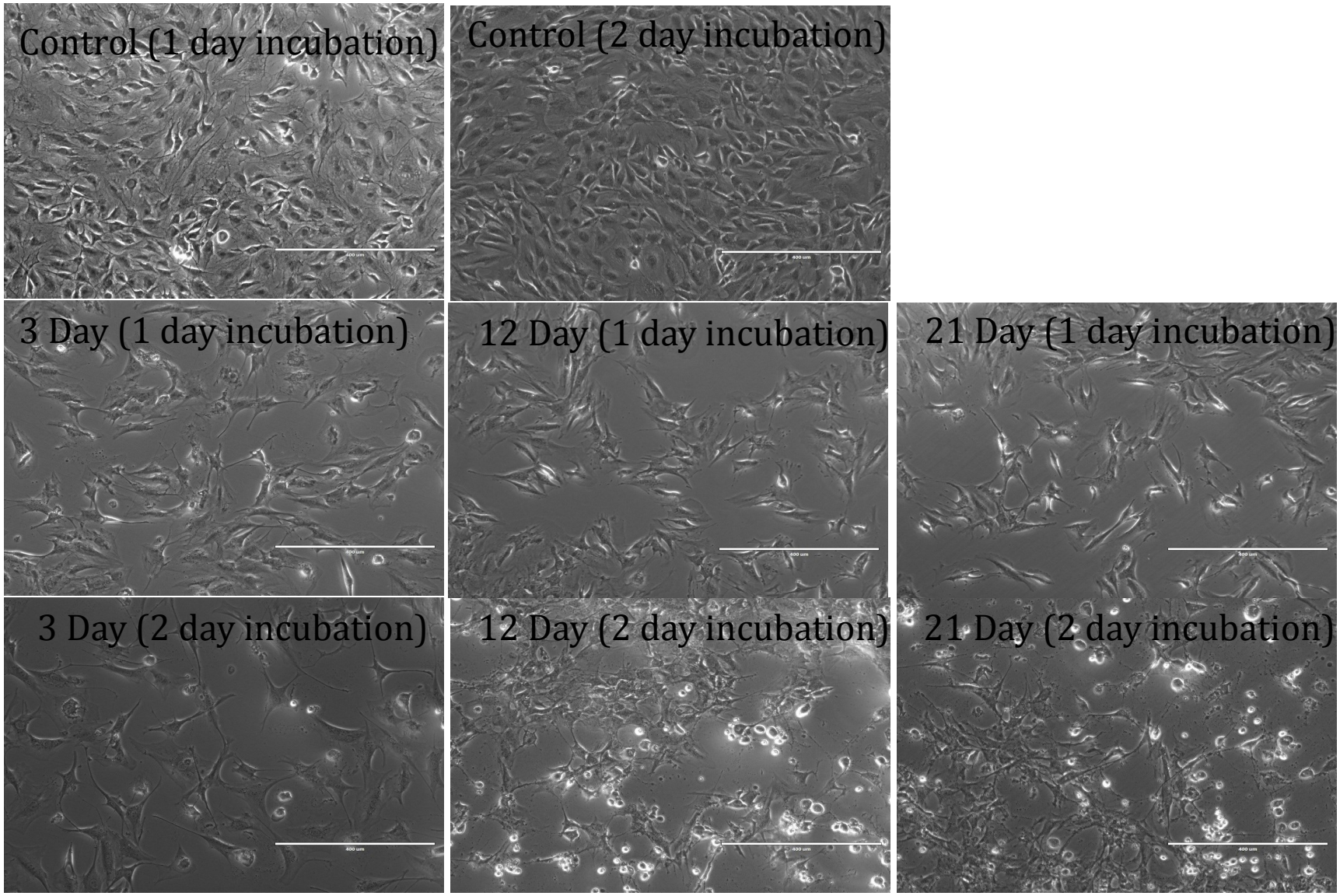

Figure 57. Effect of AZ31 anodized alloys on MC3T3 cells

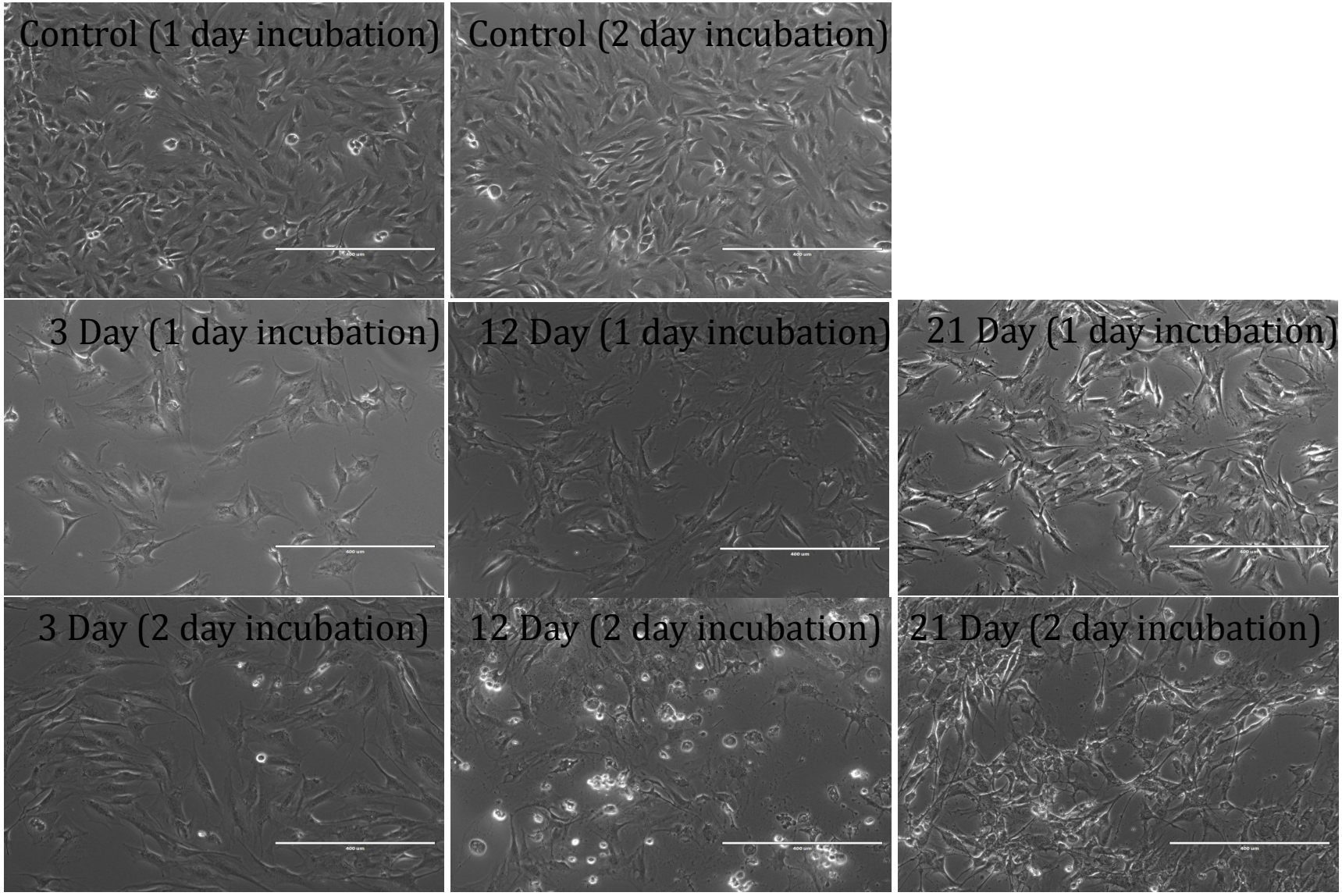

Figure 58. Effect of AZ91 untreated alloys on MC3T3 cells

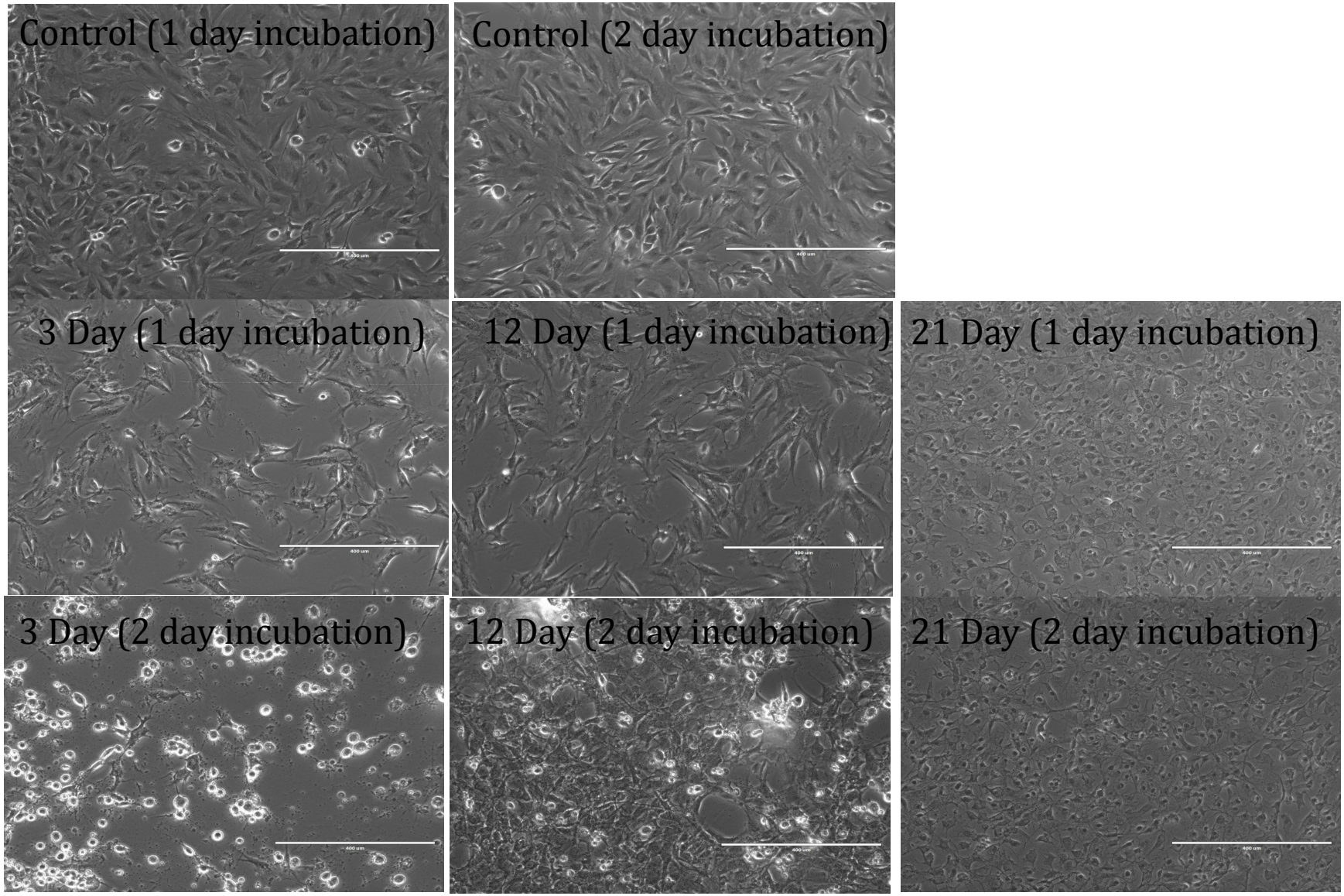

Figure 59. Effect of AZ91 anodized alloys on MC3T3 cells

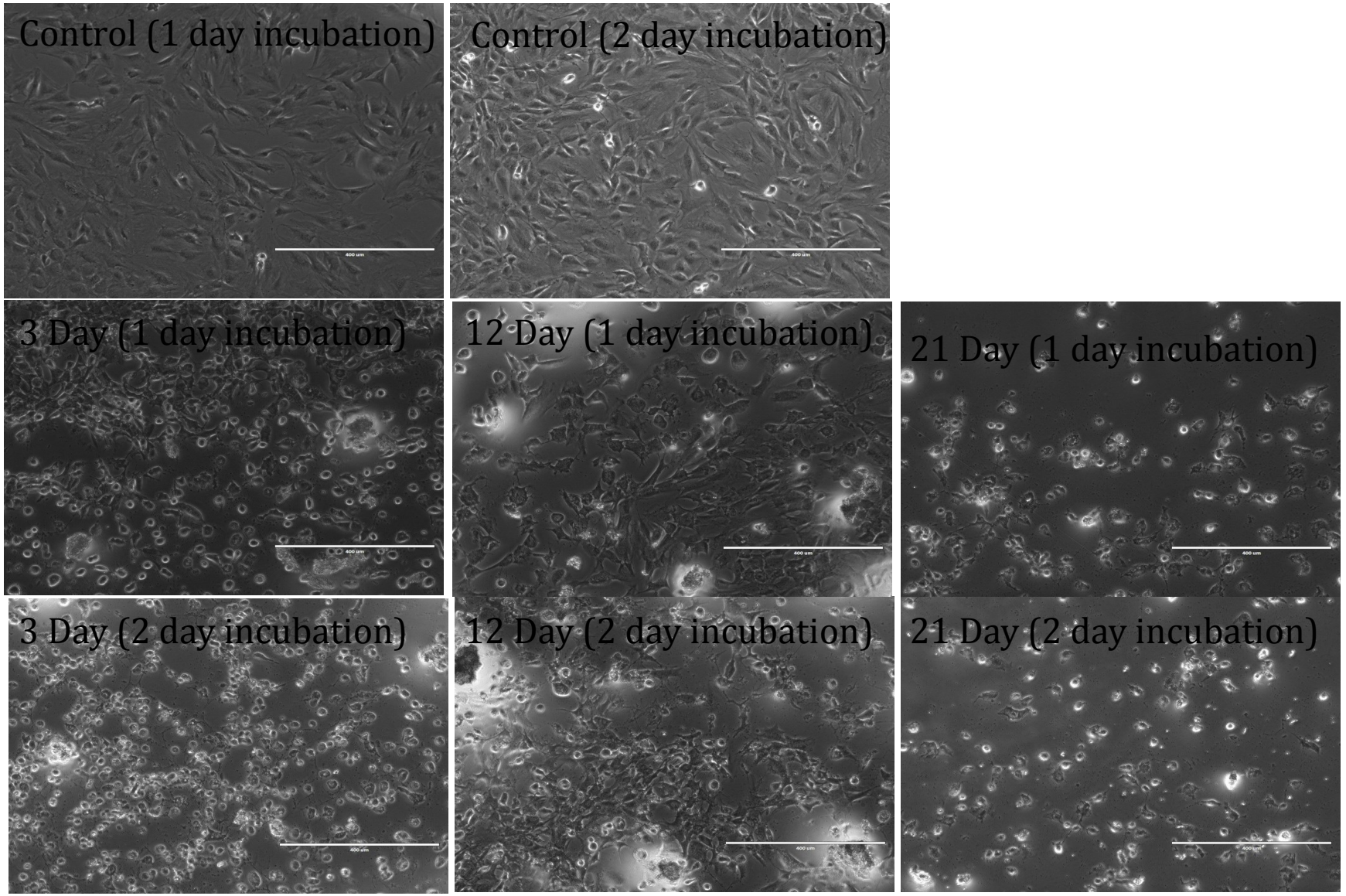

Figure 60. Effect of ZK60 untreated alloys on MC3T3 cells

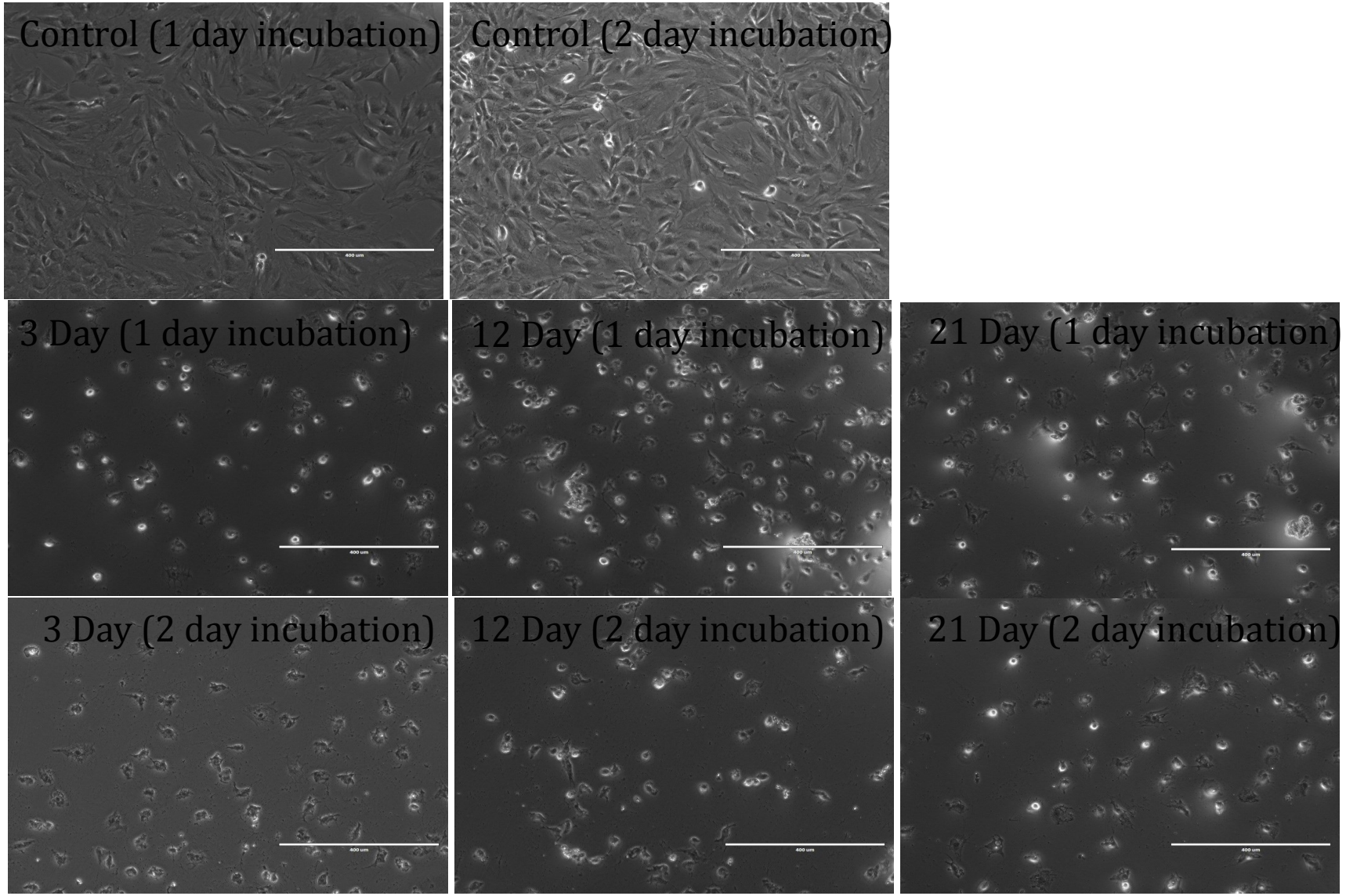

Figure 61. Effect of ZK60 anodized alloys on MC3T3 cells

4.5.2 Direct Cell Viability

The determination of endogenous intercellular signaling is related to the cell population and the surrounding environments. To mimic the natural tissue (bone) healing environment, and to optimize constituents for an engineered material as bone substitute it is important to take in consideration endogenous signaling profiles between cell populations (153). Cell density can alter the cell-cell distance. As a result, the cell density can be a critical parameter controlling subsequent cell proliferation due to in paracrine signaling distance among cells (153).

In direct viability experiments, cell are exposed or grown on top of the surface of materials. In order to evaluate the osteoblast cell proliferation, magnesium specimens were disinfected with pure ethanol, and exposed to UV light for 15 minutes. The initial cell attachment, and cell viability of the MC3T3 osteoblast cells on magnesium specimens was assessed by implementing standardization experiment trials more than three times. A different number of cell densities was seeded on samples in order to evaluate the cell proliferation. Throughout the standardization procedure it was observed that the cell density would influence the cell viability on MC3T3. After the cell seeding density was successfully studied, the cell proliferation on samples was recorded. Cells were seeded ($70x10^4$ cells) to an exposed area of 1 cm^2. The samples were incubated for 24 hours. Soon after the incubation procedure, live cell staining was assessed by adding NucBlue® (Hoechst dye) substance. Hoechst die was used to highlight the nuclei of the cells. After 25 minutes of incubation, the media was removed from the samples for the live fluorescent imaging procedure. Figures 63-65 shows the fluorescent optical images of the magnesium specimens with adherent cells. Glass control substrates were prepared to differentiate between the influences of elemental concentration and corrosion rates of

magnesium specimens on cell morphology and viability. Figure 62 shows stained cells on a glass slide as the control sample.

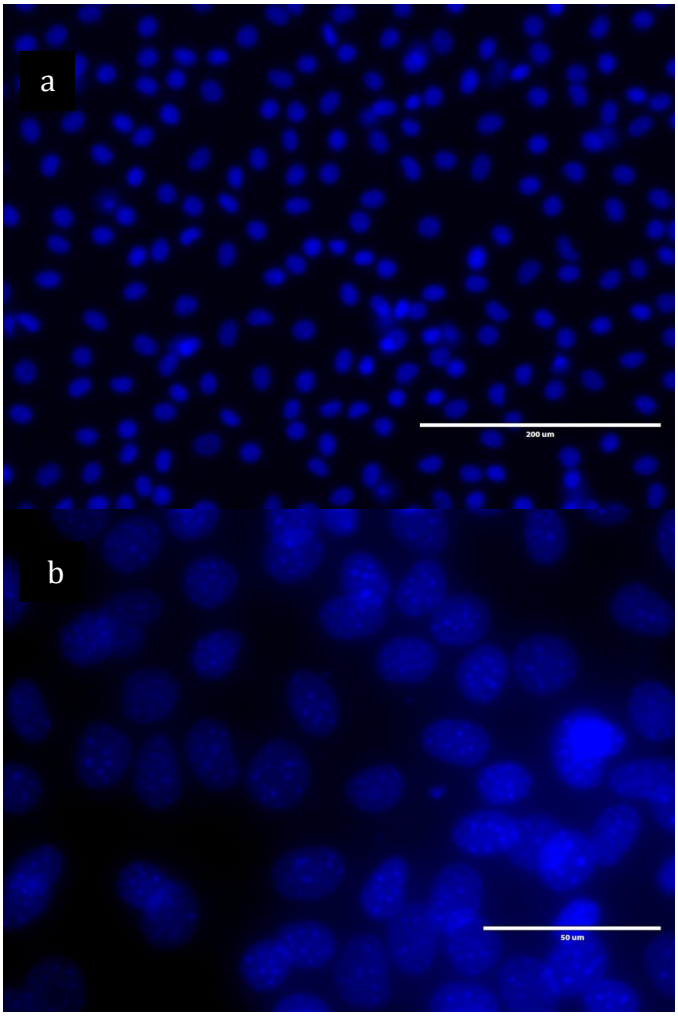

Figure 62. Healthy cell nuclei morphology a) 20X and b) 60X mag.

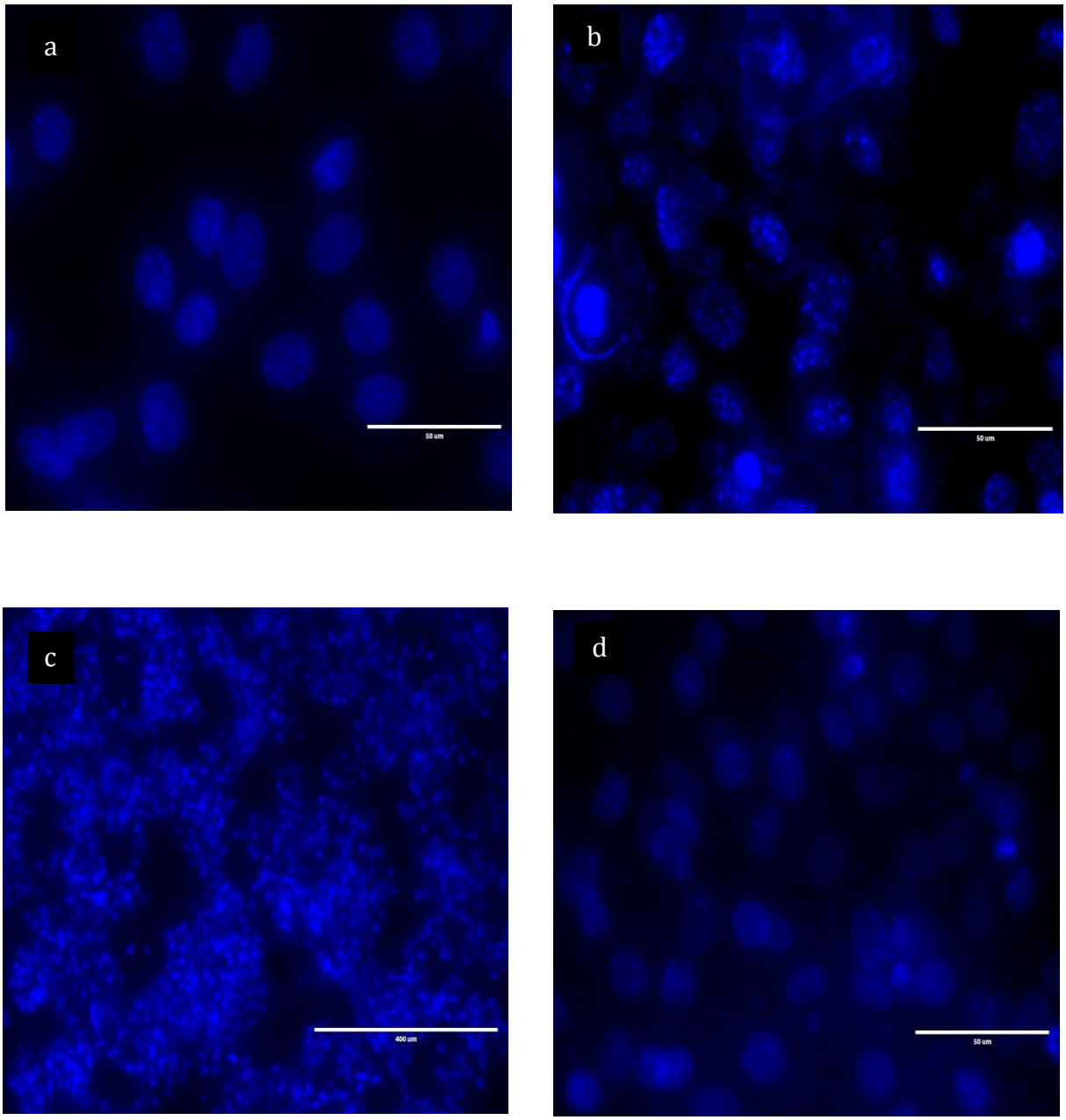

Figure 63. MC3T3 cells on AZ31 specimens a) untreated, b) anodized, c) HA, and d) PVB

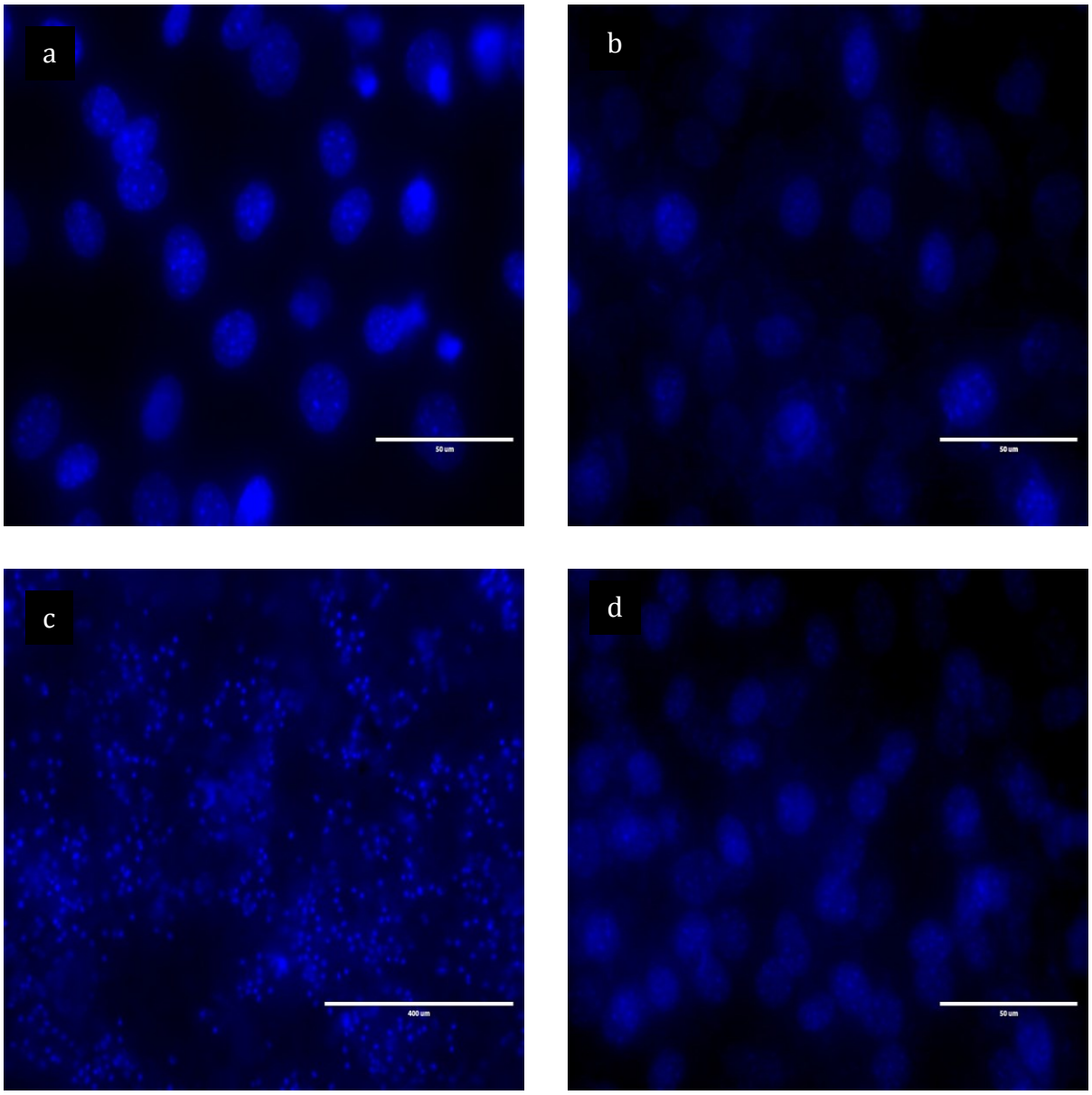

Figure 64. MC3T3 cells on AZ91 specimens a) untreated, b) anodized, c) HA, and d) PVB

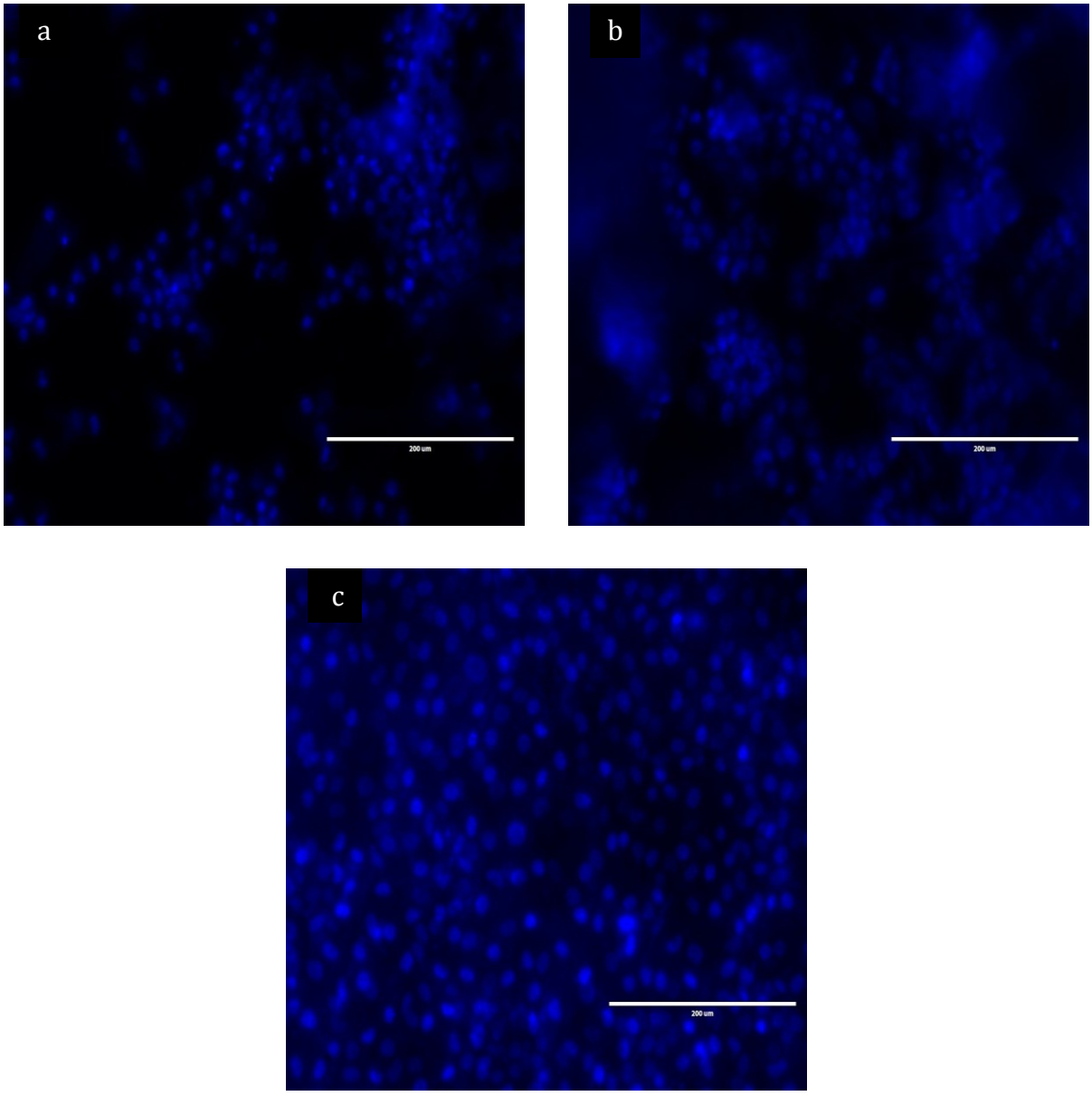

Figure 65. MC3T3 cells on ZK60 specimens a) untreated, b) anodized, c) PVB

CHAPTER V

CONCLUSIONS

Magnesium alloys as biocompatible and degradable materials, have demonstrated to be promising materials for developing future medical implants. Microstructure, corrosion behavior, and degradation characteristics play an important role for the development of efficient biodegradable implant materials focusing on magnesium and its alloys. Corrosion resistance of biodegradable magnesium alloys need to be monitor under physiological conditions in order to be improved for prevalent use as a potential implant.

A complete surface characterization is important in order to learn and understand surfaces before the actual implant use. Critical factors such as surface treatment morphology, surface roughness, surface chemistry, contact angle, and adhesion properties were studied.

The selection of alloying elements and surface modifications can successfully deliver the opportunity to design and develop Mg alloys with mechanical properties and controlled biodegradation profile that can be employed in a specific biomedical application. However, an important aspect related to biodegradable magnesium implants is the difficulty to avoid high rate of corrosion for a bare alloy surface; therefore surface engineering modifications are convenient methods to further control corrosion and degradation mechanisms.

The aim of this thesis work was to modify magnesium alloys via surface treatments and to explore the corrosion behavior in body simulated fluids implementing three electrochemical corrosion tests: potentiodynamic polarization, electrochemical impedance spectroscopy and in-

laboratory immersion tests. Compared to magnesium substrates (AZ31A, AZ91B, and ZK60A), the electrochemical treatment (anodization), decreased the corrosion rate and had a higher corrosion resistance for all treated alloys. Moreover, the calcium phosphate ceramic (hydroxyapatite) coating via plasma spraying increased corrosion rate and decreased corrosion resistance of all coated samples. The synthetic polymer PVB had a significant impact by protecting magnesium substrates against corrosion. The corrosion rate decreased, and it was obtained the lowest corrosion rate against the other surface modifications. The EIS evaluations demonstrated that the PVB coated protected magnesium alloys against the formation of any pits.

The current trend is the use of magnesium alloys as a new class of metallic biomaterials, partly, due to their capability of yielding a non-toxic corrosion product. The idea is to exploit the degradation and the inert reduction/reaction of the magnesium alloys with the perspective of developing bioabsorbable implants. This should be accomplished while presenting no adverse effects, such as the production of toxic bi-products.

This work also examined the biological performance of the different grades of magnesium alloys. Direct and in-direct cell viability practices were assessed in order to study the biocompatibility of the treated and untreated alloys. The applied viability studies indicated a good cytocompatibility. However, challenges in biomedical evaluations consist of several trials to establish the long term biocompatibility of magnesium based alloys and their corrosion products within the body, therefore further biocompatibility studies should be still performed.

REFERENCES

1. Ratner BD, Hoffman AS, Schoen FJ, Lemons J. Biomaterials Science : A Multidisciplinary Endeavor. Biomaterials Science. 2004. p. 1–20.

2. Long M, Rack HJ. Titanium alloys in total joint replacement—a materials science perspective. Biomaterials. 1998;19:1621–39.

3. Patel NR, Gohil PP. A Review on Biomaterials : Scope , Applications & Human Anatomy Significance. 2012;2(4).

4. Geetha M, Singh AK, Asokamani R, Gogia AK. Ti based biomaterials, the ultimate choice for orthopaedic implants - A review. Progress in Materials Science. 2009. p. 397–425.

5. Fries RC. Biomaterials--The Intersection of Biology and Materials Science (Temenoff, J.S. et al.; 2008) [Book reviews]. IEEE Eng Med Biol Mag. 2009;28.

6. Nasab MB, Hassan MR. Metallic biomaterials of knee and hip - A review. Trends Biomater Artif Organs [Internet]. 2010;24:69–82. Available from: http://www.sbaoi.org

7. Qin FX, Wang XM, Inoue A. Effects of Ta on Microstructure and Mechanical Property of Ti-Zr-Cu-Pd-Ta Alloys. MATERIALS TRANSACTIONS. 2007. p. 2390–4.

8. Moravej M, Mantovani D. Biodegradable metals for cardiovascular stent application: interests and new opportunities. Int J Mol Sci. 2011;12:4250–70.

9. Fadlallah SA, El-Bagoury N, Gad El-Rab SMF, Ahmed RA, El-Ousamii G. An overview of NiTi shape memory alloy: Corrosion resistance and antibacterial inhibition for dental application. J Alloys Compd. 2014;583:455–64.

10. Prymak O, Klocke A, Kahl-Nieke B, Epple M. Fatigue of orthodontic nickel-titanium (NiTi) wires in different fluids under constant mechanical stress. Mater Sci Eng A. 2004;378:110–4.

11. Meyers MA, Chen P-Y, Lin AY-M, Seki Y. Biological materials: Structure and mechanical properties. Progress in Materials Science. 2008. p. 1–206.

12. Elias CN, Lima JHC, Valiev R, Meyers MA. Biomedical Applications of Titanium and its Alloys. J Miner Met Mater Soc. 2008;46–9.

13. Thompson SA. An overview of nickel-titanium alloys used in dentistry. Int Endod J. 2000;33:297–310.

14. Srivastav A. An Overview of Metallic Biomaterials for Bone Support and Replacement. 2004;

15. Hryniewicz T, Rokosz K, Filippi M. Biomaterial Studies on AISI 316L Stainless Steel after Magnetoelectropolishing. Materials. 2009. p. 129–45.

16. Bauer S, Schmuki P, von der Mark K, Park J. Engineering biocompatible implant surfaces. Part I: Materials and surfaces. Progress in Materials Science. 2012;

17. Science H, Hermawan H, Ramdan D, Djuansjah JRP. Metals for Biomedical Applications. 2009;

18. Sáenz A, Rivera-muñoz E, Brostow W, Castaño VM, Física E De, Rica UDC, et al. CERAMIC BIOMATERIALS : AN INTRODUCTORY OVERVIEW. 1999;21:297–306.

19. Thamaraiselvi T V, Rajeswari S. Biological Evaluation of Bioceramic Materials - A Review. 2004;18(1):9–17.

20. Weiler A, Hoffmann RFG, Sta AC. Biodegradable Implants in Sports Medicine : The Biological Base. 2000;16(3):305–21.

21. Middleton JC, Tipton a J. Synthetic biodegradable polymers as orthopedic devices. Biomaterials [Internet]. 2000 Dec;21(23):2335–46. Available from: http://www.ncbi.nlm.nih.gov/pubmed/11055281

22. Tamai H, Igaki K, Kyo E, Kosuga K, Kawashima A, Matsui S, et al. Initial and 6-month results of biodegradable poly-l-lactic acid coronary stents in humans. Circulation. 2000;102:399–404.

23. Nair LS, Laurencin CT. Polymers as biomaterials for tissue engineering and controlled drug delivery. Adv Biochem Eng Biotechnol. 2006;102:47–90.

24. Hanada K, Matsuzaki K, Huang X, Chino Y. Fabrication of Mg alloy tubes for biodegradable stent application. Mater Sci Eng C Mater Biol Appl [Internet]. Elsevier B.V.; 2013 Dec 1 [cited 2014 Jan 22];33(8):4746–50. Available from: http://www.ncbi.nlm.nih.gov/pubmed/24094183

25. Salahshoor M, Guo Y. Biodegradable Orthopedic Magnesium-Calcium (MgCa) Alloys, Processing, and Corrosion Performance. Materials (Basel) [Internet]. 2012 Jan 9 [cited 2014 Feb 17];5(12):135–55. Available from: http://www.mdpi.com/1996-1944/5/1/135/

26. Zhang E, Xu L, Yu G, Pan F, Yang K. In vivo evaluation of biodegradable magnesium alloy bone implant in the first 6 months implantation. J Biomed Mater Res A [Internet].

2009 Sep 1 [cited 2014 Jan 30];90(3):882–93. Available from: http://www.ncbi.nlm.nih.gov/pubmed/18618719

27. Fekry AM. Electrochemical Corrosion Behavior of Magnesium Alloys in Biological Solutions. 2009;

28. Wang J, Tang J, Zhang P, Li Y, Wang J, Lai Y, et al. Surface modification of magnesium alloys developed for bioabsorbable orthopedic implants: a general review. J Biomed Mater Res B Appl Biomater [Internet]. 2012 Aug [cited 2014 Feb 17];100(6):1691–701. Available from: http://www.ncbi.nlm.nih.gov/pubmed/22566412

29. Wu G, Ibrahim JM, Chu PK. Surface design of biodegradable magnesium alloys — A review. Surf Coatings Technol [Internet]. Elsevier B.V.; 2013 Oct [cited 2014 Feb 4];233:2–12. Available from: http://linkinghub.elsevier.com/retrieve/pii/S0257897212009437

30. Walter R, Kannan MB, He Y, Sandham a. Effect of surface roughness on the in vitro degradation behaviour of a biodegradable magnesium-based alloy. Appl Surf Sci [Internet]. 2013 Aug [cited 2014 Mar 6];279:343–8. Available from: http://linkinghub.elsevier.com/retrieve/pii/S0169433213008003

31. Walker R. Principles and prevention of corrosion. Materials & Design. 1993. p. 207.

32. Dinodi N, Shetty AN. Electrochemical investigations on the corrosion behaviour of magnesium alloy ZE41 in a combined medium of chloride and sulphate. J Magnes Alloy [Internet]. Elsevier Ltd; 2013;41:1–9. Available from: http://dx.doi.org/10.1016/j.jma.2013.08.003

33. Shaw BA. Corrosion Resistance of Magnesium Alloys. 2003;13.

34. Staiger MP, Pietak AM, Huadmai J, Dias G. Magnesium and its alloys as orthopedic biomaterials: a review. Biomaterials. 2006;27:1728–34.

35. Wang L, Shinohara T, Zhang B-P. Influence of Deaerated Condition on the Corrosion Behavior of AZ31 Magnesium Alloy in Dilute NaCl Solutions. Mater Trans [Internet]. 2009 [cited 2014 Apr 3];50(11):2563–9. Available from: http://joi.jlc.jst.go.jp/JST.JSTAGE/matertrans/M2009191?from=CrossRef

36. Song G. Control of biodegradation of biocompatable magnesium alloys. Corrosion Science. 2007. p. 1696–701.

37. González S, Pellicer E, Suriñach S, Baró MD, Sort J. Biodegradation and Mechanical Integrity of Magnesium and Magnesium Alloys Suitable for Implants. 2013;

38. Song GL, Atrens A. Corrosion Mechanisms of Magnesium Alloys. Adv Eng Mater [Internet]. 1999;1:11–33. Available from: http://doi.wiley.com/10.1002/(SICI)1527-2648(199909)1:1<11::AID-ADEM11>3.0.CO;2-N

39. Zeng R, Dietzel W, Witte F, Hort N, Blawert C. Progress and Challenge for Magnesium Alloys as Biomaterials. Adv Eng Mater [Internet]. 2008;10:B3–B14. Available from: http://dx.doi.org/10.1002/adem.200800035

40. ZENG R, ZHANG J, HUANG W, DIETZEL W, KAINER KU, BLAWERT C, et al. Review of studies on corrosion of magnesium alloys. Transactions of Nonferrous Metals Society of China. 2006. p. s763–s771.

41. Badawy WA, Hilal NH, El-Rabiee M, Nady H. Electrochemical behavior of Mg and some Mg alloys in aqueous solutions of different pH. Electrochim Acta. 2010;55:1880–7.

42. Yao HB, Li Y, Wee ATS. XPS investigation of the oxidation/corrosion of melt-spun Mg. Appl Surf Sci. 2000;158:112–9.

43. Eddy Jai Poinern G, Brundavanam S, Fawcett D. Biomedical Magnesium Alloys: A Review of Material Properties, Surface Modifications and Potential as a Biodegradable Orthopaedic Implant. Am J Biomed Eng [Internet]. 2013 Jan 7 [cited 2014 Feb 7];2(6):218–40. Available from: http://article.sapub.org/10.5923.j.ajbe.20120206.02.html

44. Witte F, Fischer J, Nellesen J, Crostack H-A, Kaese V, Pisch A, et al. In vitro and in vivo corrosion measurements of magnesium alloys. Biomaterials [Internet]. 2006 Mar [cited 2014 Feb 10];27(7):1013–8. Available from: http://www.ncbi.nlm.nih.gov/pubmed/16122786

45. Witte F, Kaese V, Haferkamp H, Switzer E, Meyer-Lindenberg a, Wirth CJ, et al. In vivo corrosion of four magnesium alloys and the associated bone response. Biomaterials [Internet]. 2005 Jun [cited 2014 Feb 21];26(17):3557–63. Available from: http://www.ncbi.nlm.nih.gov/pubmed/15621246

46. Zhang L-N, Hou Z-T, Ye X, Xu Z-B, Bai X-L, Shang P. The effect of selected alloying element additions on properties of Mg-based alloy as bioimplants: A literature review. Front Mater Sci [Internet]. 2013 Jul 20 [cited 2014 Mar 7];7(3):227–36. Available from: http://link.springer.com/10.1007/s11706-013-0210-z

47. ASTM Standard B951. Standard Practice for Codification of Unalloyed Magnesium and Magnesium-Alloys, Cast and Wrought. ASTM Int. 2008;

48. Wu BL, Zhao YH, Du XH, Zhang YD, Wagner F, Esling C. Ductility enhancement of extruded magnesium via yttrium addition. Mater Sci Eng A. 2010;527:4334–40.

49. Reifenrath J, Bormann D, Meyer-lindenberg A. Magnesium Alloys as Promising Degradable Implant Materials in Orthopaedic Research. 2010;

50. Mushahary D, Sravanthi R, Li Y, Kumar MJ, Harishankar N, Hodgson PD, et al. Zirconium , calcium , and strontium contents in magnesium based biodegradable alloys modulate the efficiency of implant-induced osseointegration. 2013;2887–902.

51. Li Y, Wen C, Mushahary D, Sravanthi R, Harishankar N, Pande G, et al. Mg-Zr-Sr alloys as biodegradable implant materials. Acta Biomater [Internet]. Acta Materialia Inc.; 2012 Aug [cited 2014 Mar 5];8(8):3177–88. Available from: http://www.ncbi.nlm.nih.gov/pubmed/22531570

52. Gu XN, Xie XH, Li N, Zheng YF, Qin L. In vitro and in vivo studies on a Mg – Sr binary alloy system developed as a new kind of biodegradable metal. 2012;8:2360–74.

53. Yang Z, Li J, Zhang J, Lorimer G, Robson J. Review on Research and Development of Magnesium Alloys. Acta Metall Sin (English Lett [Internet]. 2008 Oct;21(5):313–28. Available from: http://linkinghub.elsevier.com/retrieve/pii/S100671910860054X

54. Persaud-Sharma D, McGoron A. Biodegradable Magnesium Alloys: A Review of Material Development and Applications. Journal of Biomimetics, Biomaterials, and Tissue Engineering. 2012. p. 25–39.

55. Yoshimoto S, Yamasaki M, Kawamura Y. Microstructure and Mechanical Properties of Extruded Mg-Zn-Y Alloys with 14H Long Period Ordered Structure Tensile Strength , σ / MPa. 2006;47(4):959–65.

56. Rho JY, Ashman RB, Turner CH. Young's modulus of trabecular and cortical bone material: Ultrasonic and microtensile measurements. J Biomech [Internet]. 1993 Feb;26(2):111–9. Available from: http://linkinghub.elsevier.com/retrieve/pii/002192909390042D

57. Zhang S, Zhang X, Zhao C, Li J, Song Y, Xie C, et al. Research on an Mg-Zn alloy as a degradable biomaterial. Acta Biomater [Internet]. Acta Materialia Inc.; 2010 Feb [cited 2014 Mar 6];6(2):626–40. Available from: http://www.ncbi.nlm.nih.gov/pubmed/19545650

58. Tapiero H, Tew KD. Trace elements in human physiology and pathology: zinc and metallothioneins. Biomed Pharmacother [Internet]. 2003 Nov [cited 2014 Mar 7];57(9):399–411. Available from: http://linkinghub.elsevier.com/retrieve/pii/S0753332203000817

59. Kim W-C, Kim J-G, Lee J-Y, Seok H-K. Influence of Ca on the corrosion properties of magnesium for biomaterials. Mater Lett [Internet]. 2008 Sep [cited 2014 Mar 7];62(25):4146–8. Available from: http://linkinghub.elsevier.com/retrieve/pii/S0167577X08005703

60. Drynda A, Hassel T, Hoehn R, Perz A, Bach F-W, Peuster M. Development and biocompatibility of a novel corrodible fluoride-coated magnesium-calcium alloy with

improved degradation kinetics and adequate mechanical properties for cardiovascular applications. J Biomed Mater Res A [Internet]. 2010 May [cited 2014 Mar 7];93(2):763–75. Available from: http://www.ncbi.nlm.nih.gov/pubmed/19653306

61. Wan Y, Xiong G, Luo H, He F, Huang Y, Zhou X. Preparation and characterization of a new biomedical magnesium–calcium alloy. Mater Des [Internet]. 2008 Dec [cited 2014 Mar 7];29(10):2034–7. Available from: http://linkinghub.elsevier.com/retrieve/pii/S0261306908000927

62. ESSENTIAL NUTRIENTS - MINERALS. Available from: http://www.fao.org/docrep/field/003/ab470e/ab470e06.htm

63. Shabestari SG. The effect of iron and manganese on the formation of intermetallic compounds in aluminum–silicon alloys. Mater Sci Eng A [Internet]. 2004 Oct [cited 2014 Feb 25];383(2):289–98. Available from: http://linkinghub.elsevier.com/retrieve/pii/S0921509304008329

64. Fraga CG. Relevance, essentiality and toxicity of trace elements in human health. Mol Aspects Med [Internet]. 2005 [cited 2014 Mar 7];26(4-5):235–44. Available from: http://www.ncbi.nlm.nih.gov/pubmed/16125765

65. Cao P, Qian M, StJohn DH. Effect of iron on grain refinement of high-purity Mg–Al alloys. Scr Mater [Internet]. 2004 Jul [cited 2014 Mar 7];51(2):125–9. Available from: http://linkinghub.elsevier.com/retrieve/pii/S1359646204001873

66. Mordike BL, Ebert T. Magnesium Properties — applications — potential. 2001;302:37–45.

67. Busk RS, Head H, Carolina S. CHAPTER 8 MAGNESIUM AND ITS ALLOYS. 2002;

68. Fu S. Review on research and development of heat resistant Magnesium alloy. 2012;(Mems):611–4.

69. Boehlert CJ, Knittel K. The microstructure, tensile properties, and creep behavior of Mg–Zn alloys containing 0–4.4wt.% Zn. Mater Sci Eng A [Internet]. 2006 Feb [cited 2014 Feb 8];417(1-2):315–21. Available from: http://linkinghub.elsevier.com/retrieve/pii/S0921509305014012

70. Jain C-C, Koo C-H. Creep and Corrosion Properties of the Extruded Magnesium Alloy Containing Rare Earth. Mater Trans [Internet]. 2007 [cited 2014 Feb 4];48(2):265–72. Available from: http://joi.jlc.jst.go.jp/JST.JSTAGE/matertrans/48.265?from=CrossRef

71. Huang ZH, Qi WJ, Zheng KH, Zhang XM, Liu M, Yu ZM, et al. Microstructures and mechanical properties of Mg – Zn – Zr – Dy. 2013;36(3):437–45.

72. Lei X, Liu T, Chen J, Miao B, Zeng W. Microstructure and Mechanical Properties of Magnesium Alloy AZ31 Processed by Compound Channel Extrusion. Mater Trans [Internet]. 2011 [cited 2014 Mar 7];52(6):1082–7. Available from: http://joi.jlc.jst.go.jp/JST.JSTAGE/matertrans/MC201004?from=CrossRef

73. Trzaska M. Studies of Resistance to Corrosion of Selected Metallic Materials Using Electrochemical Methods. 2010;

74. Müller WD, Nascimento ML, Zeddies M, Córsico M, Gassa LM, Mele MAFL de. Magnesium and its alloys as degradable biomaterials: corrosion studies using potentiodynamic and EIS electrochemical techniques. Materials Research. 2007.

75. Yang J, Cui F, Lee IS. Surface modifications of magnesium alloys for biomedical applications. Ann Biomed Eng [Internet]. 2011 Jul [cited 2014 Mar 7];39(7):1857–71. Available from: http://www.ncbi.nlm.nih.gov/pubmed/21445692

76. Abela IS. Protective Coatings for Magnesium Alloys. 2012;(December 1999).

77. Nassif N, Ghayad I. Corrosion Protection and Surface Treatment of Magnesium Alloys Used for Orthopedic Applications. 2013;2013.

78. Xu R, Yang X, Suen KW, Wu G, Li P, Chu PK. Applied Surface Science Improved corrosion resistance on biodegradable magnesium by zinc and aluminum ion implantation Atomic Concentration (%). 2012;263:608–12.

79. Shadanbaz S, Dias GJ. Calcium phosphate coatings on magnesium alloys for biomedical applications: a review. Acta Biomater [Internet]. Acta Materialia Inc.; 2012 Jan [cited 2014 Jan 29];8(1):20–30. Available from: http://www.ncbi.nlm.nih.gov/pubmed/22040686

80. Cui F, Yang J, Jiao Y, Yin Q, Zhang Y, Lee I-S. Calcium phosphate coating on magnesium alloy for modification of degradation behavior. Front Mater Sci China [Internet]. 2008 Jun 6 [cited 2014 Feb 26];2(2):143–8. Available from: http://link.springer.com/10.1007/s11706-008-0024-6

81. Gadow R, Killinger a., Stiegler N. Hydroxyapatite coatings for biomedical applications deposited by different thermal spray techniques. Surf Coatings Technol [Internet]. Elsevier B.V.; 2010 Nov [cited 2014 Mar 7];205(4):1157–64. Available from: http://linkinghub.elsevier.com/retrieve/pii/S0257897210002628

82. Orlovskii VP, Komlev VS, Barinov SM. Hydroxyapatite and Hydroxyapatite-Based Ceramics. Inorg Mater [Internet]. 2002;38:973–84. Available from: http://dx.doi.org/10.1023/A:1020585800572

83. Xu L, Zhang E, Yang K. Biocorrosion property and cytocompatibility of calcium phosphate coated Mg alloy. Trans Nonferrous Met Soc China [Internet]. 2012 Aug [cited

2014 Mar 7];22(8):2014–20. Available from: http://linkinghub.elsevier.com/retrieve/pii/S1003632611614222

84. Murakami K, Hino M, Nakai K, Kobayashi S, Saijo A, Kanadani T. Mechanism of Corrosion Protection of Anodized Magnesium Alloys. Mater Trans [Internet]. 2008 [cited 2014 Mar 7];49(5):1057–64. Available from: http://joi.jlc.jst.go.jp/JST.JSTAGE/matertrans/MC200718?from=CrossRef

85. Li N, Zheng Y. Novel Magnesium Alloys Developed for Biomedical Application : A Review. J Mater Sci Technol [Internet]. Elsevier Ltd; 2013;29(6):489–502. Available from: http://dx.doi.org/10.1016/j.jmst.2013.02.005

86. Gu X, Zheng Y, Cheng Y, Zhong S, Xi T. In vitro corrosion and biocompatibility of binary magnesium alloys. Biomaterials. 2009;30:484–98.

87. Li Z, Gu X, Lou S, Zheng Y. The development of binary Mg-Ca alloys for use as biodegradable materials within bone. Biomaterials. 2008;29:1329–44.

88. Gu XN, Li XL, Zhou WR, Cheng Y, Zheng YF. Microstructure, biocorrosion and cytotoxicity evaluations of rapid solidified Mg–3Ca alloy ribbons as a biodegradable material. Biomedical Materials. 2010. p. 035013.

89. Zhang E, Yang L. Microstructure, mechanical properties and bio-corrosion properties of Mg-Zn-Mn-Ca alloy for biomedical application. Mater Sci Eng A. 2008;497:111–8.

90. Zhang B, Hou Y, Wang X, Wang Y, Geng L. Mechanical properties, degradation performance and cytotoxicity of Mg-Zn-Ca biomedical alloys with different compositions. Mater Sci Eng C. 2011;31:1667–73.

91. Witte F, Ulrich H, Rudert M, Willbold E. Biodegradable magnesium scaffolds: Part 1: appropriate inflammatory response. J Biomed Mater Res A. 2007;81:748–56.

92. Witte F, Ulrich H, Palm C, Willbold E. Biodegradable magnesium scaffolds: Part II: peri-implant bone remodeling. J Biomed Mater Res A. 2007;81:757–65.

93. Windhagen H, Radtke K, Weizbauer A, Diekmann J, Noll Y, Kreimeyer U, et al. Biodegradable magnesium-based screw clinically equivalent to titanium screw in hallux valgus surgery: short term results of the first prospective, randomized, controlled clinical pilot study. Biomed Eng Online [Internet]. BioMedical Engineering OnLine; 2013 Jan [cited 2014 Feb 26];12(1):62. Available from: http://www.pubmedcentral.nih.gov/articlerender.fcgi?artid=3702514&tool=pmcentrez&rendertype=abstract

94. Erdmann N, Angrisani N, Reifenrath J, Lucas A, Thorey F, Bormann D, et al. Biomechanical testing and degradation analysis of MgCa0.8 alloy screws: A comparative in vivo study in rabbits. Acta Biomater. 2011;7:1421–8.

95. Kraus T, Fischerauer SF, Hänzi AC, Uggowitzer PJ, Löffler JF, Weinberg AM. Magnesium alloys for temporary implants in osteosynthesis: In vivo studies of their degradation and interaction with bone. Acta Biomater. 2012;8:1230–8.

96. Chen S, Guan S, Li W, Wang H, Chen J, Wang Y, et al. In vivo degradation and bone response of a composite coating on Mg-Zn-Ca alloy prepared by microarc oxidation and electrochemical deposition. J Biomed Mater Res B Appl Biomater [Internet]. 2011;533–43. Available from: http://www.ncbi.nlm.nih.gov/pubmed/22120974

97. ASTM. ASTM G102 - 89(2010) Standard Practice for Calculation of Corrosion Rates and Related Information from Electrochemical Measurements. Annual Book of ASTM Standards [Internet]. 2010. p. 1–7. Available from: http://www.astm.org/Standards/G102.htm

98. (G3-89) Standard Practice for Conventions Applicable to Electrochemical Measurements in Corrosion Testing.pdf.

99. (G31-72) Standard Practice for Laboratory Immersion Corrosion Testing of Metals.pdf.

100. Blawert C, Dietzel W, Ghali E, Song G. Anodizing Treatments for Magnesium Alloys and Their Effect on Corrosion Resistance in Various Environments. Adv Eng Mater [Internet]. 2006;8:511–33. Available from: http://dx.doi.org/10.1002/adem.200500257\nhttp://onlinelibrary.wiley.com/store/10.1002/adem.200500257/asset/511_ftp.pdf?v=1&t=hbd910v8&s=340f7fd21474edc9412b47f43ff6b8bd15c4bd6e

101. Tu X, Chen L, Shen J, Zhang Y, Miao C, Wu J. Effects of Sucrose on Anodized Film Formed on AZ31B Magnesium Alloy in Environmental-Friendly Electrolyte. 2012;7:9573–9.

102. Salman S a., Mori R, Ichino R, Okido M. Effect of Anodizing Potential on the Surface Morphology and Corrosion Property of AZ31 Magnesium Alloy. Mater Trans [Internet]. 2010 [cited 2014 Feb 24];51(6):1109–13. Available from: http://joi.jlc.jst.go.jp/JST.JSTAGE/matertrans/M2009380?from=CrossRef

103. Bansal NP, Singh JP, Schneider H. Innovative Processing and Synthesis of Ceramics, Glasses and Composites VIII: Proceedings of the 106th Annual Meeting of The American Ceramic Society. Ceram Trans wiley. 2004;166:223.

104. Ducheyne P, Beight J, Cuckler J, Evans B, Radin S. Effect of calcium phosphate coating characteristics on early post-operative bone tissue ingrowth. Biomaterials. 1990;11:531–40.

105. Ducheyne P, Qiu Q. Bioactive ceramics: The effect of surface reactivity on bone formation and bone cell function. Biomaterials. 1999. p. 2287–303.

106. Buma P, Van Loon PJM, Versleyen H, Weinans H, Slooff TJJH, De Groot K, et al. Histological and biomechanical analysis of bone and interface reactions around hydroxyapatite-coated intramedullary implants of different stiffness: A pilot study on the goat. Biomaterials. 1997;18:1251–60.

107. Song YW, Shan DY, Han EH. Electrodeposition of hydroxyapatite coating on AZ91D magnesium alloy for biomaterial application. Mater Lett. 2008;62:3276–9.

108. Mittal M, Nath SK, Prakash S. Characterization of Plasma Sprayed Hydroxyapatite Coatings on AISI 316L SS and Titanium Substrate and their Corrosion Behavior in Simulated Body Fluid. 2011;10(11):1041–9.

109. AYDIN E. BIODEGRADABLE POLYMER - HYDROXYAPATITE NANOCOMPOSITES FOR BONE PLATE APPLICATIONS. MIDDLE EAST TECHNICAL UNIVERSITY; 2010. p. 115.

110. Li JN, Cao P, Zhang XN, Zhang SX, He YH. In vitro degradation and cell attachment of a PLGA coated biodegradable Mg–6Zn based alloy. J Mater Sci [Internet]. 2010 Jun 15 [cited 2014 Apr 29];45(22):6038–45. Available from: http://link.springer.com/10.1007/s10853-010-4688-9

111. Chen Y, Song Y, Zhang S, Li J, Zhao C, Zhang X. Interaction between a high purity magnesium surface and PCL and PLA coatings during dynamic degradation. Biomed Mater. 2011;6:025005.

112. Ng WF, Wong MH, Cheng FT. Stearic acid coating on magnesium for enhancing corrosion resistance in Hanks' solution. Surf Coatings Technol. 2010;204:1823–30.

113. Gu XN, Zheng YF, Lan QX, Cheng Y, Zhang ZX, Xi TF, et al. Surface modification of an Mg-1Ca alloy to slow down its biocorrosion by chitosan. Biomed Mater. 2009;4:044109.

114. Gao JH, Shi XY, Yang B, Hou SS, Meng EC, Guan FX, et al. Fabrication and characterization of bioactive composite coatings on Mg-Zn-Ca alloy by MAO/sol-gel. J Mater Sci Mater Med. 2011;22:1681–7.

115. Wong HM, Yeung KWK, Lam KO, Tam V, Chu PK, Luk KDK, et al. A biodegradable polymer-based coating to control the performance of magnesium alloy orthopaedic implants. Biomaterials. 2010;31:2084–96.

116. AFM: Beginner's Guide. Available from: http://www.afmhelp.com/index.php?option=com_content&view=article&id=51:afm-beginners-guide&Itemid=57

117. L??pez-??lvarez M, Rodr??guez-Valencia C, Serra J, Gonz??lez P. Bio-inspired ceramics: Promising scaffolds for bone tissue engineering. Procedia Engineering. 2013. p. 51–8.

118. Ponsonnet L, Reybier K, Jaffrezic N, Comte V, Lagneau C, Lissac M, et al. Relationship between surface properties (roughness, wettability) of titanium and titanium alloys and cell behaviour. Mater Sci Eng C [Internet]. 2003 Jun [cited 2014 Jan 22];23(4):551–60. Available from: http://linkinghub.elsevier.com/retrieve/pii/S092849310300033X

119. Lacefield WR. Materials characteristics of uncoated/ceramic-coated implant materials. Adv Dent Res. 1999;13:21–6.

120. B Parekh R, Shetty O, Tabassum R. Surface Modifications for Endosseous Dental Implants. Mahesh L, editor. Int J Oral Implantol Clin Res [Internet]. 2012 Sep 15;3:116–21. Available from: http://www.jaypeejournals.com/eJournals/ShowText.aspx?ID=4329&Type=FREE&TYP=TOP&IN=~/eJournals/images/JPLOGO.gif&IID=337&isPDF=YES

121. Ungersb[illegible]k A, Rahn B. Methods to characterize the surface roughness of metallic implants. Journal of Materials Science: Materials in Medicine. 1994. p. 434–40.

122. Contact angle. Available from: http://www.attension.com/file/attensionan1-contact-angle-and-its measurement-techniques-250810.pdf

123. Yuan Y, Lee TR. Contact Angle and Wetting Properties. Surface Science Techniques [Internet]. 2013. p. 1–34. Available from: http://link.springer.com/10.1007/978-3-642-34243-1

124. Kyowa. Available from: http://www.face-kyowa.co.jp/english/en_products/en_contact_angle/detail-4/

125. Young T. An Essay on the Cohesion of Fluids. Philosophical Transactions of the Royal Society of London. 1805. p. 65–87.

126. Attension. Available from: http://www.attension.com/attensionan5-surfacfreeenergy-250810.pdf

127. Van Oss CJ, Chaudhury MK, Good RJ. Interfacial Lifshitz-van der Waals and polar interactions in macroscopic systems. Chem Rev [Internet]. 1988;88:927–41. Available from: http://pubs.acs.org/doi/abs/10.1021/cr00088a006

128. Ponsonnet L, Reybier K, Jaffrezic N, Comte V, Lagneau C, Lissac M, et al. Relationship between surface properties (roughness, wettability) of titanium and titanium alloys and cell behaviour. Mater Sci Eng C. 2003;23:551–60.

129. Subbiahdoss G, Grijpma DW, van der Mei HC, Busscher HJ, Kuijer R. Microbial biofilm growth versus tissue integration on biomaterials with different wettabilities and a polymer-brush coating. J Biomed Mater Res A. 2010;94:533–8.

130. Attension. Influence of topography and wettability on biocompatibility. Available from: http://www.attension.com/file/filarkiv/application-theory-notes/attensionan17roughbio.pdf

131. Attension. Influence of contact angles and surface free energies on biocompatibility of biomaterials. Available from: http://www.attension.com/file/filarkiv/application-theory-notes/attensionan4biomaterials.pdf

132. Adamson AW, Gast AP. Physical Chemistry of Surfaces Sixth Edition. SubStance. 1997;124:192C.

133. Zhu X, Chen J, Scheideler L, Reichl R, Geis-Gerstorfer J. Effects of topography and composition of titanium surface oxides on osteoblast responses. Biomaterials. 2004;25:4087–103.

134. Janssen MI, Van Leeuwen MBM, Van Kooten TG, De Vries J, Dijkhuizen L, Wösten HAB. Promotion of fibroblast activity by coating with hydrophobins in the β-sheet end state. Biomaterials. 2004;25:2731–9.

135. Gamry (Application-Notes). Available from: http://www.gamry.com/application-notes/potentiostat-fundamentals/

136. Enos DG, Scribner LL. The Potentiodynamic Polarization Scan The Potentiodynamic Polarization Scan Technical Report 33.

137. Electrochemistry P, Elements C, Equivalent C, Models C. Basics of Electrochemical Impedance Spectroscopy. Appl Note AC [Internet]. 2010;286:R491–7. Available from: http://scholar.google.com/scholar?hl=en&btnG=Search&q=intitle:Basics+of+Electrochemical+Impedance+Spectroscopy#2

138. Ates M. Review study of electrochemical impedance spectroscopy and equivalent electrical circuits of conducting polymers on carbon surfaces. Progress in Organic Coatings. 2011. p. 1–10.

139. Chang B-Y, Park S-M. Electrochemical Impedance Spectroscopy. Annual Review of Analytical Chemistry. 2010. p. 207–29.

140. Brasilien A, Naturwissenschaften D Der. Corrosion protection of magnesium AZ31 alloy sheets by polymer coatings. 2011;

141. Xin Y, Huo K, Tao H, Tang G, Chu PK. Influence of aggressive ions on the degradation behavior of biomedical magnesium alloy in physiological environment. Acta Biomater. 2008;4:2008–15.

142. Xin Y. Corrosion behavior of biomedical AZ91 magnesium alloy in. 2007;

143. Fischer J, Pröfrock D, Hort N, Willumeit R, Feyerabend F. Improved cytotoxicity testing of magnesium materials. Mater Sci Eng B [Internet]. Elsevier B.V.; 2011 Jun [cited 2014 Feb 26];176(11):830–4. Available from: http://linkinghub.elsevier.com/retrieve/pii/S0921510711001735

144. Sun Y, Kong MX, Jiao XH. In-vitro evaluation of Mg-4.0Zn-0.2Ca alloy for biomedical application. Trans Nonferrous Met Soc China (English Ed. 2011;21.

145. Niu J, Yuan G, Liao Y, Mao L, Zhang J, Wang Y, et al. Enhanced biocorrosion resistance and biocompatibility of degradable Mg-Nd-Zn-Zr alloy by brushite coating. Mater Sci Eng C. 2013;33:4833–41.

146. Gill P, Munroe N, Dua R, Ramaswamy S. Corrosion and Biocompatibility Assessment of Magnesium Alloys. 2012;2012(January):10–3.

147. Huan ZG, Leeflang MA, Zhou J, Fratila-Apachitei LE, Duszczyk J. In vitro degradation behavior and cytocompatibility of Mg-Zn-Zr alloys. J Mater Sci Mater Med. 2010;21:2623–35.

148. Hong D, Saha P, Chou D-T, Lee B, Collins BE, Tan Z, et al. In vitro degradation and cytotoxicity response of Mg-4% Zn-0.5% Zr (ZK40) alloy as a potential biodegradable material. Acta Biomater [Internet]. Acta Materialia Inc.; 2013 Nov [cited 2014 Feb 26];9(10):8534–47. Available from: http://www.ncbi.nlm.nih.gov/pubmed/23851175

149. Guan S, Hu J, Wang L, Zhu S, Wang H, Wang J, et al. Mg Alloys Development and Surface Modification for Biomedical Application. 2007;

150. Sittampalam GS, Gal-Edd N, Arkin M et al. Assay Guidance Manual. Eli Lilly & Company and the National Center for Advancing Translational Sciences; 2004.

151. Corporation P. Solution Cell Proliferation CellTiter 96 ® AQ ueous One Solution Cell Proliferation Assay.

152. EZ-Cytox Enhanced cell viability assay kit. Available from: http://www.itsbio.co.kr/main/goods_view.php?category2=57&no=119

153. Kim K (Fischell D of B. SCAFFOLD DESIGN PARAMETERS TO STIMULATE THE OSTEOGENIC SIGNAL EXPRESSION FOR BONE TISSUE ENGINEERING APPLICATIONS. University of Maryland; 2010.

APPENDIX A

APPENDIX A

ONE-WAY ANOVA STATISTICS FOR MTS CELL VIABILITY

One-way ANOVA: AZ31 Unt 50% cont, AZ31 50% 3day

Source	DF	SS	MS	F	P
Factor	1	1409.08	1409.08	281.71	0.000
Error	4	20.01	5.00		
Total	5	1429.09			

One-way ANOVA: AZ31 Unt 50% cont, AZ31 50% 6day

Source	DF	SS	MS	F	P
Factor	1	992.70	992.70	125.13	0.000
Error	4	31.73	7.93		
Total	5	1024.44			

One-way ANOVA: AZ31 Unt 50% cont, AZ31 50% 9 day

Source	DF	SS	MS	F	P
Factor	1	402.1	402.1	38.77	0.003
Error	4	41.5	10.4		
Total	5	443.6			

One-way ANOVA: AZ31 Unt 50% cont, AZ31 50% 12day

Source	DF	SS	MS	F	P
Factor	1	825	825	7.76	0.050
Error	4	425	106		
Total	5	1250			

One-way ANOVA: AZ31 Unt 50% cont, AZ31 50% 15day

Source	DF	SS	MS	F	P
Factor	1	493.9	493.9	16.24	0.016
Error	4	121.6	30.4		
Total	5	615.5			

One-way ANOVA: AZ31 Unt 50% cont, AZ31 50%18day

Source	DF	SS	MS	F	P
Factor	1	234.5	234.5	4.60	0.099
Error	4	204.1	51.0		
Total	5	438.6			

One-way ANOVA: AZ31 Unt 50% cont, AZ31 50% 21day

Source	DF	SS	MS	F	P
Factor	1	355.7	355.7	8.08	0.047
Error	4	176.1	44.0		
Total	5	531.8			

One-way ANOVA: AZ31 Unt 100% cont, AZ31 100% 3day

Source	DF	SS	MS	F	P
Factor	1	2.1	2.1	0.12	0.746
Error	4	68.3	17.1		
Total	5	70.4			

One-way ANOVA: AZ31 Unt 100% cont, AZ31 100% 6day

Source	DF	SS	MS	F	P
Factor	1	232.3	232.3	6.21	0.067
Error	4	149.7	37.4		
Total	5	382.0			

One-way ANOVA: AZ31 Unt 100% cont, AZ31 100% 9 day

Source	DF	SS	MS	F	P
Factor	1	50.5	50.5	0.90	0.396
Error	4	223.5	55.9		
Total	5	274.0			

One-way ANOVA: AZ31 Unt 100% cont, AZ31 100% 12day

Source	DF	SS	MS	F	P
Factor	1	31.3	31.3	0.54	0.502
Error	4	229.7	57.4		
Total	5	260.9			

One-way ANOVA: AZ31 Unt 100% cont, AZ31 100% 15day

Source	DF	SS	MS	F	P
Factor	1	47.1	47.1	0.93	0.390
Error	4	203.6	50.9		
Total	5	250.7			

One-way ANOVA: AZ31 Unt 100% cont, AZ31 100%18day

Source	DF	SS	MS	F	P
Factor	1	93.4	93.4	1.61	0.274
Error	4	232.8	58.2		
Total	5	326.2			

One-way ANOVA: AZ31 Unt 100% cont, AZ31 100% 21day

Source	DF	SS	MS	F	P
Factor	1	113.4	113.4	5.14	0.086
Error	4	88.2	22.1		
Total	5	201.6			

One-way ANOVA: AZ31 ANOD 50% cont, AZ31 ANOD 50% 3day

Source	DF	SS	MS	F	P
Factor	1	2106.10	2106.10	300.37	0.000
Error	4	28.05	7.01		
Total	5	2134.15			

One-way ANOVA: AZ31 ANOD 50% cont, AZ31 ANOD 50% 6day

Source	DF	SS	MS	F	P
Factor	1	1569.33	1569.33	1100.59	0.000
Error	4	5.70	1.43		

One-way ANOVA: AZ31 ANOD 50% cont, AZ31 ANOD 50% 9 day

Source	DF	SS	MS	F	P
Factor	1	1327.7	1327.7	24.96	0.008
Error	4	212.8	53.2		
Total	5	1540.4			

One-way ANOVA: AZ31 ANOD 50% cont, AZ31 ANOD 50% 12day

Source	DF	SS	MS	F	P
Factor	1	520.582	520.582	545.15	0.000
Error	4	3.820	0.955		
Total	5	524.402			

One-way ANOVA: AZ31 ANOD 50% cont, AZ31 ANOD 50% 15day

Source	DF	SS	MS	F	P
Factor	1	427.67	427.67	83.68	0.001
Error	4	20.44	5.11		
Total	5	448.11			

One-way ANOVA: AZ31 ANOD 50% cont, AZ31 ANOD 50%18day

Source	DF	SS	MS	F	P
Factor	1	391.84	391.84	92.85	0.001
Error	4	16.88	4.22		
Total	5	408.72			

One-way ANOVA: AZ31 ANOD 50% cont, AZ31 ANOD 50% 21day

Source	DF	SS	MS	F	P
Factor	1	443.76	443.76	46.13	0.002
Error	4	38.48	9.62		
Total	5	482.24			

One-way ANOVA: AZ31 ANOD 100% cont, AZ31 ANOD 100% 3day

Source	DF	SS	MS	F	P
Factor	1	469.7	469.7	26.30	0.007
Error	4	71.4	17.9		
Total	5	541.2			

One-way ANOVA: AZ31 ANOD 100% cont, AZ31 ANOD 100% 6day

Source	DF	SS	MS	F	P
Factor	1	1175.39	1175.39	143.93	0.000
Error	4	32.67	8.17		
Total	5	1208.05			

One-way ANOVA: AZ31 ANOD 100% cont, AZ31 ANOD 100% 9 day

Source	DF	SS	MS	F	P
Factor	1	1809.4	1809.4	93.65	0.001
Error	4	77.3	19.3		
Total	5	1886.7			

One-way ANOVA: AZ31 ANOD 100% cont, AZ31 ANOD 100% 12day

Source	DF	SS	MS	F	P
Factor	1	1297.0	1297.0	78.65	0.001
Error	4	66.0	16.5		
Total	5	1363.0			

One-way ANOVA: AZ31 ANOD 100% cont, AZ31 ANOD 100% 15day

Source	DF	SS	MS	F	P
Factor	1	1251.9	1251.9	91.26	0.001
Error	4	54.9	13.7		
Total	5	1306.8			

One-way ANOVA: AZ31 ANOD 100% cont, AZ31 ANOD 100%18day

Source	DF	SS	MS	F	P
Factor	1	1028.37	1028.37	891.71	0.000
Error	4	4.61	1.15		
Total	5	1032.99			

One-way ANOVA: AZ31 ANOD 100% cont, AZ31 ANOD 100% 21day

Source	DF	SS	MS	F	P
Factor	1	1598.81	1598.81	339.90	0.000
Error	4	18.82	4.70		
Total	5	1617.63			

One-way ANOVA: AZ91 UNT 50% cont, AZ91 UNT 50% 3day

Source	DF	SS	MS	F	P
Factor	1	1391.1	1391.1	67.87	0.001
Error	4	82.0	20.5		
Total	5	1473.1			

One-way ANOVA: AZ91 UNT 50% cont, AZ91 UNT 50% 6day

Source	DF	SS	MS	F	P
Factor	1	808.7	808.7	47.58	0.002
Error	4	68.0	17.0		
Total	5	876.7			

One-way ANOVA: AZ91 UNT 50% cont, AZ91 UNT 100% 9 day

Source	DF	SS	MS	F	P
Factor	1	488.4	488.4	33.23	0.004
Error	4	58.8	14.7		
Total	5	547.2			

One-way ANOVA: AZ91 UNT 50% cont, AZ91 UNT 50% 12day

Source	DF	SS	MS	F	P
Factor	1	334.40	334.40	50.45	0.002
Error	4	26.51	6.63		
Total	5	360.91			

One-way ANOVA: AZ91 UNT 50% cont, AZ91 UNT 50% 15day

Source	DF	SS	MS	F	P
Factor	1	596.6	596.6	9.88	0.035

```
Error     4  241.7   60.4
Total     5  838.3
```

One-way ANOVA: AZ91 UNT 50% cont, AZ91 UNT 50%18day

```
Source  DF      SS      MS      F      P
Factor   1  386.35  386.35  40.76  0.003
Error    4   37.92    9.48
Total    5  424.27
```

One-way ANOVA: AZ91 UNT 50% cont, AZ91 UNT 50% 21day

```
Source  DF     SS     MS      F      P
Factor   1  291.1  291.1  19.22  0.012
Error    4   60.6   15.1
Total    5  351.7
```

One-way ANOVA: AZ91 UNT 100% cont, AZ91 UNT 100% 3day

```
Source  DF   SS   MS     F      P
Factor   1    3    3  0.03  0.865
Error    4  420  105
Total    5  424
```

One-way ANOVA: AZ91 UNT 100% cont, AZ91 UNT 100% 6day

```
Source  DF      SS      MS      F      P
Factor   1  1242.7  1242.7  67.02  0.001
Error    4    74.2    18.5
Total    5  1316.9
```

One-way ANOVA: AZ91 UNT 100% cont, AZ91 UNT 100% 9 day

```
Source  DF      SS      MS       F      P
Factor   1  654.91  654.91  264.24  0.000
Error    4    9.91    2.48
Total    5  664.83
```

One-way ANOVA: AZ91 UNT 100% cont, AZ91 UNT 100% 12day

```
Source  DF     SS     MS      F      P
Factor   1  337.4  337.4  24.76  0.008
Error    4   54.5   13.6
Total    5  392.0
```

One-way ANOVA: AZ91 UNT 100% cont, AZ91 UNT 100% 15day

```
Source  DF      SS      MS      F      P
Factor   1  379.98  379.98  38.09  0.003
Error    4   39.90    9.97
Total    5  419.88
```

One-way ANOVA: AZ91 UNT 100% cont, AZ91 UNT 100%18day

```
Source  DF    SS   MS     F      P
Factor   1   801  801  4.03  0.115
Error    4   795  199
Total    5  1596
```

One-way ANOVA: AZ91 UNT 100% cont, AZ91 UNT 100% 21day

```
Source  DF     SS     MS     F      P
Factor   1  248.7  248.7  7.52  0.052
Error    4  132.3   33.1
Total    5  380.9
```

One-way ANOVA: AZ91 ANOD 50% cont, AZ91 ANOD 50% 3day

```
Source  DF       SS       MS       F      P
Factor   1  1507.49  1507.49  274.96  0.000
Error    4    21.93     5.48
Total    5  1529.43
```

One-way ANOVA: AZ91 ANOD 50% cont, AZ91 ANOD 50% 6day

```
Source  DF      SS      MS       F      P
Factor   1  461.26  461.26  125.05  0.000
Error    4   14.75    3.69
Total    5  476.02
```

One-way ANOVA: AZ91 ANOD 50% cont, AZ91 ANOD 50% 9 day

```
Source  DF       SS       MS        F      P
Factor   1  270.916  270.916  2554.70  0.000
Error    4    0.424    0.106
Total    5  271.340
```

One-way ANOVA: AZ91 ANOD 50% cont, AZ91 ANOD 50% 12day

```
Source  DF      SS      MS      F      P
Factor   1  156.45  156.45  91.21  0.001
Error    4    6.86    1.72
Total    5  163.31
```

One-way ANOVA: AZ91 ANOD 50% cont, AZ91 ANOD 50% 15day

```
Source  DF        SS        MS        F
P
Factor   1  55.85178  55.85178  7974.61
0.000
Error    4   0.02801   0.00700
Total    5  55.87980
```

One-way ANOVA: AZ91 ANOD 50% cont, AZ91 ANOD 50%18day

```
Source  DF     SS     MS     F      P
Factor   1  22.94  22.94  5.16  0.086
Error    4  17.79   4.45
Total    5  40.73
```

One-way ANOVA: AZ91 ANOD 50% cont, AZ91 ANOD 50% 21day

```
Source  DF    SS    MS     F      P
Factor   1  0.02  0.02  0.01  0.929
Error    4  8.90  2.22
Total    5  8.92
```

One-way ANOVA: AZ91 ANOD 100% cont, AZ91 ANOD 100% 3day

```
Source  DF       SS       MS       F      P
```

Factor	1	1016.19	1016.19	600.29	0.000
Error	4	6.77	1.69		
Total	5	1022.96			

One-way ANOVA: AZ91 ANOD 100% cont, AZ91 ANOD 100% 6day

Source	DF	SS	MS	F	P
Factor	1	154.9	154.9	3.68	0.128
Error	4	168.4	42.1		
Total	5	323.4			

One-way ANOVA: AZ91 ANOD 100% cont, AZ91 ANOD 100% 9 day

Source	DF	SS	MS	F	P
Factor	1	27.9	27.9	1.24	0.327
Error	4	89.5	22.4		
Total	5	117.4			

One-way ANOVA: AZ91 ANOD 100% cont, AZ91 ANOD 100% 12day

Source	DF	SS	MS	F	P
Factor	1	2.6	2.6	0.07	0.800
Error	4	143.7	35.9		
Total	5	146.4			

One-way ANOVA: AZ91 ANOD 100% cont, AZ91 ANOD 100% 15day

Source	DF	SS	MS	F	P
Factor	1	17.2	17.2	0.69	0.452
Error	4	99.2	24.8		
Total	5	116.4			

One-way ANOVA: AZ91 ANOD 100% cont, AZ91 ANOD 100%18day

Source	DF	SS	MS	F	P
Factor	1	4.5	4.5	0.10	0.767
Error	4	180.8	45.2		
Total	5	185.3			

One-way ANOVA: AZ91 ANOD 100% cont, AZ91 ANOD 100% 21day

Source	DF	SS	MS	F	P
Factor	1	4.6	4.6	0.06	0.815
Error	4	293.3	73.3		
Total	5	297.9			

One-way ANOVA: ZK60 UNT 50% cont, ZK60 UNT 50% 3day

Source	DF	SS	MS	F	P
Factor	1	35	35	0.34	0.593
Error	4	415	104		
Total	5	450			

One-way ANOVA: ZK60 UNT 50% cont, ZK60 UNT 50% 6day

Source	DF	SS	MS	F	P
Factor	1	17	17	0.17	0.704
Error	4	405	101		
Total	5	422			

One-way ANOVA: ZK60 UNT 50% cont, ZK60 UNT 50% 9 day

Source	DF	SS	MS	F	P
Factor	1	338.27	338.27	220.80	0.000
Error	4	6.13	1.53		
Total	5	344.40			

One-way ANOVA: ZK60 UNT 50% cont, ZK60 UNT 50% 12day

Source	DF	SS	MS	F	P
Factor	1	604.19	604.19	86.30	0.001
Error	4	28.00	7.00		
Total	5	632.20			

One-way ANOVA: ZK60 UNT 50% cont, ZK60 UNT 50% 15day

Source	DF	SS	MS	F	P
Factor	1	487.37	487.37	84.19	0.001
Error	4	23.15	5.79		
Total	5	510.53			

One-way ANOVA: ZK60 UNT 50% cont, ZK60 UNT 50%18day

Source	DF	SS	MS	F	P
Factor	1	165.39	165.39	88.26	0.001
Error	4	7.50	1.87		
Total	5	172.89			

One-way ANOVA: ZK60 UNT 50% cont, ZK60 UNT 50% 21day

Source	DF	SS	MS	F	P
Factor	1	46.54	46.54	8.38	0.044
Error	4	22.22	5.56		
Total	5	68.76			

One-way ANOVA: ZK60 UNT 100% cont, ZK60 UNT 100% 3day

Source	DF	SS	MS	F	P
Factor	1	1179.89	1179.89	250.71	0.000
Error	4	18.82	4.71		
Total	5	1198.72			

One-way ANOVA: ZK60 UNT 100% cont, ZK60 UNT 100% 6day

Source	DF	SS	MS	F	P
Factor	1	307.6	307.6	11.74	0.027
Error	4	104.8	26.2		
Total	5	412.4			

One-way ANOVA: ZK60 UNT 100% cont, ZK60 UNT 100% 9 day

Source	DF	SS	MS	F	P
Factor	1	138.2	138.2	9.25	0.038
Error	4	59.8	14.9		
Total	5	198.0			

One-way ANOVA: ZK60 UNT 100% cont, ZK60 UNT 100% 12day

Source	DF	SS	MS	F	P
Factor	1	36.5	36.5	2.19	0.213
Error	4	66.8	16.7		

Total	5	103.4			

One-way ANOVA: ZK60 UNT 100% cont, ZK60 UNT 100% 15day

Source	DF	SS	MS	F	P
Factor	1	583.4	583.4	30.53	0.005
Error	4	76.4	19.1		
Total	5	659.8			

One-way ANOVA: ZK60 UNT 100% cont, ZK60 UNT 100%18day

Source	DF	SS	MS	F	P
Factor	1	6325.5	6325.5	255.79	0.000
Error	4	98.9	24.7		
Total	5	6424.4			

One-way ANOVA: ZK60 UNT 100% cont, ZK60 UNT 100% 21day

Source	DF	SS	MS	F	P
Factor	1	6865.9	6865.9	156.47	0.000
Error	4	175.5	43.9		
Total	5	7041.4			

One-way ANOVA: ZK60 ANOD 50% cont, ZK60 ANOD 50% 3day

Source	DF	SS	MS	F	P
Factor	1	137.7	137.7	4.93	0.091
Error	4	111.8	27.9		
Total	5	249.5			

One-way ANOVA: ZK60 ANOD 50% cont, ZK60 ANOD 50% 6day

Source	DF	SS	MS	F	P
Factor	1	106.89	106.89	90.57	0.001
Error	4	4.72	1.18		
Total	5	111.61			

One-way ANOVA: ZK60 ANOD 50% cont, ZK60 ANOD 50% 9day

Source	DF	SS	MS	F	P
Factor	1	621.87	621.87	145.94	0.000
Error	4	17.04	4.26		
Total	5	638.92			

One-way ANOVA: ZK60 ANOD 50% cont, ZK60 ANOD 50% 12day

Source	DF	SS	MS	F	P
Factor	1	633.19	633.19	248.40	0.000
Error	4	10.20	2.55		
Total	5	643.38			

One-way ANOVA: ZK60 ANOD 50% cont, ZK60 ANOD 50% 15day

Source	DF	SS	MS	F	P
Factor	1	310.82	310.82	48.16	0.002
Error	4	25.82	6.45		
Total	5	336.64			

One-way ANOVA: ZK60 ANOD 50% cont, ZK60 ANOD 50%18day

Source	DF	SS	MS	F	P
Factor	1	100.6411	100.6411	53861.43	0.000
Error	4	0.0075	0.0019		
Total	5	100.6486			

One-way ANOVA: ZK60 ANOD 50% cont, ZK60 ANOD 50% 21day

Source	DF	SS	MS	F	P
Factor	1	129.4	129.4	2.83	0.168
Error	4	182.7	45.7		
Total	5	312.1			

One-way ANOVA: ZK60 ANOD 100% cont, ZK60 ANOD 100% 3day

Source	DF	SS	MS	F	P
Factor	1	6913	6913	10.84	0.017
Error	6	3827	638		
Total	7	10740			

One-way ANOVA: ZK60 ANOD 100% cont, ZK60 ANOD 100% 6day

Source	DF	SS	MS	F	P
Factor	1	6202	6202	6.59	0.043
Error	6	5648	941		
Total	7	11850			

One-way ANOVA: ZK60 ANOD 100% cont, ZK60 ANOD 100% 9day

Source	DF	SS	MS	F	P
Factor	1	2440	2440	3.37	0.116
Error	6	4343	724		
Total	7	6783			

One-way ANOVA: ZK60 ANOD 100% cont, ZK60 ANOD 100% 12day

Source	DF	SS	MS	F	P
Factor	1	3761	3761	3.93	0.095
Error	6	5745	958		
Total	7	9507			

One-way ANOVA: ZK60 ANOD 100% cont, ZK60 ANOD 100% 15day

Source	DF	SS	MS	F	P
Factor	1	5618	5618	5.22	0.062
Error	6	6459	1077		
Total	7	12077			

One-way ANOVA: ZK60 ANOD 100% cont, ZK60 ANOD 100%18day

Source	DF	SS	MS	F	P
Factor	1	6177	6177	6.80	0.040
Error	6	5452	909		
Total	7	11629			

One-way ANOVA: ZK60 ANOD 100% cont, ZK60 ANOD 100% 21day

Source	DF	SS	MS	F	P
Factor	1	6329	6329	10.17	0.019
Error	6	3735	623		
Total	7	1006			

BIOGRAPHICAL SKETCH

Luis Enrique Pompa earned his Bachelor of Engineering (August 2011) and his Master of Science degree (May 2014) in Mechanical Engineering from the University of Texas-Pan American. He also participated in a study abroad program in Rouen, France the year of 2011. While pursuing his degree, Mr. Pompa worked as a graduate research assistant and laboratory manager.

Mr. Luis Pompa has presented his research work at international conferences meetings and workshops including: The National Association of Corrosion Engineers (NACE) Conference, The Materials Science and Technology (MS&T) Conference and Exhibition, and The Minerals, Metals and Materials (TMS) 142nd Annual Meeting & Exhibition. Additionally, Mr. Pompa has submitted his research work to international journals.

Mr. Pompa has been recipient of numerous honors and awards. Some of the most recent (Master's career) awards include: Graduate Travel Scholarship, Billy Eugene Minnis Schol Scholarship, and first and second place, technical poster competition as co-author, during 142nd Annual Meeting & Exhibition, TMS 2013 in San Antonio, TX.

Mr. Pompa's thesis, Corrosion Assessment And Enhanced Biocompatibility Analysis of Biodegradable Magnesium-Based Alloys, was supervised by Dr. Waseem Haider.

Address:1015 E. Sanchez St. Pharr, TX. 78577
Email: lepompa@broncs.utpa.edu